ATOMIC MASS DIFFERENCES AND NUCLEON SEPARATION AND PAIRING ENERGIES, $60 \leq Z \leq 72$

A Thesis

Submitted to the Faculty of Graduate Studies

University of Manitoba

In partial fulfillment

of the Requirements for the Degree

Doctor of Philosophy

by

John Ogilvie Meredith

Winnipeg, Canada

August 1971

Doctor of Philosophy (1971) University of Manitoba

Physics Winnipeg, Manitoba

Title: Atomic Mass Differences and Nucleon Separation and Pairing Energies, $60 \leq Z \leq 72$

Author: John Ogilvie Meredith, B.Sc.(Hons.), University of Manitoba

Supervisor: Professor R. C. Barber

Pages: viii, 140

Scope and Contents:

A high resolution double focusing mass spectrometer has been constructed with a working resolving power of 100,000 at the base of the peaks. The spacings of 25 mass spectral doublets, with a typical precision of 5 parts in 10^9, are reported.

A method of peak matching using a digital computer has been developed. The spacings of 13 of the above doublets have been determined using this new technique.

The resulting mass differences are combined with precise atomic masses, and nuclear reaction and decay Q-values in two overlapping adjustments to obtain least squares adjusted masses for $59 \leq Z \leq 72$.

The quantities S_{2n}, S_n, P_n, S_{2p}, S_p, P_p, $Q(\beta^-)$ and $Q(\alpha)$ are calculated for each nuclide wherever possible, and their systematic variations are commented upon.

ACKNOWLEDGEMENTS

This research has been supported by the National Research Council. Financial assistance from the University of Manitoba is gratefully acknowledged.

I wish to thank my supervisor, Dr. R. C. Barber for his encouragement and guidance during this research project. I also wish to give particular credit to Dr. H. E. Duckworth for his valuable comments. He is responsible for this programme of precise atomic mass determinations.

Many other people in the research group have helped over the years and I would like to thank Drs. R. L. Bishop, B. G. Hogg and P. Williams, Messrs. D. Burrell, G. Southon and P. van Rookhuysen.

Special mention should be made of my wife, Helen, who was partially responsible for a delay due to marriage during July 1971.

CONTENTS

LIST OF TABLES

LIST OF FIGURES

CHAPTER 1

INTRODUCTION

The importance of atomic mass determinations and the related standards of atomic mass are discussed. Various methods of atomic mass determinations are briefly presented.

Mass and Mass Standards

The mass of any object or particle is one of the most useful and revealing pieces of information available about that particle. In the macroscopic world, the mass of a solid object gives one some idea of its size, and certainly gives information about whether or not one can lift or move it. The standard for this sort of mass is the international kilogram, maintained at the Bureau International des Poids et Mesures at Sèvres, France. This is a platinum - iridium bar, carefully protected, but certainly not indestructible, and not exactly reproducible.

On the atomic scale, the unit of mass has been chosen so that one atom ^{12}C has a mass of exactly 12 u. (Mattauch 1960). This has the advantage of being a universal quantity, available to any laboratory interested in making measurements

relative to it. In mass spectroscopy it is especially useful since many atomic mass determinations may be made directly against a hydrocarbon fragment containing ^{12}C only, or ^{12}C and ^{1}H only. Thus, a secondary mass standard is ^{1}H. As will become evident in later chapters, the atomic mass difference ^{37}Cl-^{35}Cl is very important to this research group. A recent compilation of experimental values by Meredith et al (1971) gives these secondary masses as:

$$^{1}H = 1.007825\ 035 \pm 14\ u$$

$$^{37}Cl\text{-}^{35}Cl = 1.997049\ 720 \pm 90\ u$$

The relation between the kilogram and the atomic mass unit is known to a precision of 6.6 parts per million (ppm), and is: $1\ u = 1.660531 \pm 11 \times 10^{-27}$ kg as calculated in a least squares adjustment of fundamental constants by Taylor et al (1970).

A third unit of mass, used on the atomic, nuclear and sub-nuclear scale is the electron volt (eV) and its multiples. This is defined as the amount of energy an electron gains when it falls through a potential of one volt. The relation of energy to mass follows from Einstein's famous equation

$$E = mc^2$$

in his special theory of relativity in 1905. At present, the conversion factor between eV (energy) and kg (mass) is known to a precision of 4.4 ppm, and between eV and the

atomic mass unit, 5.5 ppm. The energy conversion factors from Taylor et al (1970) are:

$$1 \text{ kg} = 5.609538 \pm 24 \times 10^{29} \text{ MeV}$$

$$1 \text{ u} = 931.4812 \pm 52 \text{ MeV}$$

Importance of Atomic Mass Determinations

Just as mass is important in the macroscopic world, it is equally, if not more, important on the atomic scale. Mass, along with charge uniquely identifies an atom, and with spin included, any sub-atomic particle is specified.

Since mass and energy are different forms of the same quantity, the mass of an atom gives a measure of the energy of the atom. An atom's mass is less than that of its constituent protons, neutrons and electrons. This missing mass is called the binding energy of the atom.

The mass defect (or missing mass) is of great importance in the studying of nuclear structure, since the effect of the electronic binding energy is small and varies gradually with atomic number. The magnitude of the binding energy gives information on possible nuclear transformations and decays. Variations in the binding energy from nucleus to nucleus show the effects of proton or neutron shells, (the so-called magic numbers), and also of collective nucleon behaviour.

Methods of Atomic Mass Determinations

Alpha-decay - Most of the atomic mass information for nuclides heavier than lead has been obtained by α-decay energy determinations. The α-decay of a parent nucleus may be represented as

$$ {}^{A}_{Z}M \rightarrow {}^{A-4}_{Z-2}M + {}^{4}_{2}He + Q $$

The energy of the particle is usually determined by a magnetic analyser. These analysers are usually calibrated with the ^{210}Po α particle whose energy is 5304.5 ± 0.5 keV. (Wapstra, 1964). More recently, solid state detectors have proved useful in determining E_{α}. The recoil energy of the daughter nucleus is calculated, and the sum of the two energies, and the mass of the $^{4}_{2}He$ allows the mass difference between parent and daughter nuclei to be calculated, usually with a final precision of ∿25 keV and occasionally as low as ∿5 keV.

Beta decay - The β-decay of unstable nuclides can be represented by:

$$ {}^{A}_{Z}M \begin{cases} \nearrow \\ \searrow \end{cases} \begin{matrix} {}^{A}_{Z-1}M + \beta^{+} + \nu + Q \text{ or (e.c.) if } Q < 2\, m_o c^2 \\ {}^{A}_{Z+1}M + \beta^{-} + \bar{\nu} + Q \end{matrix} $$

An accurate determination of the end point of the β-spectrum, and energies of correlated γ-rays is necessary. The large magnetic spectrometer at Chalk River has achieved precision of ∿0.1 keV, but most determinations are ±∿10 keV

or more. The total decay energy in cases of electron capture (ec) is more difficult to determine.

Induced Nuclear Reactions - Many induced nuclear reactions involve charged particles from accelerators (e.g. p, d, t, ^{3}He, α, ^{12}C, ^{16}O, etc.) as well as neutrons, photons, and virtual photons (in the form of high energy electrons from LINACs). The reaction can be represented as:

$$x(a,b)Y$$

or $Q = (M_x+M_a-M_b-M_y)C^2$ where x and y are the initial and final nuclei, a is the incoming particle and b the outgoing one. The energies of a, b and y must all be determined to obtain Q. In reactions such as (n,γ) with thermal neutrons, precision <1 keV is obtainable with the recent GeLi detectors. More typical precision of Q values from charged particle reaction is $\sim$10 keV.

Mass Spectroscopy - Here the mass of ions may be determined directly by deflecting them in electric and magnetic fields. This method can be applied to any stable or naturally occurring nuclide, and also to unstable nuclides having sufficiently long half-lives.

Generally the doublet method is used in which the unknown mass is compared to a well known one (say a hydrocarbon fragment or other secondary standard) of almost the same m/e.

The precision attainable with such doublets is about 5 parts in 10^9, or about 1 keV at mass 200. Thus the relative masses may be determined from .1 to 1 keV. Also mass differences are established to the same precision. In studying the mass surface, and the systematic variation in nuclear binding energies, mass differences determined by close doublets are as important as the masses and are more easily obtained.

References for Chapter 1

Mattauch, J.H.E. (1960) Proc. Int. Conf. Nuclidic Masses (University of Toronto Press) p.459

Meredith, J.O., Barber, R.C. and Duckworth, H.E. (1971) (to be published)

Taylor, B.N. Parker, W.H. and Langenberg, D.N. (1970) The Fundamental Constants and Quantum Electrodynamics (Academic Press, New York)

CHAPTER 2

MASS SPECTROSCOPY

The early development of mass spectroscopy is outlined. The direction focusing properties of uniform magnetic and radial electric fields, and double focusing in tandem are presented to first order. The results of second order theory are outlined. Electrical detection and current performance of several instruments are discussed.

Historical Development

Mass spectroscopy had its origins in the late 19th century with the discovery by Goldstein (1886) of "positive-rays" in discharge tubes. However, they remained a curiosity until 1912 when J. J. Thompson used his positive ray parabola apparatus to show that Goldstein's positive rays were actually positively charged atoms and molecules. Thus, Thompson (1913) had constructed the first mass spectroscope. Using this instrument with a resolution of about 1/20, Thompson found evidence for the existence of two stable isotopes of neon.

F. W. Aston continued Thompson's investigation of the existence of isotopes. By 1919 he had a velocity focusing

instrument with a resolution of about 130, and proved that neon indeed had two isotopes (Aston 1920). During the next decade he carried out a systematic study of the periodic table, showing most elements had several isotopes. This measurement of the masses of the nuclides lead to his famous binding energy and packing fraction curves (Aston 1933). In these 'preneutron days' he defined the packing fraction, P, as: $P = \frac{M-A}{A}$ where A is the mass number.

Simultaneously, A. J. Dempster at the University of Chicago exploited the direction focusing property of the 180° magnetic field (Dempster 1918). He also carried out extensive investigations of nuclear binding energy over the next two decades (Dempster 1938 a,b).

In 1933 K. T. Bainbridge added a Wien velocity filter to the original Dempster instrument.

General focusing equations were presented by Herzog (1934), and subsequently many new double focusing instruments were constructed, notably by Dempster at Chicago, Bainbridge and Jordan at Harvard, Mattauch and Herzog at Vienna, and Nier at Minnesota. A more detailed account of the development of mass spectroscopy is given by Duckworth (1958).

Positive Ion Optics

An ion of mass m and charge q moving with a velocity v in an electromagnetic field experiences a force $\bar{F}$ given by:

$$\bar{F} = q\bar{E} + q\bar{v} \times \bar{B} \qquad (1)$$

Uniform Magnetic Fields - In this case the equation (1) reduces to $F = q\bar{v} \times \bar{B}$. If $\bar{v}$ is perpendicular to $\bar{B}$, the ion is constrained to move in a circle of radius a_m, so that

$$\frac{mv^2}{a_m} = qvB$$

Thus, a uniform magnetic field is a momentum analyser. To examine the direction focusing properties, we refer to Fig. 2-1; the terminology is that of Herzog (1934). Ions of mass m_o leave the point 0 (object slit) with a velocity v_o and half angular spread α. Herzog compared this to the optical arrangement of prism plus cylindrical lens. The divergent beam comes to a focus again at I, the image. Note that I, the centre of curvature, and O lie on the same straight line, as pointed out by Barber (1933).

Radial Electric Fields - Here the equation (1) reduces to $\bar{F} = q\bar{E}$. The field $\bar{E}$ is usually established by a voltage V applied to the plates of a cylindrical capacitor, of mean radius a_e and separation 2k.

Then $$\frac{mv^2}{a_e} \approx q\frac{V}{2k} \qquad (3)$$

Thus, such a configuration is an energy analyser.

Fig. 2-2 shows the direction focusing properties of a radial electrostatic field. Note that it does not obey Barber's rule as was the case for the uniform magnetic field. A geometric construction, which corresponds to Fig. 2-1, may be

made, if a_e is divided by $\sqrt{2}$ and Φ_e is multiplied by $\sqrt{2}$. Then Barber's rule may be applied as for the magnetic field.

Double Focusing - So far we have assumed mono-energetic ions. If a velocity spread is considered, i.e. $v = v_o(1 \pm \beta)$, then each of the magnetic and electric fields produce a velocity dispersion. That is, the direction focused image is blurred because ions of different v come to a focus at a different position perpendicular to the median beam.

It is possible to construct an instrument in which the velocity dispersion of one element is cancelled by that of the other. The usual arrangement is to use the direction focus of the electrostatic analyser (ESA) to serve as the object of the magnetic analyser. Thus, direction focusing is preserved, and a double focus (i.e. focused both in α and β) may be achieved.

Resolution - The resolving power of an instrument is a measure of the peak width (or image width); we say that the two peaks are just resolved if they are just separated at the base. For a mass spectroscope, the two peaks of a doublet are approximately mass M, and differ by a small amount ΔM. The resolving power required to just spearate them is then $M/\Delta M$ and for a symmetrical ESA ($l_e' = l_e''$)

$$\frac{M}{\Delta M} = \frac{a_e}{S_o} \qquad (4)$$

where S_o is the width of the object slit. Here we see that as small a slit as possible should be used with as large an

ESA as possible for maximum resolving power. (The reciprocal of resolving power, the resolution, may alternately be used.)

Second-Order Focusing - The theory of Herzog (1934) ignores the effects of second-and higher-order terms in α and β. These lead to image aberrations, as do the effects of fringing fields.

Effective boundaries for the ESA may be established by use of grounded diaphragms placed according to Herzog (1935), and for the magnet, iron diaphragms have been discussed by Herzog (1955) and by Konig and Hintenberger (1955). Alternatively, the position of the effective boundary may be calculated by integration of the fringing field. As a rule of thumb, the effective boundary is one gap width beyond the physical boundary. (See for example, Kerwin 1958.)

Second order terms in α and β have been included in the theory of Hintenberger and Konig (1957a, 1957b). The aberrations of the final image of a double focusing instrument may be written as:

$$Y_B = a_m (B_1\alpha + B_2\beta + B_{11}\alpha^2 + B_{12}\alpha\beta + B_{22}\beta^2). \qquad (5)$$

Here Y_B is the lateral displacement of an ion from the central path ($\alpha=\beta=o$). The coefficients B_{ij} are functions of the instrument geometry. When $B_1 = B_2 = 0$ there is a first order double focus. If, in addition, $B_{11} = B_{12} = B_{22} = 0$, there is complete second order double focusing. Hintenberger and Konig have calculated a solution of the second order equations

and have proposed geometrical arrangements for many complete and partial second order double focusing spectrometers. A more complete description of first and second order focusing for mass spectrometers is given by Barber (1962).

Current High Resolution Spectroscopes

Most instruments at the present time employ electrical, rather than photographic detection. This means that the ion beam is modulated across a collector slit, and the current which passes through the slit is amplified by some high gain electron multiplier. Following the nomenclature of Aston, these instruments are call mass spectrometers, while those employing photographic detection are call mass spectrographs.

If photographic detection is employed, the resolution of the instrument is as calculated previously, but in addition the dispersion of the instrument must be known in order to calculate a mass difference. Also, the precision of locating the centroid of line on a plate is limited to $\sim$ 1/50 of its width.

For instruments using electrical detection, the resolution is reduced since the expression now includes the width of the collector slit (S_c).

$$\Delta M/M = (S_o + S_c)/a_m \qquad (6)$$

However, this is more than compensated for by increase in precision in locating a peak. The peak matching method will be described in the next Chapter, but we will note here that the precision of matching is about 1/500 of a peak width for visual matching to 1/5000 for signal averaging and computer analysis.

The peak matching method of determining a mass difference depends on a theorem due to Bleakney (1936). If we start with $\bar{F} = m\bar{a} = q\ (\bar{E} + \bar{v} \times \bar{B})$ it can be shown that two different ions of mass m and m' will follow the identical trajectory if all $\bar{E}$ are changed to $\bar{E}'$ in the ratio $E/E' = m/m'$ while B remains fixed. In practice, this means that E' is varied until m and m' do appear to follow the same trajectory (i.e. the peaks are matched). Then Δm, the mass difference may be calculated from $\frac{\Delta m}{m'} = \frac{\Delta E}{E}$.

The major instruments are compared in Table 2-I, which gives the parameters of the ESA and magnetic analyser, along with the calculated resolving power for 4μ width object slit. (Matsuda, 1970), the achieved resolving power, and the second order coefficients calculated as noted. The type of measuring technique is given on the second line for each instrument, and special features are pointed out.

An excellent review article by Duckworth (1970) covers the development of high resolution mass spectrometry over the

last two decades and shows general trends in the precise determinations of atomic mass differences.

References for Chapter 2

Aston, F.W. (1920) Phil.Mag. 39, 449

Aston, F.W. (1933) Mass Spectra and Isotopes, Edward Arnold & Co., London

Bainbridge, K.T. (1933) Phys.Rev. 44, 123L

Barber (1933) Proc. Leeds Phil.Lit.Soc. 2, 427

Barber, R.C. (1962) Ph.D. Thesis, McMaster University

Barber, R.C., Bishop, R.L., Cambey, L.A., Duckworth, H.E., Macdougall, J.D., McLatchie, W., Ormrod, J.H. and van Rookhuyzen, P. (1963) Proc. 2nd Int. Conf. on Nucl. Masses, Springer Verlag, Vienna, p.373.

Barber, R.C., Meredith, J.O., Bishop, R.L., Duckworth, H.E., Kettner, M.E. and van Rookhuyzen, P. (1967) Proc. 3rd Int. Conf. on Atomic Masses, University of Manitoba Press, p.717

Barber, R.C., Bishop, R.L., Duckworth, H.E., Meredith, J.O., Southon, F.C.G., van Rookhuyzen, P. and Williams, P. (1971) Rev.Sci. Instrum. 42, 1.

Bleakney, W. (1936) Amer.Phys.Teacher 4, 12

Collins, T.L. and Bainbridge, K.T. (1957) Nuclear Masses and Their Determinations, Pergamon Press, London, p.213

Demirkhanov, Dorokhov and Dzkuya (1965) Izv. AN.SSSR. ser.fiz. 29, N5 857

Dempster, A.J. (1918) Phys.Rev. 11, 316

Dempster, A.J. (1938a,b) Phys.Rev. 53, 64, 869

Duckworth, H.E. (1958) Mass Spectroscopy, Cambridge University Press

Duckworth, H.E. (1970) Recent Developments in Mass Spectroscopy, University of Tokyo Press, p.26

Fukumoto, S. and Matsuo, T. (1970) Nucl.Instrum. and Methods, 83, 58

Goldstein (1886) Berl.Ber. 39, 691

Herzog, R. (1934) Z. Phys. 89, 447

Herzog, R. (1935) Z. Phys. 97, 596

Herzog, R. (1955) Z. Naturforshg. 10a, 887

Hintenberger, H. and Konig, L.A. (1957 a,b) Z. Naturforschg. 12a, 140, 773

Hintenberger, H. and Konig, L.A. (1959) Advances in Mass Spectroscopy (Pergamon Press, London) p.16

Hintenberger, H,, Mattauch, J.H.E., Muller-Warmuth, W., Voshage, H. and Wende, H. (1960) Proc. Int.Conf. on Nucl. Masses, University of Toronto Press, p.387

Hintenberger, H., Mattauch, J.H.E., Wende, H., Voshage, H. and Muller-Warmuth, W. (1963) Adv. in Mass Spec. Vol. 2, p.180

Kerwin, L. (1958) Can. J. Phys. 36, 711

Konig, L.A. and Hintenberger, H. (1955) Z. Naturforshg. 10a, 877

Matsuda, H., Fukumoto, S., Kuroda, Y. and Nojiri, M. (1966 a,b) Z. Naturforshg. 21a, 25, 1304

Matsuda, H., Fukumoto, S. and Matsuo, T. (1967) Proc. 3rd Int. Conf. on Atomic Masses, University of Manitoba Press p.733

Matsuda, H. (1970) Int. Conf. on Mass Spectroscopy, Brussels

Moreland, P.E. and Bainbridge, K.T. (1963) Proc. 2nd Int. Conf. Nucl. Masses, Springer Verlag Vienna p.423

Nier, A.O.C. (1957) Nuclear Masses and Their Determinations, Pergamon Press, London p.185

Ogata, K. and Matsuda, H. (1955) Z. Naturforschg. 10a, 843

Smith, L.G. (1967) Proc. 3rd Int. Conf. on Atomic Masses, University of Manitoba Press, p.811

Stevens, C., Terandy, J. Lobell, G., Wolfe, J., Beyer, N. and Lewis, R. (1960) Proc. Int. Conf. on Nuclidic Masses, University of Toronto Press, p.403

Stevens, C. and Moreland, P.E. (1967) Proc. 3rd Int. Conf. on Atomic Masses, University of Manitoba Press, p.673

Thompson, J.J. (1913) Rays of Positive Electricity, Longmans Green and Co. London

TABLE 2-I

CURRENT HIGH RESOLUTION DOUBLE FOCUSING MASS SPECTROMETERS

		ESA a_e(cm)	ESA Φ_e	Magnet a_m(cm)	Magnet Φ_m	Dispersion γ(cm)	Resolving Power calc.(4μ)	Resolving Power Achieved	Calc.2nd Order Coeff* B_{11}	B_{12}	B_{22}
Argonne	a)	254	75°	254	110°	170	317,000	350,000	<.01	- 6.69	-10.3 k)
		Peak matching with signal averager and computer.									
Harvard	b)	213.4	31.8°	126.8	90°	63	133,000	165,000	-.0012	6.14	- 1.39
		Peak matching with lock-in amplifier.									
Mainz	c)	542.6	48.4°	100.0	167°	99	340,000	150,000	-.0015	-12.1	-10.0
		Largest radius. Photographic and peak matching. No measurement since 1964.									
Manitoba I	d)	273.1	90°	273.1	180°	273	340,000	150,000	.7	- 0.36	- 2.12
		Originally at McMaster. Peak matching with signal averager.									
Manitoba II	e)	100.0	94.65°	62.74	90°	54	134,000	250,000	-.0003	.0009	- .0006
									.0963	.310	1.29**
		Peak matching with signal averager and computer.							<.1	<.2	<.5 ++
Minnesota	f)	50.3	90°	40.6	60°	34	63,000	100,000	.0010	.649	.275
		Peak matching with signal averager.									
Osaka I	g)	109.3	84.8°	120.0	60°	224	200,000	150,000	4.54	-13.2	2.93
		Photographic, and Peak matching. No measurements since 1964.									
Osaka II	h)	30.0	118.7°	120.0	30°	475	580,000	500,000	0.40	- 0.61	0.31+
		Largest dispersion, achieved by 1/r magnetic field between the ESA and the mass discriminating magnetic field. Peak matching, or photographic detection.									
Princeton	i)	21.5	90°X	4.5	720°X			100,000	-	-	-
		This is an r.f. mass spectrometer.									
USSR	j)	Photographic detection						80,000			

Figure 2-1

Direction Focusing in a Uniform Magnetic Field

Figure 2-2

Direction Focusing in a Radial Electric Field

TABLE 2-I cont'd.

* Except where otherwise noted, these coefficients are as calculated by Matsuda (1970), with no fringing fields.

**Calculated by Matsuda (1970) with fringing fields.

++Measured by Barber et al (1971)

+ Measured by Fukumoto and Matsuo (1970)

X r.f. mass spectrometer

a) Stevens & Moreland (1967)

b) Collins & Bainbridge (1957)
Moreland & Bainbridge (1963)

c) Hintenberger et al (1960)
Hintenberger et al (1963)

d) Barber et al (1963)

e) Barber et al (1967)
Barber et al (1971)

f) Nier (1957)

g) Ogata & Matsuda (1955)

h) Matsuda et al (1966,a,b)

i) Smith (1967)

j) Demirkhanov et al (1965)

k) Stevens et al (1960)

FIGURE 2 - 1

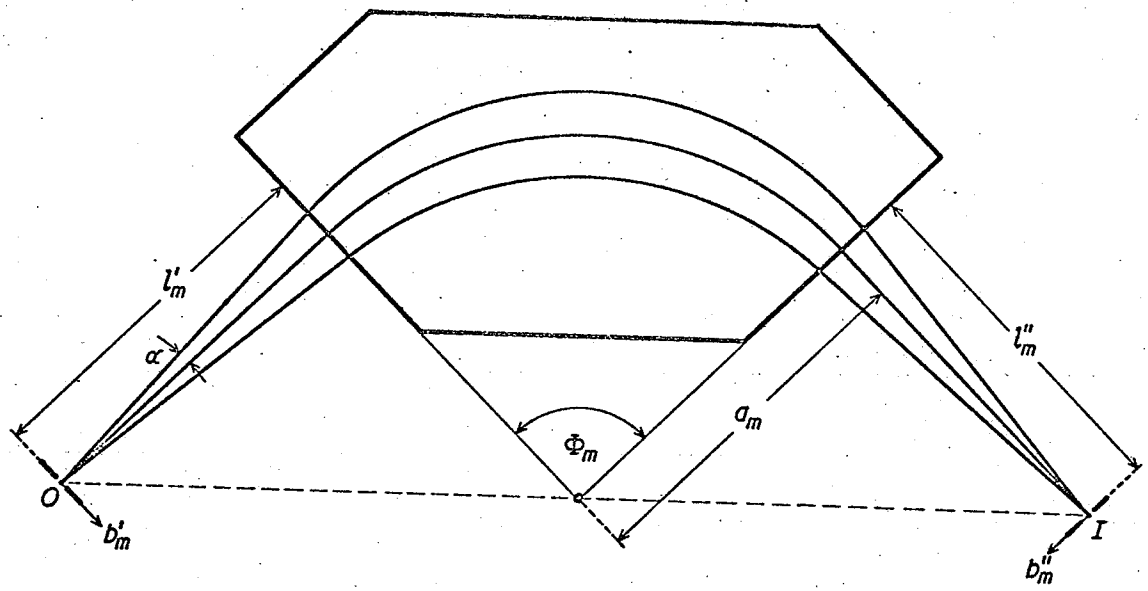

FIGURE 2 - 2

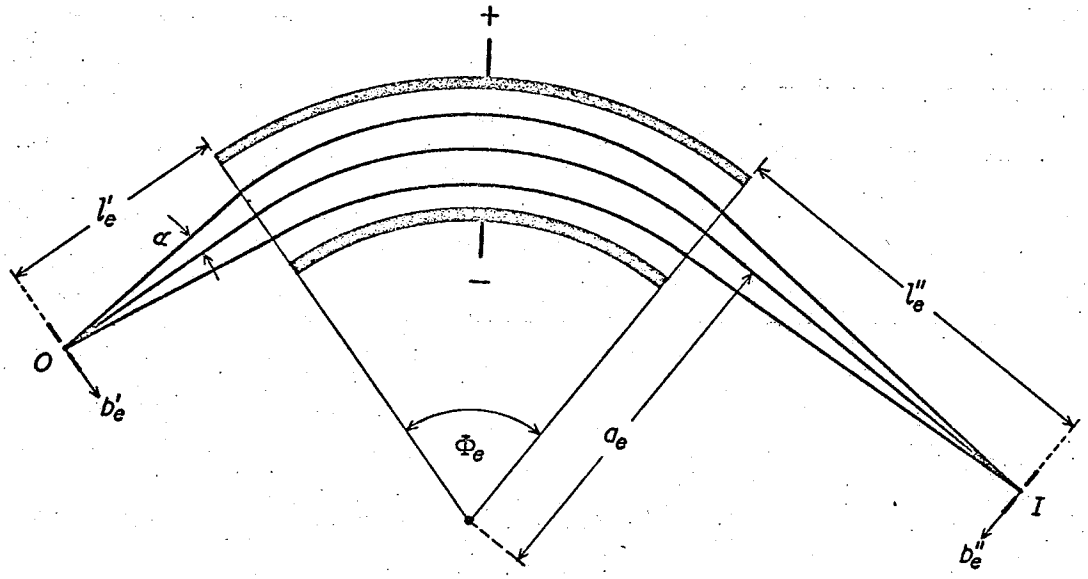

CHAPTER 3

THE SECOND ORDER SPECTROMETER

The second-order double-focusing mass spectrometer at the University of Manitoba is briefly presented. The "visual null" matching method and recent modifications associated with the new computer matching system are described.

Geometry and Construction

The geometrical arrangement of the instrument, one of many proposed by Hintenberger and Konig (1959), is shown in Fig. 3-1. The advantages of this particular design are: (i) an intermediate direction focus with an energy resolution of ∿1eV, (ii) straight rather than curved magnetic field boundaries and (iii) compact shape.

Detailed descriptions of the apparatus in its early (Barber et al 1968) and present forms (Barber et al 1971, hereinafter called Paper I) have previously been published. Certain of the most important features of the instrument are presented here.

The overall size is determined by choosing the radius of curvature of the electrostatic analyser (ESA) to be 1.000 m. The total path length is 4.59 m and the overall magnification

is 0.50. The width of the object slit S_o is variable, but for a resolving power of 200,000 at the base of the peaks, the calculated width of S_o is 2.7μ. The collector slit S_c then must be 1.8μ wide. The slits S_α at the entrance to the ESA are normally used to limit α to $\sim\pm 2 \times 10^{-3}$ radians, although a maximum value of $\pm 10^{-2}$ radians is available. At the exit of the ESA, the slits S_β are used to limit the energy spread of the beam; usually β is $\pm 8 \times 10^{-4}$. The height slits at the entrance to the magnet are generally set about 2mm to limit the vertical spread of the beam and thereby to ensure that ions reaching S_c have all gone through the same magnetic field.

The angle of deflection in the ESA is 94.65°, and a direction focus is formed 17.63 cm beyond the exit boundary. The field is terminated at the physical boundaries of the plates by fringe blocks positioned according to the theory of Herzog (1935).

The angle of deflection in the magnetic analyser is 90.00° and the pole gap is 2.540 cm, with a field uniformity of 1/5000 over the range 3-8 kG.

As can be seen in Fig. 3-2, the whole instrument is mounted on a rigid steel table one inch thick and 5 x 12 feet. The table is supported by eight pneumatic mounts to isolate the instrument from building vibrations. The vacuum chamber of the spectrometer is made of stainless steel. Two oil

diffusion pumps provide differential pumping on the source arm. The 140 l/sec and a 50 l/sec ion pumps on the main chamber maintain a pressure of about 5×10^{-8} Torr. during operation of the instrument.

The source, shown in Fig.3-3, has been described in Paper I and also by Bishop (1969). It is a variation of the Finkelstein source (as referred to by Von Ardenne, 1962), with a stainless steel or tantalum oven and a rhenium or tungsten heating filament. The electron emission filament is usually coated with LaB_6 for better emission and is 50-300V negative with respect to the oven. An electromagnet provides a magnetic field of $\sim$1 kG in the region of the oven, parallel to the source axis. For emission currents of 5-20 mA the ion current is usually 1 to 5 μA.

The ions are extracted from the plasma through the front hole of the source toward the ground electrode just outside the front plate. The ion beam can be steered horizontally and vertically by separate pairs of electrostatic deflection plates, and are subsequently focused on the principal slit by an electrostatic quadrupole lens. The theory of the operation of the quadrupole lens is given by Enge (1959), and details of the steering and focusing are presented by Southon (1971).

The principal slit can be moved in a horizontal direction perpendicular to the ion beam, and also parallel to the ion beam by means of two lathe slides. In addition, the source

may be rotated about a vertical axis at the principal slit by a rotary table. The analyser and source arm can be swung as a unit about a pivot located directly below the intermediate direction focus.

Peak Matching and Focusing

The peak-matching method of determining the separation of a mass doublet depends on Bleakney's theorem outlined in Chapter 2. If all potentials V_i are changed to V_i' according to the relation $MV_i = M'V_i'$, then the ions of mass M' will be 'matched' with ions of mass M. In order to judge this match, the potentials are switched at a frequency of ∿19 cps, and the electron multiplier output displayed.

The control circuitry is shown in Fig.3-4. The master trigger signal is derived from a mechanical chopper, which also switches the ΔV applied to the ESA voltage V. This trigger signal supplies the start signal for the sweep of the display oscilloscope and of the FT1052 signal averager. The horizontal sawtooth sweep of the display oscilloscope is amplified and drives the Helmholtz coils which sweep the ion beam across the collector slit. The fly-back of the sawtooth triggers a flip-flop which controls relays to (i) switch the signal through gain A or B, (ii) displace alternate sweeps vertically on the display oscilloscope, and (iii) switch a neon light which

subsequently switches V_a. There is also provision for switching the voltages applied to the quadrupole lens electrodes, although this is not necessary for narrow doublets.

Gain A or gain B is adjusted so that the peaks M and M' are the same amplitude and ΔV is adjusted so that the two peaks appear at the same stage of the oscilloscope sweep. Alternate traces can be displaced vertically for focusing or visual matching, as described in detail by Barber et al (1964).

More recently a signal averager was used on-line to detect the lack of coincidence of the peaks (the "visual null" method). This method was developed at the University of Minnesota (Benson and Johnson, 1966) and used subsequently by this group at McMaster University (Macdougall, 1966) and at the University of Manitoba as described in Paper I. In this method, the gains A and B are adjusted, but the display is not split. The trace corresponding to mass M is added to the memory on odd numbered sweeps while the trace corresponding to mass M' (with ΔV applied to the plates), is subtracted from the memory on even numbered sweeps. Thus, at match, there is a null signal. A slight mismatch (i.e. ΔV too big or too small) results in an S-shaped error signal. ΔV is then adjusted to obtain a null.

Either M or M' may be used as the reference peak, the reference peak may be routed through either gain A or gain B,

and the ion beam may be swept in either of two directions across the collector slit. Permutation of these arrangements results in eight different matching configurations. To reduce the chance of systematic error, the unweighted average is taken as one run. Since there may be systematic differences between configurations due to instrumental or operator biases, the spread of the eight values does not necessarily represent the statistical error to be associated with one run. In the past about 20 runs have been used to determine the mass difference, and the standard deviation of the mean of the set of 20 has been used as the error for the doublet. This point will be discussed further in Chapter 4 when the visual null method is compared with the new computer matching method.

In order to reduce operator biases, two people are involved. One, the operator, judges the match, while the other runs the potentiometer to determine ΔV. Moreover, values for individual runs are obtained on at least three different days and by several different operators.

The voltage supply for the electrostatic analyser is still basically as described by Bishop and Barber (1970). Each of the eight 97.2 V mercury batteries is actually a set of twelve 8.1 V mercury batteries (Mallory TR-136R). The supply which presents ΔV to the chopper is much as described by Bishop (1966).

Additionally there is now the option of providing small voltages δV to ΔV and applying the signal to an alternate chopper. This optional arrangement is the one used for peak matching using the computer method described in Chapter 4. The details of the circuit are deferred to that Chapter.

The precision potentiometer developed by Bishop (1969) and described by Bishop and Barber (1970) is used to determine both V and ΔV relative to the same standard. It is used in the same manner when the technique to be described in the next Chapter is applied to peak matching.

The switching circuits described above are also used during the focusing of the spectrometer. The general focusing procedure and adjustments have been described in Paper I. To check the velocity focus, ΔV_a is increased to $\sim$22V (ΔV is not applied to the ESA) and alternate sweeps of the oscilloscope are displaced. Lack of velocity focusing results in the peak on one trace being displaced sideways with respect to the one on the other trace. A small movement of the collector slit perpendicular to the ion beam usually results in a velocity focus. If a more sensitive velocity focusing test is required, the degree of mismatch may be detected by the signal averager (as used in the "visual null" method).

The direction focus is characterized by a marked improvement in the resolution of the peaks. As the ESA is swung about its pivot, the optimum position is chosen. In addition,

with a tightly focused beam at the principal slit, the quadrupole lens and steering plates may be used to change α. At the direction focus, the peaks will not be sensitive to this change.

On the basis of current performance, the upper limits for the second order coefficients are estimated as $B_{11}<0.1$, $B_{12}<0.2$ and $B_{22}<0.5$. If B_{12} is large, the velocity and direction foci are not coincident. A comparison of the coefficients of this instrument with those of other instruments now operating is made in the previous chapter.

References for Chapter 3

Barber, R.C., Bishop, R.L., Cambey, L.A., Duckworth, H.E., Macdougall, J.D., McLatchie, W. Ormrod, J.H. and van Rookhuyzen, P. (1964), Proc. 2nd Int. Conf. Nuclidic Masses (W.H. Johnson, Ed.) Springer Verlag, Vienna, p.393

Barber, R.C., Meredith, J.O., Bishop, R.L., Duckworth, H.E., Kettner, M.E. and van Rookhuyzen, P. (1968) Proc. 3rd Int. Conf. on Atomic Masses, University of Manitoba Press, p.717

Barber, R.C., Bishop, R.L., Duckworth, H.E., Meredith, J.O., Southon, F.C.G., van Rookhuysen, P. and Williams, P. (1971) Rev. Sci. Instrum. 42, 1

Benson, J.L. and Johnson, W.H. Jr. (1966) Phys. Rev. 141, 1112

Bishop, R.L. (1969) Ph.D. Thesis, University of Manitoba

Bishop, R.L. and Barber, R.C. (1970) Rev. Sci. Instrum. 41, 370

Enge, H.A. (1959) Rev. Sci. Instrum. 30, 248

Finkelstein, A.T. (1962) referred to by M. von Ardenne, Tabellen zur Angewandten Physik, (VEB Deutscher Verlag der Wissenschaften, Berlin 1962) Vol. 1, p.646

Herzog, R. (1935) Z. Phys. 97, 596

Hintenberger, H. and Konig, L.A. (1959) Advances in Mass Spectrometry (Pergamon Press, London, 1959) p.16

Macdougall, J.D., McLatchie, W., Whineray, S. and Duckworth, H.E. (1966) Z. Naturforschg. 21a, 63

Southon, F.C.G. (1971) Ph.D. Thesis, University of Manitoba

Figure 3-1

Geometry of Manitoba II

FIGURE 3 - 1

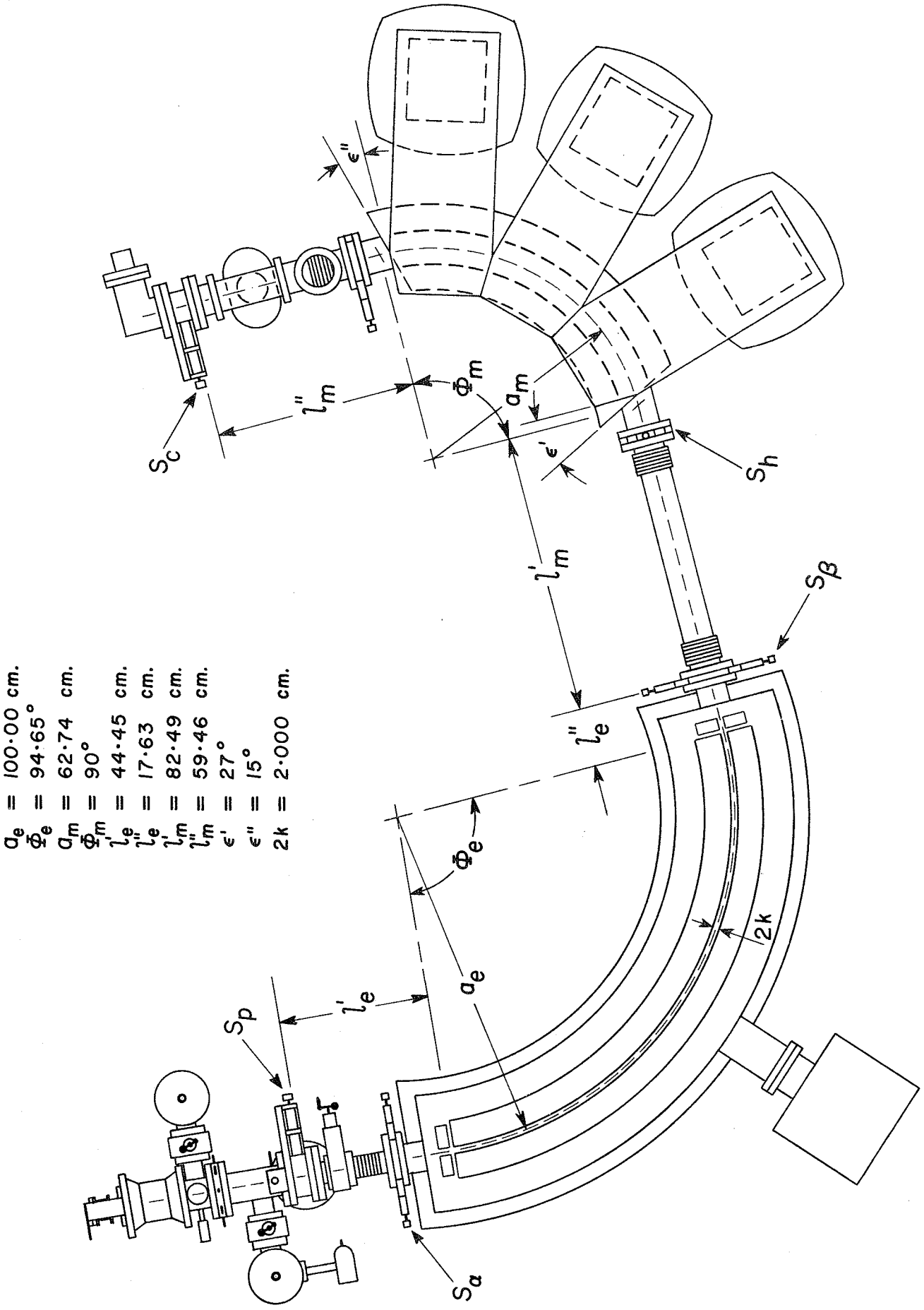
a_e = 100·00 cm.
Φ_e = 94·65°
a_m = 62·74 cm.
Φ_m = 90°
l'_e = 44·45 cm.
l''_e = 17·63 cm.
l'_m = 82·49 cm.
l''_m = 59·46 cm.
ϵ' = 27°
ϵ'' = 15°
2k = 2·000 cm.
S_c
S_h
S_β
S_p
S_a
l''_m
l'_m
Φ_m
a_m
ϵ'
ϵ''
l''_e
Φ_e
a_e
l'_e
2k

Figure 3-2

Photograph of the Mass Spectrometer

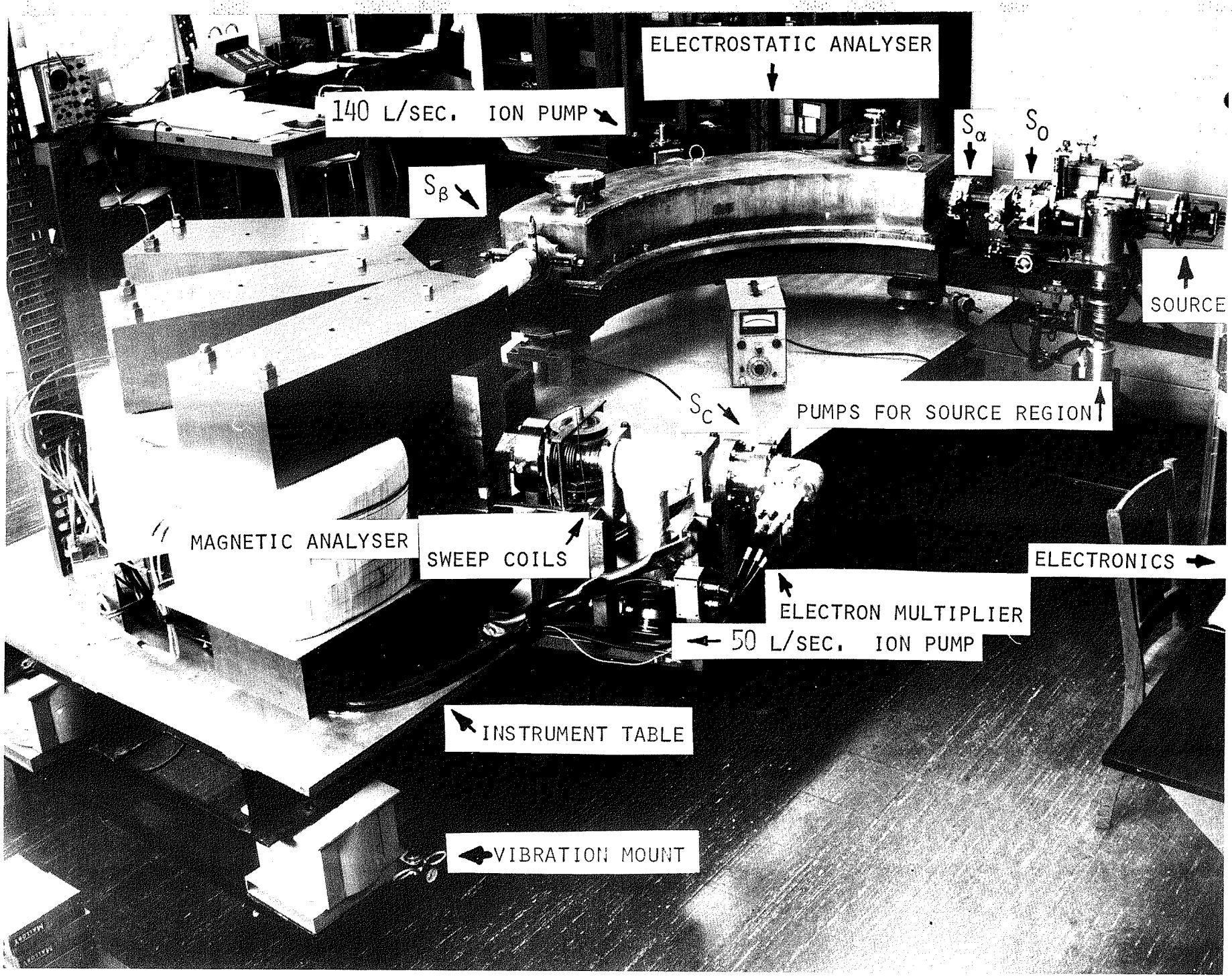
ELECTROSTATIC ANALYSER
140 L/SEC. ION PUMP
S_α
S_o
S_β
SOURCE
S_c
PUMPS FOR SOURCE REGION
MAGNETIC ANALYSER
SWEEP COILS
ELECTRONICS
ELECTRON MULTIPLIER
50 L/SEC. ION PUMP
INSTRUMENT TABLE
VIBRATION MOUNT

FIGURE 3 - 2

Figure 3-3

The Ion Source

Figure 3-4

Block Diagram for the Control Circuitry

FIGURE 3 - 3

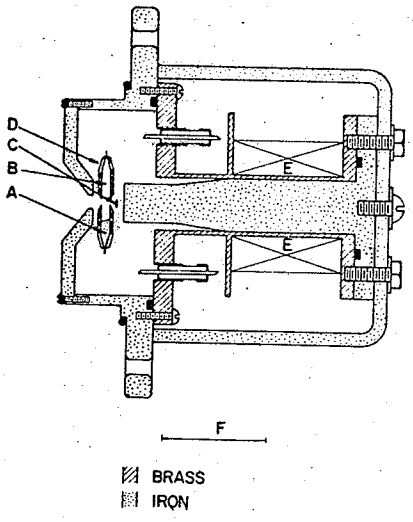

Ion source. A—Sample; B—oven; C—Re filament (coated with LaB_6); D—ribbon heater and BN insulation; E—Cu windings for electromagnet; F—5 cm.

FIGURE 3 - 4

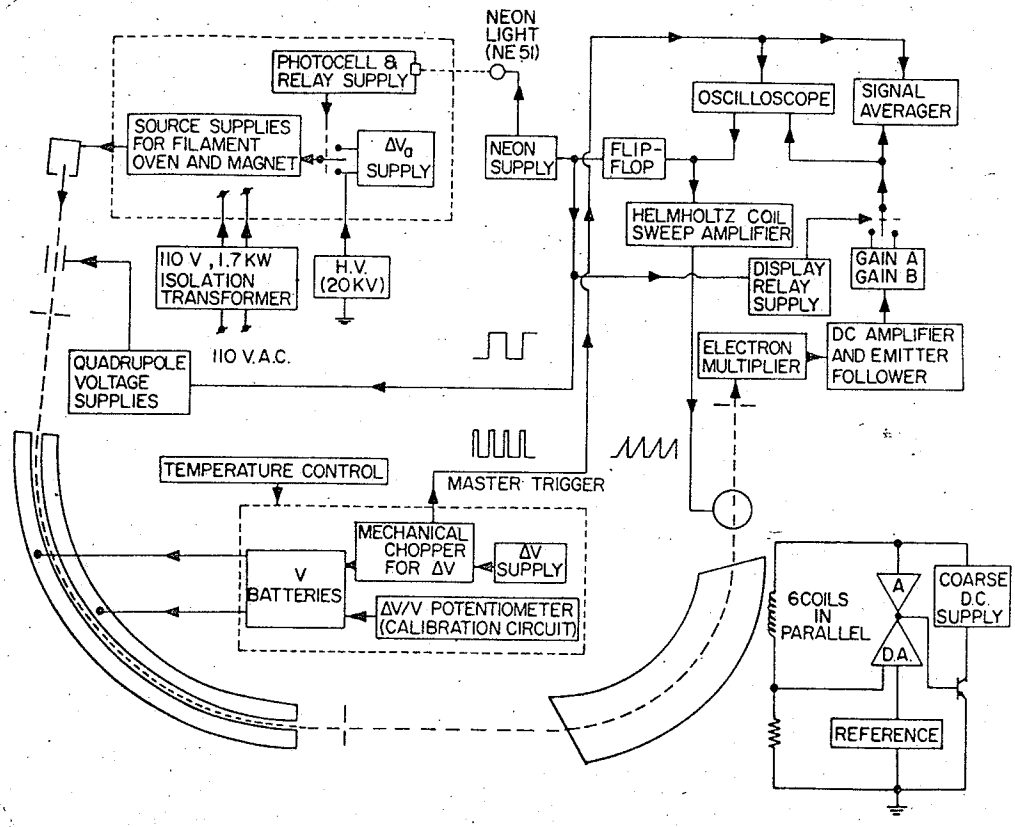

doublets where the precision was worse than $5/10^9$, the intensity of the peaks was below the average intensity for rare earth chlorides. In all cases, the precision was not limited by the potentiometer used to determine $\Delta V/V$.

The highest resolving power obtained to date has been $\sim$200 000 measured at the base of the peaks, and involved the intense peaks in the $CdCl_2$ spectrum. The low intensity available for most of these rare earth doublets has made it expedient to operate at resolving powers in the range 100 000–150 000.

ACKNOWLEDGMENTS

The advice of J. A. Barber regarding some of the structural problems in the design of this instrument is gratefully acknowledged. During the design and initial construction stages, T. H. Bryden and H. Howell of McMaster University made valuable contributions of advice and skill that are greatly appreciated. We are also grateful to R. H. Batten for technical assistance in the later work at the University of Manitoba and to M. E. Kettner and B. G. Hogg for their support in the early stages of construction.

* This work has been supported by the National Research Council of Canada.

† Holder of a National Research Council of Canada Studentship, 1966–67 and on leave 1966–69 from Acadia University, Wolfville, Nova Scotia, Canada.

‡ Now with TRIUMF Project; c/o University of British Columbia, Vancouver, Canada.

[1] R. Herzog, Z. Physik **89**, 447 (1934).
[2] A. O. Nier and T. R. Roberts, Phys. Rev. **81**, 507 (1951).
[3] E. G. Johnson and A. O. Nier, Phys. Rev. **91**, 10 (1953).
[4] F. Everling, H. Hintenberger, L. A. König, J. Mattauch, W. Müller-Warmuth, and H. Wende, *Nuclear Masses and Their Determination* (Pergamon, London, 1957), p. 221.
[5] T. L. Collins and K. T. Bainbridge, *Nuclear Masses and Their Determination* (Pergamon, London, 1957), p. 213.
[6] C. M. Stevens, J. Terandy, G. Lobell, J. Wolfe, N. Beyer, and R. Lewis, Proc. Int. Conf. Nuclidic Masses, Hamilton, Ont., 1960 401 (1960).
[7] H. Hintenberger and L. A. König, Advan. Mass Spectrometry, Proc. Conf. Univ. London, 1958, **1**, 16 (1959).
[8] H. Matsuda, Mass Spectrosc. (Japan) **11**, 127 (1964).
[9] H. Matsuda, S. Fukumoto, Y. Kuroda, and M. Nojiri, Z. Naturforsch. **21a**, 25 (1966).
[10] H. Matsuda, S. Fukumoto, T. Matsuo, and M. Nojiri, Z. Naturforsch. **21a**, 1304 (1966).
[11] H. Matsuda, S. Fukumoto, and T. Matsuo, Int. Conf. Mass Spectrom., Kyoto, Japan (1969).
[12] R. C. Barber, J. O. Meredith, R. L. Bishop, H. E. Duckworth, M. E. Kettner, and P. Van Rookhuyzen, *Proceedings of the Third International Conference on Atomic Masses* (Manitoba U. P., Winnipeg, 1968), p. 717.
[13] A. T. Finkelstein, as referred to by M. von Ardenne, *Tabellen zur Angewandten Physik*, (VEB Deutscher Verlag der Wissenschaften, Berlin, 1962), Vol. 1, p. 646.
[14] R. Herzog, Z. Naturforsch. **10a**, 887 (1955).
[15] R. C. Barber, Can. J. Phys. **43**, 716 (1965).
[16] D. A. Burrell and R. C. Barber (to be published).
[17] R. C. Barber, R. L. Bishop, L. A. Cambey, H. E. Duckworth, J. D. Macdougall, W. McLatchie, J. H. Ormrod, and P. Van Rookhuyzen, Proc. Int. Conf. Nuclidic Masses, 2nd Vienna, 1963, 393 (1964).
[18] W. Bleakney, Amer. Phys. Teacher **4**, 12 (1936).
[19] R. L. Bishop and R. C. Barber, Rev. Sci. Instrum. **41**, 327 (1970).
[20] H. Matsuda, S. Fukumoto and T. Matsuo, *Proceedings of the Third International Conference on Atomic Masses* (Manitoba U. P., Winnipeg 1968), p. 733.
[21] A. O. Nier, *Nuclear Masses and Their Determination* (Pergamon London, 1957), p. 185.
[22] W. McLatchie, Ph.D. thesis, McMaster University, 1966 (unpublished).
[23] K. T. Bainbridge and P. E. Moreland, Jr., Proc. Int. Conf. Nuclidic Masses, 3rd Winnipeg, 1967, 460 (1968).
[24] J. L. Benson and W. H. Johnson, Phys. Rev. **141**, 1112 (1966).
[25] J. D. Macdougall, Ph.D. thesis, McMaster University, 1966 (unpublished).
[26] R. C. Barber, R. L. Bishop, H. E. Duckworth, J. O. Meredith, F. C. G. Southon, P. Van Rookhuyzen, and P. Williams (to be published).

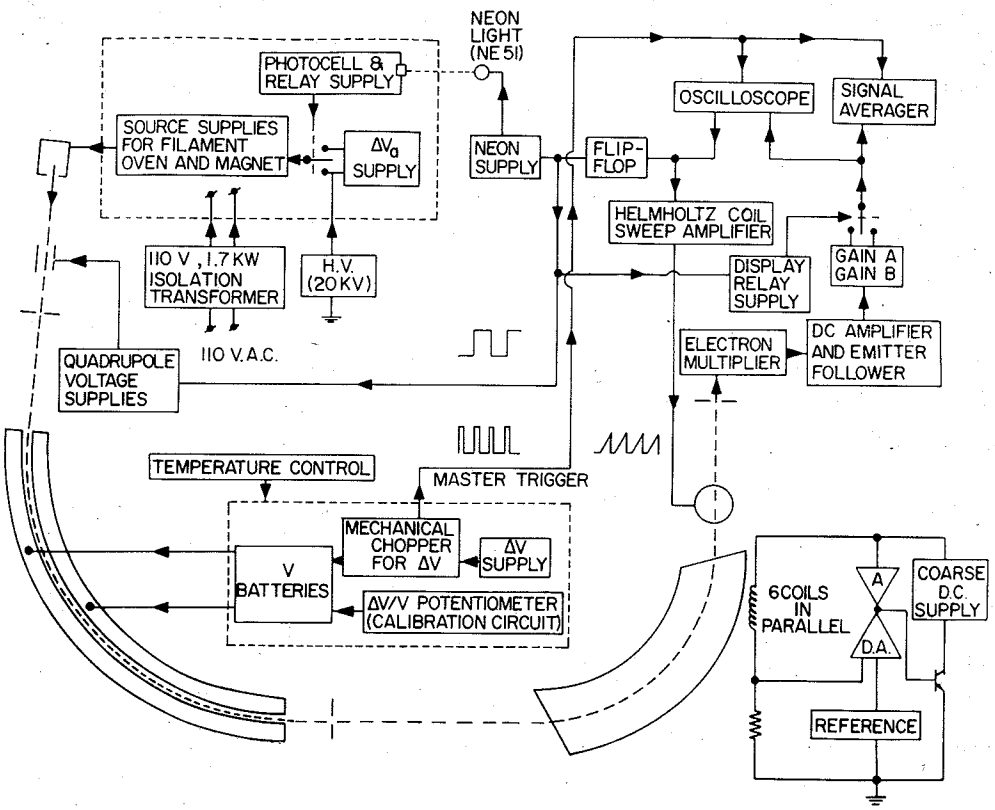

FIG. 7. Block diagram for the control circuitry.

signal whose phase indicates the appropriate adjustment to be made in ΔV to obtain a null.

The mass difference of a doublet may be determined as described above in eight different ways which are permutations of the following variables: the direction of sweeping the ion beam across the collector slit, the routing of the reference peak (M) through gain A or gain B, and the choice of reference peak (i.e., the choice whether ΔV is added to or subtracted from V). In order greatly to reduce the likelihood of systematic error in the final result, the unweighted average is taken of these eight values. Before each run, the instrument is refocused in at least a minor way. Approximately 20 such runs are taken by at least three different operators and from these values the mean and the standard deviation of the mean are calculated.

It should be noted that, when the instrument is operated as described, it is adequate to test for velocity focusing by visual observation of the live display. This means that the routine velocity focusing is actually a first order focusing. However, the signal averager permits a very sensitive method of performing the test, viz. by setting $\Delta V=0$, $\Delta V_a=22$ V, and matching a peak to itself. Such a test becomes important when a small number of runs is to be used to determine a mass difference.

II. PRECISION

In its present form, this instrument has been used to obtain values for a number of close doublets ($\Delta M/M$ $\sim 1/50\,000$) in the spectra of various rare earth chlorides. These values will be presented elsewhere.[26] The precision of this work is shown in Fig. 8 which gives a histogram of the values of $\delta M/M$ obtained for the first 12 doublets studied with the instrument as described. Here δM is the error assigned to a mass difference, and M is the mass at which it occurs. The number of runs corresponding to each value is indicated in the square representing that value. It is seen that a typical precision for these results is $\sim 5/10^9$. The best was $2.5/10^9$ and was obtained for the relatively intense doublet

$$^{169}Tb^{35}Cl_2 - ^{165}Ho^{37}Cl_2$$

on the basis of only 18 runs.

In general the precision appears to be closely related to the intensity of peaks being matched. For the seven

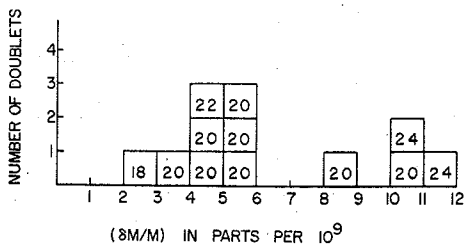

FIG. 8. Precision achieved with the mass spectrometer. This is a histogram of values of $\delta M/M$ for 12 doublets studied (δM is the error for a given determination and M is the mass at which it occurs). The number of runs for each doublet is indicated in the square representing the doublet.

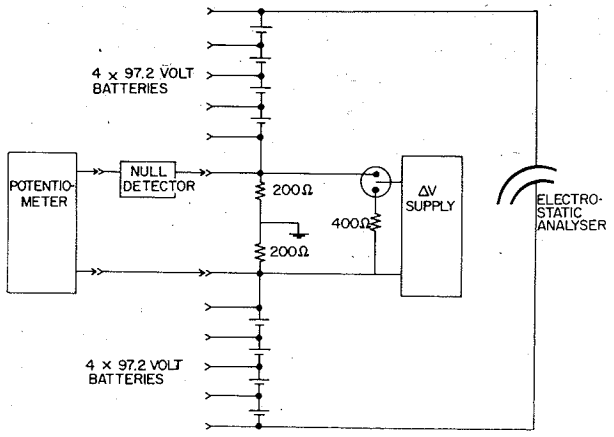

FIG. 6. Potential supply for electrostatic analyzer.

As the instrument is double focusing, the peak position is insensitive to the accelerating potential. However, strictly to satisfy Bleakney's theorem and thus to ensure that the two ion groups traverse the identical path, V_a is changed by ΔV_a in the same fashion as V. The same is true, in a strict sense, for the voltages provided to the quadrupole lens. However, for the narrow doublets studied to date, the appropriate changes in the lens voltages produce a negligible effect on the doublet separation. When the two members of a doublet are chemically identical, they are formed in the source with the same energy distribution. Thus the change ΔV_a in the voltage V_a may be calculated precisely from ΔM, M, and V_a.

When the two members of a doublet are chemically dissimilar, ΔV_a may be set and checked in the following manner. With the instrument set up for the visual peak matching of a given doublet, the ion accelerating potential is varied slowly so that the ion beam is cut off by one of the edges of the slit S_β which is located at the direction focus of the electrostatic analyzer. ΔV_a is adjusted so that the two members of the doublet disappear simultaneously. In this test, a deviation of ~ 1 eV in energy from the value required by Bleakney's theorem may be readily detected.

The potential supply for the electrostatic analyzer is shown in Fig. 6. V is provided by eight 97.2 V mercury reference batteries (Eveready E 302 462) while ΔV is presented to the chopper and the resulting square wave is applied across the two 200 Ω resistors. A precision potentiometer, described by Bishop and Barber,[19] is then used to determine both V and ΔV relative to the same standard.

The power supply for this traveling potentiometer has as its reference an additional 97.2 V mercury battery which is identical to the others and is located in the same temperature controlled box. Thus, although the absolute values of the potentials of the mercury batteries may change, the measured values are very stable, and the precision to which $\Delta V/V$ can be determined depends on the calibration of the divider chain in the potentiometer.

Although this technique is basically similar to one used previously in our laboratory[17] and more recently by Matsuda *et al.*,[20] the precision attained with this new potentiometer is significantly better. This method also differs from that of Nier[21] and McLatchie[22] and that of Bainbridge and Moreland.[23] For both latter arrangements, V and ΔV are supplied by a battery driven resistor chain. In Nier's circuit, the resistor chain is a π network and $\Delta V/V$ is determined from a calibration of the resistances. The circuit of Bainbridge and Moreland consists of a series chain of 22 resistors and two voltage dividers. The measurement of $\Delta V/V$ can be carried out either by the calibration of the resistances or by measuring voltages by a traveling potentiometer.

The present arrangement offers certain advantages over these other networks. Since there is no current drain from the batteries, relatively low capacity batteries may be used and the problem of drift in the value of V is absent. Secondly, the impedance between the analyzer plates and ground is low so that problems of pickup and of ion currents arriving at the analyzer plates are much reduced.

The mechanical chopper which switches ΔV on and off also includes a switch used to supply a master trigger pulse at a repetition rate of ~ 19 cps (Figs. 6 and 7). This pulse is used as the external trigger for the display oscilloscope and the Fabri-Tek 1024 channel signal averager (FT1052).

The output of the electron multiplier is amplified and applied to the display oscilloscope and to the signal averager. The sawtooth voltage from the oscilloscope is amplified in order to drive the Helmholtz coils which modulate the beam position. The differentiated sawtooth triggers a flipflop which (a) switches the electron multiplier information through gain A or gain B, (b) switches the neon light on or off subsequently to switch V_a, and (c) switches the voltages applied to the quadrupole lenses.

The signal averager effectively divides the trace into 1024 intervals, integrates the voltage over each time interval, and stores a number from -64 to $+64$ proportional to the integrated voltage in the corresponding memory location. Successive traces are added in order to improve the signal-to-noise ratio. The memory contents are continuously displayed on a second oscilloscope.

The application of the signal averager to peak matching follows closely the work of Benson and Johnson[24] and that of Macdougall.[25] A circuit, incorporated in the averager, switches between add and subtract modes on successive sweeps. A peak for mass M is added to the memory on odd numbered sweeps while a peak for mass M' is subtracted on even numbered sweeps. Thus, when the peak heights are made equal by gains A and B, and the peaks appear at the same stage of the oscilloscope trace a null signal results. A slight mismatch results in an S-shaped error

In particular the effect on the focusing of a nonuniform magnetic field was studied.

For ions traveling in the median plane of the magnetic field, it was found that, while the individual widths of the velocity focus ($a_m B_{22}\beta^2$) and direction focus ($a_m B_{11}\alpha^2$) would not be altered by small radial or azimuthal variations in the field, their positions would be shifted differentially so that a double focus would not be formed. In this case, of course, B_{12} would no longer be zero. A suitable small correction could be made so that the two foci would again coincide, although not necessarily at the theoretical position for the double focus, and B_{12} would be virtually zero.

Thus the calculations suggested that it would be sufficient to adjust the instrument to obtain a first order double focus. Because the second order aberrations are relatively insensitive to geometry we should then obtain a second order focus as well.

The calculations have recently been extended[16] to study the effect produced by the actual magnetic fringing field on the double focus. This work indicates that, in general, the effect is similar to the case of the nonuniform field described above, although there may also be a small deterioration in the second-order focusing properties.

The general procedure and tests for focusing are similar to those used in focusing the 2.74 m radius mass spectrometer formerly at McMaster University.[17] To check the velocity focus, the ion energy is changed by ~22 V on every second sweep of the display oscilloscope. Lack of velocity focusing results in one peak being displaced with respect to itself. The direction focus is characterized by a marked improvement in the resolution of the peaks. Additionally, the quadrupole lens may be used to vary α and thus permit a test of the direction focus.

In the initial focusing, the principal slit was positioned at its theoretical location relative to the electrostatic analyzer and the distances ($l''_e+l'_m$) and l''_m (see Fig. 1) were set at their nominal values. The electrostatic analyzer plus source arm was then adjusted relative to the magnet to correct for the fringing field.

In the subsequent routine focusing, the first half of the instrument consisting of electrostatic analyzer plus source arm is swung about the intermediate direction focus. The field necessary to bring the ions to the same point on the oscilloscope screen is a maximum for some particular angle. If the direction focus occurs at this same angle, then the direction focus of the electrostatic analyzer is being formed at the pivot axis. Invariably both the direction and velocity foci occur near this angle and a minor adjustment in l'_m (to move the direction focus) or a lateral movement of the collector (to move the velocity focus) is sufficient to achieve a double focus.

Near the double focused arrangement, a further test for the coincidence of the two foci may be made. As noted earlier, when the two foci are separated, B_{12} is of appreciable size. During the velocity focusing test described above, the angle α may be varied by means of the quadrupole lens. If, under these circumstances, the velocity focused condition is α dependent, B_{12} is large and the velocity and direction foci are not coincident.

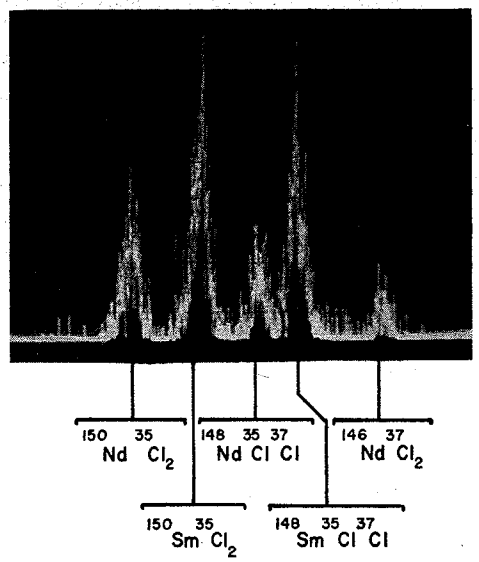

FIG. 5. Oscilloscope display of the electron multiplier output. From the left the peaks are $^{150}Nd^{35}Cl_2$, $^{150}Sm^{35}Cl_2$, $^{148}Nd^{35}Cl^{37}Cl$, $^{148}Sm^{35}Cl^{37}Cl$, and $^{146}Nd^{37}Cl_2$. The base resolving power in this case is ~ 110 000.

On the basis of the current performance of the instrument we have estimated the following upper limits for the second order focusing coefficients: $B_{11}<0.1$, $B_{12}<0.2$, and $B_{22}<0.5$. Further, it would appear that slit quality and uniformity of the deflecting fields are the limiting factors in achieving more definitive values of these coefficients.

G. Peak Matching and the Control Circuitry

The method of obtaining a mass difference is a variation of the well established peak matching technique, which in turn depends on Bleakney's theorem.[18] Let us suppose that an ion of mass M traverses a given path through the instrument in which certain fixed potentials are applied to various electrodes (V_i would be applied to the ith electrode.) Then an ion of mass M' will follow exactly the same path through the instrument if all the magnetic fields are maintained constant and all the potentials are changed according to the relation

$$MV_i=M'V'_i. \tag{2}$$

Provision is therefore made for changing the electrostatic analyzer voltage from V to $V+\Delta V$, on alternate sweeps. The magnitude of ΔV is adjusted in order to bring M' to the same stage of the oscilloscope sweep as M. ΔV is then determined. The mass difference, $\Delta M=M'-M$, is calculated from $\Delta V/V$ and M.

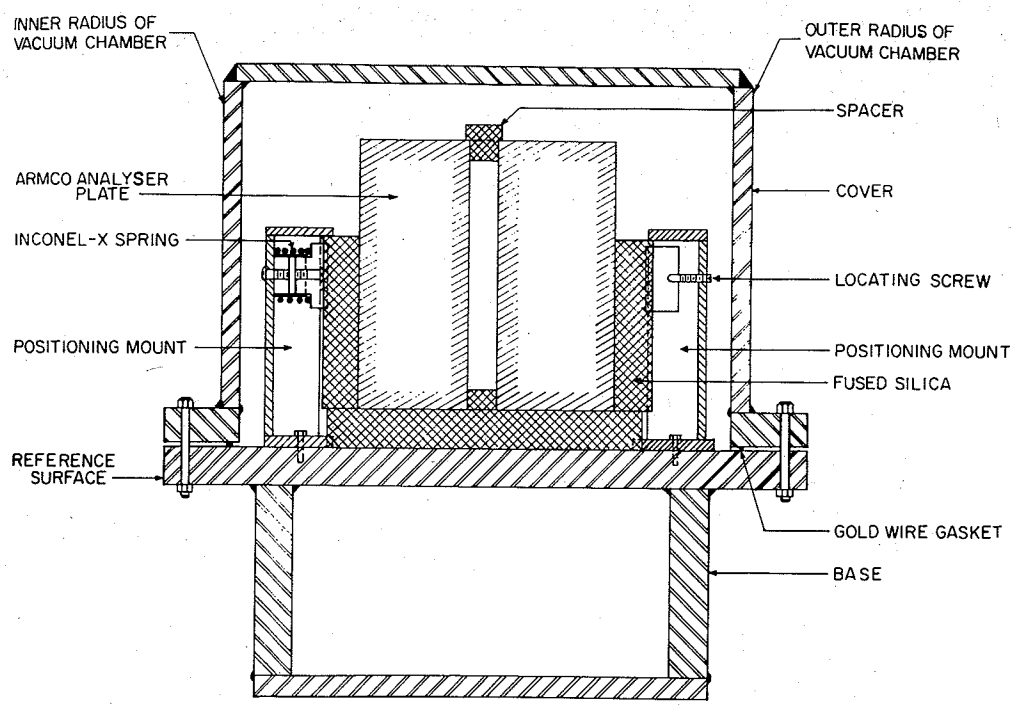

FIG. 4. Cross section of the electrostatic analyzer through one pair of the positioning mounts.

and above the pole pieces a small shimming gap has been introduced to improve the homogeneity of the field. Some adjustment of the field uniformity can be made by changing the width of the upper shimming gap. The yoke is made in three sectors with two water-cooled exciting coils on each sector. The six coils are connected in parallel electrically and in three parallel branches of two coils each for cooling.

The field can be varied over the range 3–8 kG with a typical uniformity of 1/5000 throughout the entire volume to within one gap width from the boundary of the field. Below 3 kG the inhomogeneity remains at ~0.5 G. The stability of the magnetic current supply is 1 ppm or better over a period of several minutes.

The entire instrument is mounted on a rigid table made of 150×366×2.5 cm steel plate with a grid of 20 cm I-beams welded to its lower side. This table is supported by eight pneumatic mounts which isolate the instrument from building vibrations. Each mount contains a pressure regulator and a rubber bellows which will support two tons when inflated to a pressure of 7 $kg \cdot cm^{-2}$. A cylinder of nitrogen will operate the system for over a month. In the event of a pressure failure the spectrometer table simply settles onto steel supports. The table and five of the vibration mounts are visible in Fig. 3.

As mounted, the spectrometer has a highly damped natural frequency of ~1 cps. For frequencies of about 30 cps and greater (typical of building vibrations), the isolation efficiency is better than 0.99.

E. Collector Arm

The collector arm shown in the middle of Fig. 3 is supported by a stainless steel frame attached to the spectrometer table. A second ion pump (50 liters/sec) is suspended from the collector arm and typically produces a pressure of $\sim 3\times10^{-8}$ Torr during operation of the instrument.

A pair of Helmholtz coils located between the magnet and the collector slit (Fig. 3) is driven by a sawtooth current with a repetition rate of ~19 cps. The resultant magnetic field sweeps the ion beam across the collector slit. All ions passing through the slit are detected by a high gain, low noise magnetic electron multiplier (Bendix M310). The resultant signal is amplified and viewed on the oscilloscope from which the sawtooth is derived. Figure 5 is a photograph of a trace in which five peaks are shown. The base resolving power in this case is ~110 000.

Because of the location of the 50 liter/sec ion pump, it contributes a noise current of $\sim 10^{-18}$ A in the electron multiplier which can be objectionable when peaks of very low intensity are studied. In this case the pump may be switched off and the noise thereby reduced to less than 10^{-19} A.

F. Focusing Procedure

Prior to the start of construction the focusing properties of this instrument were investigated in some detail.[15]

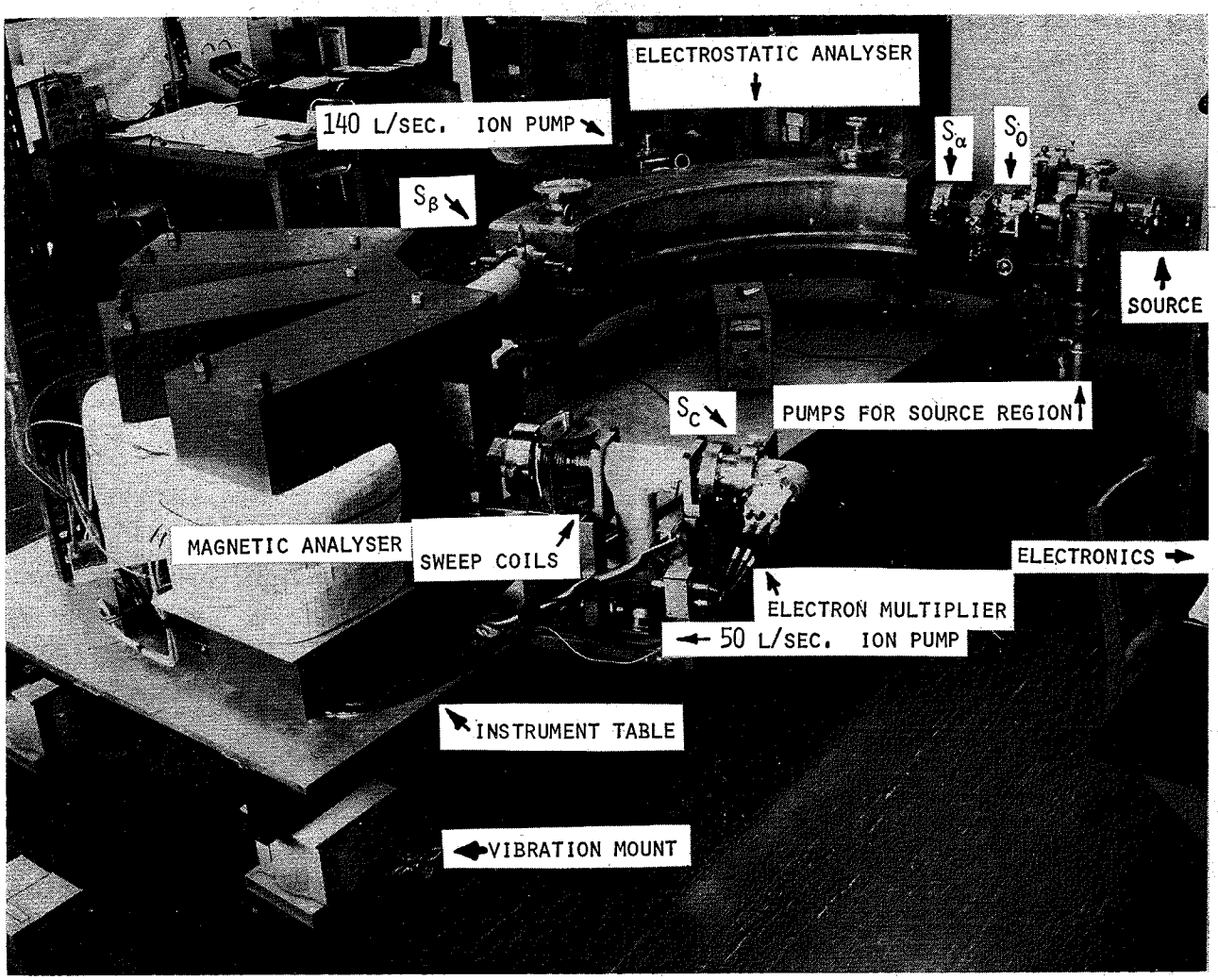

FIG. 3. The mass spectrometer.

Further details of the construction of the analyzer are shown in Fig. 4 which is a cross sectional view through one of the five positioning assemblies. The analyzer plates, which are made of gold plated Armco iron, are supported by fused silica blocks which, in turn, rest on the analyzer base. The size of the gap is determined at each assembly by a pair of cylindrical fused silica spacers. The position of the plates relative to the reference surface may be adjusted by means of the locating screws on each of the outer mounts. The inner mounts have an Inconel-X spring arrangement which presses the entire assembly together and against the outer positioning mounts. In this arrangement, the total variation in the mean radius of the analyzer is $\sim$0.003 cm (with respect to the reference surface). The total variation in the gap is $\sim$0.001 cm over the entire area of the plates and much less in the more limited region through which the ion beam actually travels. This results primarily from differences in spacers (ground to 2.0000 $\pm$0.0003 cm) and variations arising in the grinding and electroplating of the plates.

The cover and base of the electrostatic analyzer are made of 304 stainless steel. The vacuum seal between cover and base is made with a 1 mm diam gold wire gasket. The pressure measured by the 140 liter/sec ion pump is $\sim 5\times 10^{-8}$ Torr when the valve between the source and the electrostatic analyzer is open.

The electrostatic analyzer and source arm are supported on three ball bearings located approximately at the entrance and exit boundaries of the electrostatic field, and at the intersection of the tangents to the ion paths at these points. A pivot is located directly below the direction focus of the electrostatic analyzer. Thus, the first half of the instrument, consisting of electrostatic analyzer plus source arm, may be rotated as a unit about this pivot during focusing.

D. Magnetic Analyzer

Each of the pole pieces of the magnet (shown at left in Fig. 3) is a single block of Armco iron. The gap between them is established by 2.540 cm Inconel spacers. Below

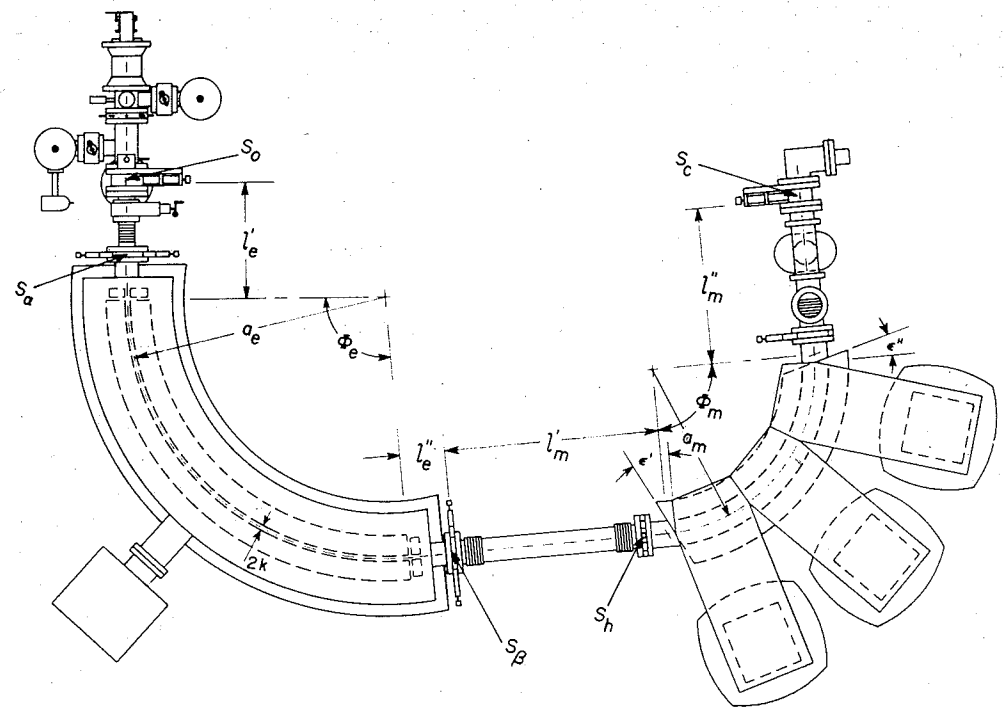

FIG. 1. Geometry of the mass spectrometer: $a_e=100.00$ cm; $\Phi_e=94.65°$; $a_m=62.74$ cm; $\Phi_m=90°$; $l'_e=44.45$ cm; $l''_e=17.63$ cm; $l'_m=82.49$ cm; $l''_m=59.46$ cm; $\epsilon'=27°$; $\epsilon''=15°$; $2k=2.000$ cm.

The object slit S_0 is variable in width and orientation, as is the collector slit S_c. For a resolving power of 200 000 at the base of the peaks and with the image width equal to the width of S_c, S_0 is 2.7 μ width. The maximum value of α is $\pm 10^{-2}$ rad, although S_α is usually set to limit α to $\pm 2\times 10^{-3}$ rad. S_β is typically set to correspond to $\beta=\pm 8\times 10^{-4}$. The height of the beam is limited normally to $\sim$ 2 mm to ensure that all ions reaching the detector have experienced the same magnetic field.

B. The Source

The ion source, shown in Fig. 2, is a variation of the Finkelstein[13] source. The oven is made of tantalum, coated with boron nitride insulation, and wrapped with a rhenium heating filament. The electromagnet is excited by the coil E so that there is, in the central region of the oven, a magnetic field of $\sim$1 kG directed parallel to the axis of the source. The ion accelerating potential V_a ($\sim$20 kV) is applied to the oven. The filament is 50–500 V, and the brass and iron parts of the source housing are 100–500 V, negative with respect to the oven. Thus, electrons are emitted from the filament and are constrained to follow a path along the axis of the source, passing through the hole in the back of the oven and then oscillating back and forth. Within the oven a plasma is formed from which ions are extracted through the front hole.

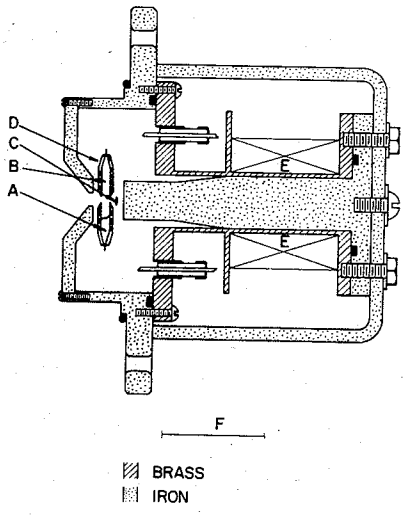

FIG. 2. Ion source. A—Sample; B—oven; C—Re filament (coated with LaB_6); D—ribbon heater and BN insulation; E—Cu windings for electromagnet; F—5 cm.

For total electron emission currents of 5 to 100 mA, ion currents from 0.5 to 25 μA have been obtained with an energy spread of less than 2 eV. In the work done to date, the samples have been solids ($CdCl_2$ or rare earth chlorides) which are vaporized in the oven.

The source arm is shown in the upper right corner of Fig. 3, which gives a view of the entire instrument. The ion beam is centered and focused on the principal slit by means of an electrostatic quadrupole lens. The position of the slit S_0 relative to the electrostatic analyzer can be adjusted by a rotary table mounted on the I-beam support which, in turn, is bolted to the electrostatic analyzer base.

C. Electrostatic Analyzer

The electrostatic analyzer is a cylindrical condenser of mean radius $a_e=1$ m and sector angle $\phi_e=94.65°$, as indicated in Fig. 1. The analyzer gap is 2 cm and the field is terminated at the physical boundaries by blocks positioned according to Herzog's theory.[14]

Reprinted from THE REVIEW OF SCIENTIFIC INSTRUMENTS, Vol. 42, No. 1, 1-8, January 1971
Printed in U. S. A.

A High Resolution Mass Spectrometer for Atomic Mass Determinations*

R. C. BARBER, R. L. BISHOP,† H. E. DUCKWORTH, J. O. MEREDITH,
F. C. G. SOUTHON, P. VAN ROOKHUYZEN,‡ AND P. WILLIAMS
Department of Physics, University of Manitoba, Winnipeg, Canada
(Received 10 August 1970; and in final form, 24 September 1970)

A high resolution, second-order double-focusing mass spectrometer has been constructed for the precise determination of atomic mass differences. The instrument has a mean radius of curvature in the electrostatic analyzer of 1 m and has operated with a resolving power at the base of the peaks of ~200 000. Details of current operation are given. The best precision achieved to date is 2.5×10^{-9}, corresponding to ~250 eV at $M=100$ amu; typical precision is $\sim5\times10^{-9}$.

INTRODUCTION

HIGH resolution mass spectrometers which are used for the precise determination of atomic masses are normally deflection instruments consisting of electric and magnetic fields in tandem. For this type of arrangement, ions emerging from an object slit of zero width with half angular divergence α and velocity $v=v_0(1+\beta)$ will fall a perpendicular distance

$$y_B=a_m\{B_1\alpha+B_2\beta+B_{11}\alpha^2+B_{12}\alpha\beta+B_{22}\beta^2\} \quad (1)$$

from the optic axis after traversing the two fields. The coefficients depend upon the distance l''_m traveled from the magnetic field boundary.

The well known theory of Herzog[1] allows field arrangements to be chosen for which $B_1=B_2=0$ (for a particular l''_m), thus providing first order double focusing. Subsequently several instruments which additionally provide $B_{11}=0$ were designed and built.[2-6] Finally, in 1959, Hintenberger and König[7] reported an extensive study of the second order focusing properties of such fields and proposed a number of arrangements which provide complete second-order double focusing ($B_{11}=B_{12}=B_{22}=0$).

In 1963, when planning of the present instrument was begun, no high resolution mass spectrometer possessed complete second-order double focusing. Since then, Matsuda *et al.*[8-10] have described a novel high resolution mass spectrometer which theoretically achieves this objective. In practice, however, the measured second-order coefficients differ significantly from zero.[11]

Although a brief preliminary description of the design and construction of the new Manitoba mass spectrometer has been given elsewhere[12] we here present further details together with information concerning its performance.

I. THE MASS SPECTROMETER

A. Geometry

Of the many instruments proposed by Hintenberger and König,[7] the geometry chosen for our purpose has deflection in the same sense in both electric and magnetic fields plus straight magnetic field boundaries. The advantages in choosing this arrangement, shown in Fig. 1, are the following.

(1) An intermediate direction focus is formed (at l''_e) by the electrostatic analyzer. This permits the use of the electrostatic analyzer as an energy analyzer capable of resolving ~ 1 eV.

(2) The total ion path is reasonably short compared to the mean radius of curvature in the electrostatic analyzer, a_e. The individual lengths $l'_{e'}$ $l''_{e'}$ l'_m, and l''_m are also relatively short so that problems due to mechanical vibration and stray magnetic fields are minimized.

(3) It is not necessary for the ion beam to cross a curved magnetic field boundary at a prescribed angle.

The scale of the mass spectrometer was determined by choosing $a_e=1$ m. The total length of the ion path is 4.59 m and the over-all magnification is 0.50. The values of the other geometric parameters are given in Fig. 1.

*Work supported by the National Research Council of nada, and until 1965 by the Air Force Office of Scitific Research, U. S. Air Force.

†Now at the Department of Physics, University of anitoba, Winnipeg, Man., Canada.

‡Now with TRIUMF project, c/o University of Brith Columbia, Vancouver, B. C., Canada.

§Now with Sprague Electric Company, North Adams, ass.

‖Now at the Department of Physics, Queen's Univerty, Kingston, Ont., Canada.

**Now at the Australian National University, Canber-, Australia.

††On leave 1966-1969 from Acadia University, Wolfle, N. S., Canada.

‡‡On leave 1966-1967 from Brandon College, Bran-n, Man., Canada.

[1]R. C. Barber, H. E. Duckworth, B. G. Hogg, J. D. acdougall, W. McLatchie, and P. Van Rookhuyzen, ys. Rev. Letters 12, 597 (1964).

[2]H. E. Duckworth, R. C. Barber, B. G. Hogg, J. D. acdougall, W. McLatchie, and P. Van Rookhuyzen, in ongrès International de Physique Nucléaire, edited by Gugenberger (Centre National de la Recherche Scitifique, Paris, France, 1964), Vol. II, p. 557.

[3]J. D. Macdougall, W. McLatchie, S. Whineray, and E. Duckworth, Z. Naturforsch. 21a, 63 (1966).

[4]R. C. Barber, R. L. Bishop, L. A. Cambey, H. E. Duckworth, J. D. Macdougall, W. McLatchie, J. H. Ormrod, and P. Van Rookhuyzen, in Proceedings of the Second International Conference on Nuclidic Masses (Springer Verlag, Berlin, Germany, 1964), p. 393.

[5]R. C. Barber, J. O. Meredith, R. L. Bishop, H. E. Duckworth, M. E. Kettner, and P. Van Rookhuyzen, in Proceedings of the Third International Conference on Atomic Masses (University of Manitoba Press, Winnipeg, Man., Canada, 1968), p. 717.

[6]J. L. Benson and W. H. Johnson, Phys. Rev. 141, 1112 (1966).

[7]J. W. Dewdney and K. T. Bainbridge, Phys. Rev. 138, B540 (1965).

[8]J. H. E. Mattauch, W. Thiele, and A. H. Wapstra, Nucl. Phys. 67, 1 (1965).

[9]W. H. Johnson, Jr., and A. O. C. Nier, Phys. Rev. 105, 1014 (1957).

[10]R. A. Damerow, R. R. Ries, and W. H. Johnson, Jr., Phys. Rev. 132, 1673 (1963).

[11]R. L. Bishop, R. C. Barber, W. McLatchie, J. D. Macdougall, P. Van Rookhuyzen, and H. E. Duckworth, Can. J. Phys. 41, 1532 (1963).

[12]S. G. Nilsson and O. Prior, Kgl. Danske Videnskab. Selskab, Mat.-Fys. Medd. 32, No. 16 (1961).

[13]W. H. Johnson, Jr., and V. B. Bhanot, Phys. Rev. 107, 1669 (1957).

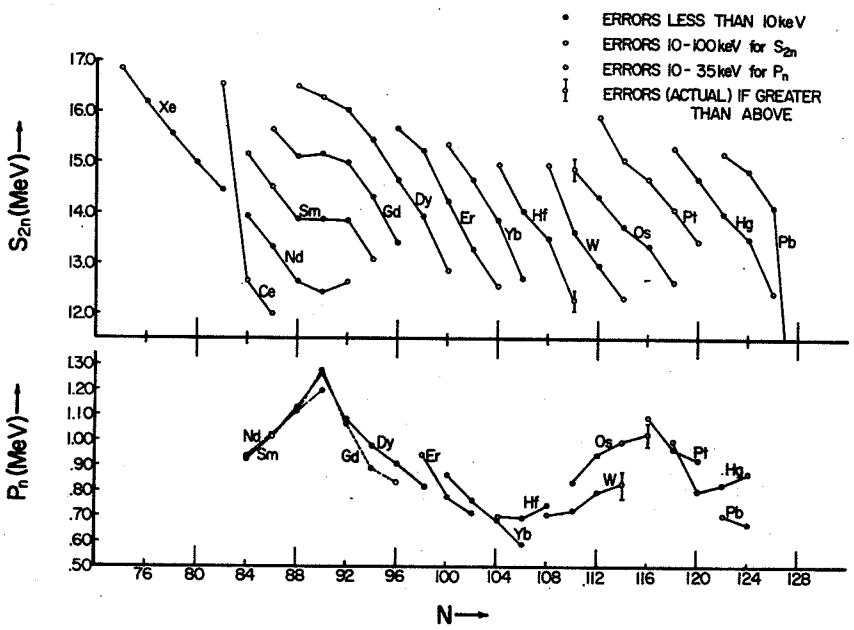

FIG. 1. Plot of double-neutron separation energy (S_{2n}) and of neutron-pairing energy (P_n), both as functions of neutron number. Data are for isotopes of the even-Z elements in the region $82 \lesssim N \lesssim 126$.

(b) The energy of deformation exhibited by nuclides with $N = 90$ is least for $Z = 60$ (Nd) and shows a small but steady increase in going to $Z = 62$ (Sm) and $Z = 64$ (Dy). The relatively high value of S_{2n} at ^{154}Dy ($N = 88$, $Z = 66$) may suggest that this nuclide has already acquired a small ground-state deformation. But in going from $N = 90$ to $N = 92$, although there is also a Z dependence, the incremental effect is greatest for $Z = 60$ (Nd).

(c) When viewed over a range of two neutrons the segments of adjacent curves are usually parallel to one another, that is, irregularities are reproduced for the same neutron numbers.

(d) The most conspicuous irregularities lie in the region $106 \leq N \leq 110$.

(e) Below $N \sim 106$ the shape of the curves (which are strikingly different from the "regular" curves referred to earlier) indicates that for certain elements the mass effect associated with deformation continues well beyond 92, but at a more gradual rate.

(f) The curves above $N \sim 110$ do not individually reveal the disapperance of deformation, rather, this disappearance is indicated by the large separations between the curves for $Z = 74$ (W), $Z = 76$ (Os), and $Z = 78$ (Pt).

In the lower portion of Fig. 1 is a plot of neutron-pairing energies for the majority of nuclides represented in the upper portion, calculated according to the relationship[12]

$$P_n(N) = (-1)^N \tfrac{1}{4}[2S_N(N) - S_n(N-1) - S_n(N+1)]. \quad (3)$$

These pairing-energy curves are a refinement and an extension of the pioneer work of Johnson and Nier[9] and Johnson and Bhanot[13] who drew attention to maxima in the region of 90 and 116 neutrons. With reference to the lower portion of Fig. 1, attention is now drawn to the following specific features:

(g) At $N = 90$ the neutron-pairing energies show a definite maximum for $Z = 62$ (Sm) and $Z = 64$ (Gd), a probable maximum for $Z = 60$ (Nd), and a possible maximum for $Z = 66$ (Dy). The greatest effect appears to occur at $Z = 62$ (Sm) and $Z = 64$ (Gd).

(h) A second maximum in the neutron-pairing energy appears to occur at $N = 116$, although the curve for no element actually passes through the maximum. But the curves for $Z = 76$ (Os) and $Z = 78$ (Pt) suggest the existence of this maximum, and those for $Z = 74$ (W) and $Z = 80$ (Hg) are not inconsistent with this hypothesis.

(i) Between these two maxima, the neutron-pairing energy appears to decline steadily to a minimum in the region $106 \leq N \leq 108$. This is undoubtedly related to the transition region referred to in comments (d), (e), and (f) above.

(j) The pairing energies for $Z = 80$ (Hg) and $Z = 82$ (Pb) appear not to follow the same trend as they approach the 126-neutron shell.

We are indebted to a number of individuals for prepublication information, and appropriate acknowledgement for this will be made in the subsequent detailed papers.

NEUTRON SEPARATION AND PAIRING ENERGIES IN THE REGION $82 \leq N \leq 126$*

H. E. Duckworth,† R. C. Barber,† and P. Van Rookhuysen‡
Department of Physics, McMaster University, Hamilton, Ontario, Canada,
and Department of Physics, University of Manitoba, Winnipeg, Manitoba, Canada

and

J. D. Macdougall,§ W. McLatchie,‖ and S. Whineray**
Department of Physics, McMaster University, Hamilton, Ontario, Canada

and

R. L. Bishop,†† J. O. Meredith, P. Williams, G. Southon, W. Wong,‡‡ B. G. Hogg, and M. E. Kettner
Department of Physics, University of Manitoba, Winnipeg, Manitoba, Canada

(Received 31 July 1969)

Results of a systematic study of atomic-mass differences in the region $82 \leq N \leq 126$ are presented as plots of double-neutron separation energy and neutron-pairing energy. These plots provide information concerning the extent of the nuclear deformation which begins in the region of 90 neutrons, its dependence upon Z, and its gradual dissappearance in the region $106 \lesssim N \lesssim 116$.

In 1964[1,2] and 1965[3] some of us reported a series of precise atomic-mass differences in the region $N \sim 90$, which provided accurate information concerning the mass effect associated with the onset of nuclear deformation in that region. We have since extended this work substantially, using improved techniques and employing both the original high-resolution mass spectrometer[4] and a newly constructed one,[5] and can now provide a fairly complete picture of the mass surface between the 82- and 126-neutron shells. The details of this work, including the major comments on its interpretation, will be reported in due course in a series of papers, but the overall picture is sufficiently informative to warrant its prior presentation.

As in earlier work, most of the mass differences have been obtained by studying doublets of the type

$$\Delta M = {}^{A}X_1{}^{35}\mathrm{Cl} - {}^{A-2}X_2{}^{37}\mathrm{Cl}, \tag{1}$$

where X_1 and X_2 may or may not be isotopes of the same element. The fractional spacing of the various doublets studied ranged from one part in 8400 to one part in 115 800. The error associated with ΔM was usually in the range 1-4 keV. Since the $^{37}\mathrm{Cl}-{}^{35}\mathrm{Cl}$ mass difference is known to 0.4 keV,[6,7] double-neutron separation energies S_{2n} can be calculated to virtually the same precision as ΔM, viz.

$$S_{2n} = 2n - ({}^{A}X_1 - {}^{A-2}X_1)$$

$$= 2n - (^{37}\mathrm{Cl} - {}^{35}\mathrm{Cl}) - \Delta M \tag{2}$$

for cases in which the doublet contains isotopes of the same element. For cases in which isotopes of different elements are involved, the available data are frequently accurate enough to introduce negligible error in the calculation of S_{2n} for the nuclides concerned.

The upper portion of Fig. 1 is a plot of S_{2n} for even-Z, even-N nuclides from $N = 74$ to $N = 126$. The many data relating to odd-Z and/or odd-N nuclides are omitted in order to avoid congestion in the figure. The values for Xe and Ce (taken from the 1965 mass table[8] which in this region is based primarily on the work of Johnson and Nier[9] and Damerow, Ries, and Johnson[10]) are included to show the characteristically "regular" shape of the curves of S_{2n} vs N in the region $50 \leq N \leq 82$,[11] and to remind the reader of the sudden decrease in S_{2n} which occurs as the 82-neutron shell is exceeded. The values for the other elements are based mainly on some 70 mass differences determined in our laboratory during the past four years. Most of these values are derived directly from Eq. (2), but a few require for their calculation the use of accurate reaction Q's or disintegration energies.

As was mentioned, some of the curves shown in the upper portion of Fig. 1 for $N \sim 90$ were published earlier, at which time attention was drawn to the major discontinuity in slope at $N = 88$, the apparent charge dependence of this effect, and the suggestion that the slopes for $N \geq 92$ are similar to those for $N < 88$. Also, the relationship between these effects and the deformation of the nucleus was commented upon. Additional points now to be noted include these:

(a) The injection of the new data has produced a marked increase in the regularity of the S_{2n} curves in the region $92 \leq N \leq 126$. One may now ascribe special significance to the irregularities that remain.

MACFARLANE (McMaster): In this respect we've started to measure some Q-values for thermal neutron (n,α) reactions in this region. And there will probably be about eight or nine cases that we'll be able to measure and this will provide some connection between elements.

DUCKWORTH: I'd like to say at the risk of delaying all of us, that we had at McMaster University before we moved to the University of Manitoba, a uniquely harmonious arrangement, and I use the word unique in its true sense because I am sure it has not existed before. We were determining these binding energies in the 90 neutron region. Ron MacFarlane was determining α-decay energies in the same region and Terry Kennett and others were doing capture γ-ray work using the new Ge(Li) techniques in the same region. And we had at the same time Preston and Sprung who were interested in calculating the binding energy of nuclear matter. I don't think ever in one laboratory, certainly not in a small laboratory, have so many people been together with common interest. And when we would have a new value we'd run upstairs to MacFarlane to see if he would have something that would compare with it. And sometimes he would run down with new values that he had. It was tremendously stimulating. In a way, it was a microcosm of what this conference represents. That was one of the great regrets that I had, and the rest of us, when we decided to move to the University of Manitoba.

Now that is purely gratuitous but it is in the spirit of the conference.

HINTENBERGER (Mainz): You now have some connections between nuclides of different elements. Can you say anything about the β-decay energy of ^{187}Re from your new measurements?

DUCKWORTH: I have it in the tabulation. Many decay energies, of course, can be calculated and my recollection is that we have re-calculated this and agree within the limits of the error with what appears in the Mass Table.

that I notice there and I was wondering whether there was any real physical significance in it. If you look at the 3 Xenon points, they seem to extend right in across the break to the Nd and the Ba seems to extend across directly to the Sm, the Ce to the Gd and, in fact, the first two Gd points seem to line up with the Sm last two points. There seems to be an identification of corresponding energy levels from Ba into Sm in some way.

DUCKWORTH: We'll hear perhaps from Zeldes in a minute, but I should think this is fortuitous. Before the 82 neutron shell, the curves are regular and they are spaced by roughly regular amounts. And then after the 82 neutron shell things adjust to reasonable regularity again and, once again, the spacings are about the same between elements as was before. So that if one had a fortuitous coincidence between Nd say and Xe, then he would have many others, because of this equality of the spacings. Perhaps Zeldes can read more meaning into this, but I think it is fortuitous.

ZELDES: I agree with that.

It would be nice to measure as much as possible doublets connecting different elements, because now after this nice work you know almost perfectly about neutron effects on shell effects, deformation effects and so on. But still the information about the protons is much worse, and you had four isolated groups or even more with no connections between them in your four slides. So it's very good if you can extend these doublets with different elements.

DUCKWORTH: Yes, we are aware that the connections between different elements are especially valuable. You will understand that they are harder to do because one has to have in the source material that will produce ions of both elements. And I think that the gap between the region I and the region II which involves Tb would have been covered if it hadn't been that the students who were working on their theses and those who were planning to move the instrument were both working to a deadline. We ran out of time last summer before the Tb connections were made. However, I don't think those are difficult, I think they'll be made soon when we resume the program, hopefully before Christmas.

DISCUSSION

ZELDES (Jerusalem): This is in connection with the proton shell effect. If you look at α-decay energies from the 1961 table (which is essentially based on Bhanot, Johnson and Nier's doublets) and from the 1964 table (which is based mainly on the Russian doublets) you see at the peak, a gap beyond Gd, and you go from Gd to Dy which shows a gap beyond 64 protons as it should be in spherical nuclides because the $g_{7/2}d_{5/2}$ shell closes there.

But then when you go to the right into the deformed region then the line of Dy is much steeper than that of Gd and the gap above Gd disappears. Now it seemed that there is a big gap beyond Dy, between Dy and Er. And in the Nilsson diagrams you can also find something above the 66 protons. But then with the newer data, the gap beyond Gd on the left exists, but when you go to the right, the gap above Dy has almost disappeared. I mean, there is something, but if you go from Er say to Yb it's more or less the same as from Dy to Er.

So I want to know if your new data can say something about the situation. I noticed you have connections within elements from 66, from Dy,to 71. So from your data you could plot the up-to-date graph and tell what happens above 66, above Dy.

DUCKWORTH (Manitoba): Your Dy curve, of course, extends very much further than the limited curve that we showed.

ZELDES: From your data and from the nuclear decay and reaction data I think you can calculate the α-decays appearing in this figure into the deformed region.

DUCKWORTH: The only analysis we've done is the plot of the double neutron separation energies, so all that I could say now would be what one could infer from that curve that was shown on the boards.

ZELDES: You have the data to calculate double proton separation energies and find out.

DUCKWORTH: Yes.

COHEN (North American Aviation): In your plot of double neutron separation energies, there is an intriguing trend

The total electrostatic analyzer voltage V is measured in two steps by a digital voltmeter and the change in voltage ΔV is determined by means of a potentiometer. When the error introduced by these instruments is added, the error in the new determination is increased to 2.3 μu.

As shown in this figure the new value is in good agreement with several values for this doublet obtained over a number of years in our laboratory using the 9' radius instrument and various measuring equipment. In particular, it should be noted that the last value was obtained with a set of equipment which, except for the enhancetron, is distinct from that used to obtain the new value.

The part of the error representing the reproducibility of the results is unfortunately, somewhat larger than we expected. We believe, however, that this reflects borderline intensity coupled with small fluctuations in peak position which were quite common during these measurements. Accordingly, an effort will be made to correct these problems before we commence the work in the upper rare earth region of the periodic table.

REFERENCES

1. H. Hintenberger and L. A. König, Advances in Mass Spectrometry (Pergamon Press, London, 1960) p. 16.
2. R. C. Barber, Can. J. Phys. 43, 716 (1965).
3. R. L. Bishop, R. C. Barber, W. McLatchie, J. D. Macdougall, P. Van Rookhuyzen and H. E. Duckworth, Can. J. Phys. 41, 1532 (1963).
4. J. D. Macdougall, W. McLatchie, S. Whineray and H. E. Duckworth, Zeits Fur Naturf. 21a, 63(1966).
5. W. McLatchie, Ph. D. Thesis McMaster University 1966.

*Work supported by the National Research Council of Canada

TABLE I - Comparison of Values for $^{114}Cd^{35}Cl$ - $^{112}Cd^{37}Cl$ Mass Difference (mu)

Mass Difference	Date	Method of Peak Matching	Measurements of $\Delta V/V$	Instrument	Reference
3.5470 ± 23	1967	visual	voltmeter/ potentiometer	1 m. radius	Present work
3.547 ± 2	1963	"	"	9' radius	3
3.546 ± 3	1966	"	"	"	4
3.547 ± 3	1966	enhancetron	"	"	4
3.548 ± 2	1966	"	resistance network	"	5

After these basic geometrical adjustments have been made, routine focusing is carried out as follows. When the electrostatic analyzer is moved about its pivot, the field necessary to bring the ions to the same stage of the oscilloscope trace is a maximum for some angle. If the direction focus occurs at this angle also, it indicates that the electrostatic analyzer is direction focusing correctly. Our experience is that the direction and velocity foci invariably occur near this angle and either a minor correction in the source position (to move the direction focus) or a lateral movement of the collector (to move the velocity focus) is sufficient to achieve a double focus.

Fig. 8 is a photograph of the live display of the triplet $^{114}Cd^{35}Cl_2$ - $^{112}Cd^{35}Cl^{37}Cl$ - $^{110}Cd^{37}Cl_2$ at mass 184. The mass difference between the two strong members is 1/52,000 so that the resolution here is about 1/160,000 at the base of the peaks.

The sum of many traces of this type as accumulated by the enhancetron is shown in Fig. 9. This picture confirms that the noise to the left of the $^{114}Cd^{35}Cl_2$ peak is random.

We have not as yet carried out a systematic investigation to measure the upper limits of B_{11}, B_{12} and B_{22}. However it appears that the present limitation to the resolution arises from the low intensity which we are able to pass through the principal slit. The maximum useable resolution achieved to date is 1/200,000 (base).

Results

As a check on the performance of the instrument we have re-determined the $^{114}Cd^{35}Cl$ - $^{112}Cd^{37}Cl$ mass difference. This was done using the peak matching technique and the enhancetron null detection system which was described earlier by Professor Duckworth.

Each run consists of 4 determinations which represent the possible permutations of adding or subtracting ΔV and sweeping the ion beam across the collector slit in both directions. The mean of these 4 values is then the value for that run. The mean which we have shown in Table I is the mean of the values for 19 runs made on 5 days of operation. The standard deviation of the results is 2.0 μu.

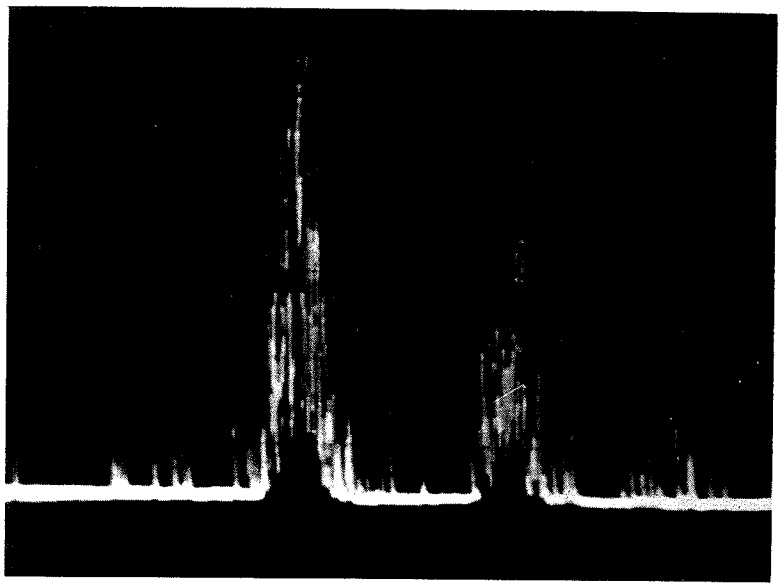

Fig.8 Live display of the triplet $^{114}Cd^{35}Cl_2$ - $^{112}Cd^{35}Cl^{37}Cl$ - $^{110}Cd^{37}Cl_2$. The mass difference between the two intense peaks is 1/52,000.

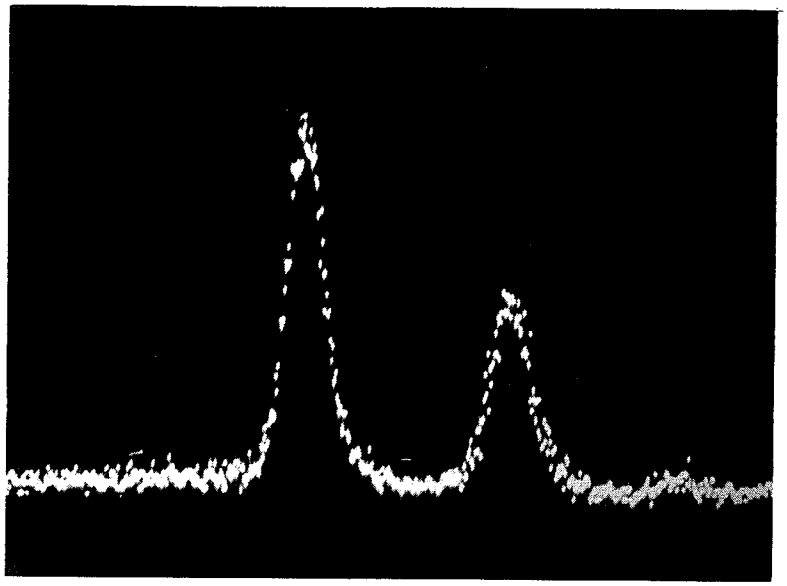

Fig.9 Contents of the digital memory after many sweeps of the display shown in Fig. 8.

amplified signal from the electron multiplier is viewed on the same oscilloscope that provides the sawtooth.

Focusing

The focusing properties of this instrument were investigated in some detail before construction began (2). In particular, the focusing was examined for the case where the instrument is set up to the designed dimensions but the magnet field is not uniform.

It was found that the individual widths of the "velocity and direction foci" are not altered although the foci may be separated and moved from the theoretical position of double focus as illustrated in Fig. 7. In this case, of course, $B_{12} \neq 0$. A suitable small correction could be made to bring the two foci together althought not necessarily at the theoretical position of double focus. In this case B_{12} was virtually zero (for $\Delta M/M = 1/500,000$) as well.

Our conclusioh from this was that it was necessary to find only the correct position for a first order double focus. Since the second-order aberrations are not extremely sensitive to geometry we would then have a second order focus as well.

The focusing procedure and the tests for focusing are similar to those used in operating the large mass spectrometer. The ion energy is changed by 22-1/2 volts on every second sweep of the oscilloscope. Lack of velocity focusing results in a peak being displaced with respect to itself. The displacement may be detected either on the live display or by using the enhancetron to match a peak with itself. The direction focus is characterized by a marked increase in the resolution of the peaks.

In the initial focusing, the principal slit was placed at its theoretical position with respect to the electrostatic analyzer The distance between the electrostatic analyzer and magnet and the distance from the magnetic field to the collector were also set. Then the entire instrument was adjusted relative to the magnet to correct for the fringing field of the magnet. This adjustment is equivalent to moving the magnet along the bisector of the angle defined by its entrance and exit boundaries.

Fig.6 Complementary view of entire instrument.

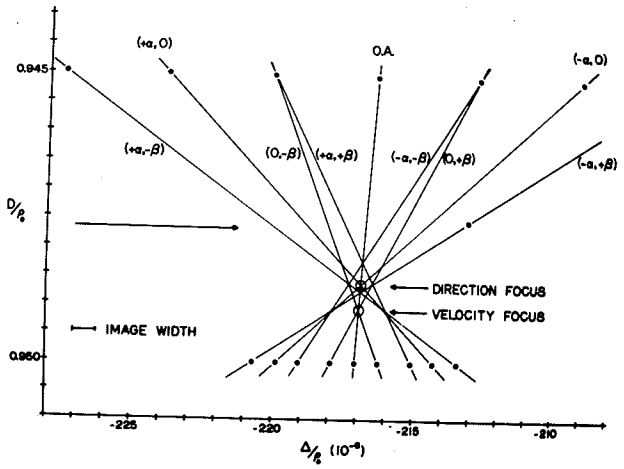

Fig.7 Calculated ion trajectories at the final image of the instrument for a non-uniform magnetic field.

inner positioning mounts.

The electrostatic field is terminated at the physical boundaries of the condenser by Herzog terminating blocks.

The analyzer cover is made of 304 stainless steel with the vacuum seal between cover and base being made with a gold wire.

The analyzer is supported by 3 ball bearings located approximately along the tangents to the ion path at the entrance and exit of the electric field. A pivot is located directly below the direction focus of the electrostatic analyzer. This arrangement allows the analyzer to be moved easily by hand during focusing.

Magnet

The pole pieces of the magnet shown in Figs. 5 and 6, are each a single block of Armco Iron and separated by 1" inconel spacers. Below and above these pole pieces a shimming gap has been introduced to improve the uniformity of the field produced. The yoke is made in three sectors with 2 exciting coils on each sector. Some adjustment of the field can be accomplished by adjusting the width of the upper shimming gap.

The typical uniformity for any field in the range 3-8 kgauss is 1/5,000 over the entire region to within about one gap width of the boundary.

The magnet coils are water-cooled and are designed for a 60 amp, 100 volt supply. A transistorized current regulator maintains the current constant to about $1/10^6$ (or better) for short term.

Figs. 5 and 6 show how the entire instrument is mounted on a rigid steel table. Should vibrations prove to be a problem when we improve the resolution, we propose to equip the legs of the table with standard spring shock mounts.

Detection

A pair of Helmholtz coils, located (Fig. 6) at the exit boundary of the magnetic field, is driven by a sawtooth current. The resulting magnetic field sweeps the ion beam across the collector slit at 30 cps. All ions passing through the collector slit are detected by a low-noise high-gain electron multiplier (Bendix, M310). The

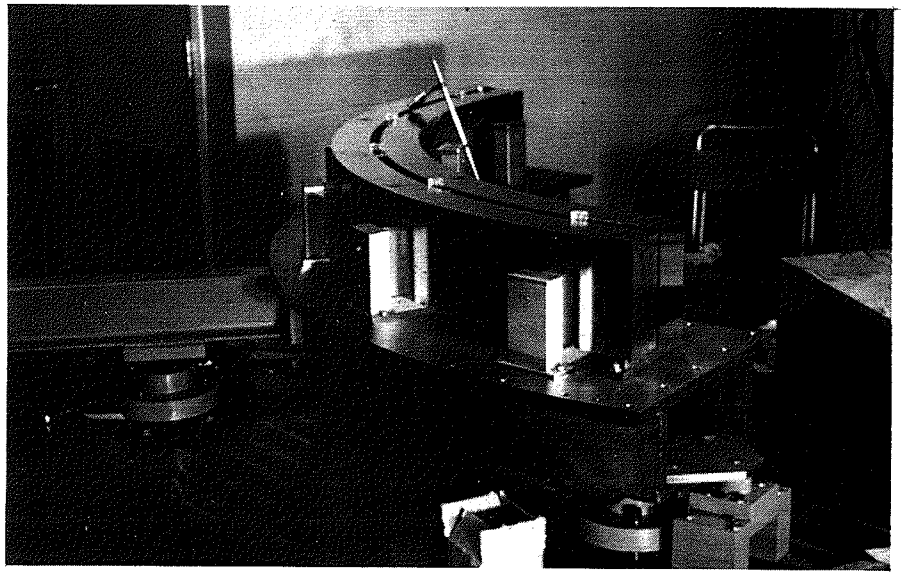

Fig.4 Interior of electrostatic analyzer.

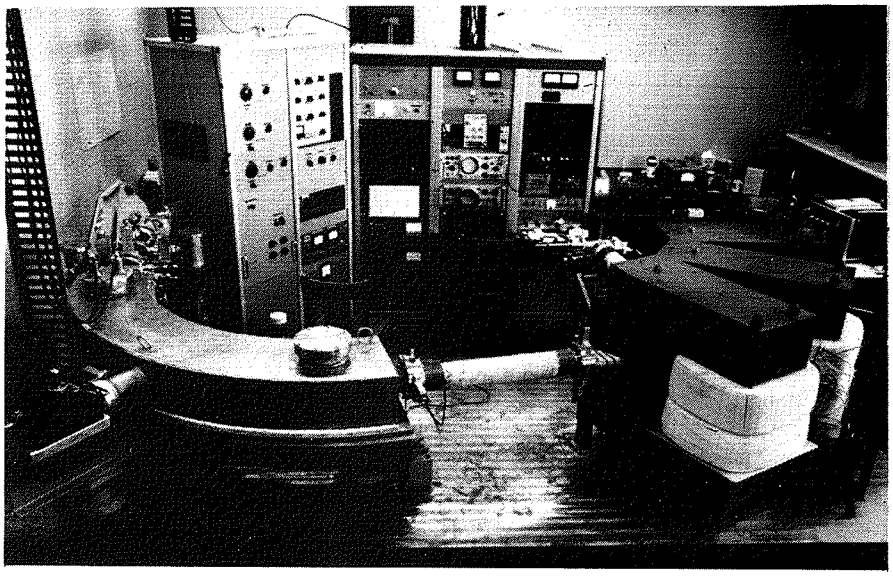

Fig.5 View of entire instrument showing control panel.

is a conventional electron bombardment source which may be fitted either with a gas leak or with a small oven mounted on the back of the repeller electrode. The source potential, ~ 20kV, is derived from a commercial supply which was modified to provide a short term variation in voltage of less than 1/20, 000. The ion beam from the source is focused on the principal slit by means of an electrostatic quadrupole lens designed to produce a line image at the principal slit and a parallel beam in the Z- direction. Beam centering is accomplished by applying small bias voltages to the quadrupole lens.

The position of the principal slit in the horizontal plane may be adjusted relative to the electrostatic analyzer by the rotary table which is mounted on the "I" beam support. The slit is directly over the center of the table. The supporting "I" beam is bolted to the electrostatic analyzer base so that the entire source assembly may be moved with the electrostatic analyzer as a unit.

Electrostatic Analyzer

The interior of the electrostatic analyzer is shown in Fig. 4.

Each of the two electrostatic analyzer plates is made of Armco iron and is gold plated. The plates are positioned relative to the inner edge of the stainless steel base plate. The mean radius of curvature is 1. 00 metre as noted previously, and the separation of the plates is 2. 000 cm. The variation in the radius of curvature is ~ 0. 003 mm. (. 0015") and the variation in the gap is ~ 0. 01 mm. (. 0004).

The plates are supported by 5 quartz blocks which have been accurately ground to the same thickness (~. 01 mm. or . 0004"). The gap is determined by 5 pairs of quartz spacers, which are ground to 2. 0000 ± 3 cm. Of each pair, one spacer is at the bottom of the plates and the other is at the top. The position of the plates relative to the reference circle may be adjusted by a locating screw on each of the inner mounts. The outer mounts have an inconel spring arrangement which presses the entire assembly together and against the

Vacuum System

The entire vacuum system is made using 304 stainless steel. Metal gaskets are used throughout except in the valves and on the source side of the principal slit where Viton "O" rings have been used. The main chamber is evacuated by a 140 l/sec ion pump, located on the electrostatic analyzer and a 50 l/sec ion pump, between the magnet and the collector assembly. Typical pressures at these two pumps are 2×10^{-7} torr and 6×10^{-8} torr respectively.

Fig. 3 is a photograph of the source arm, showing the source, slit controls and vacuum arrangement. The two oil diffusion pumps, which provide differential pumping in the source and lens regions, have an untrapped speed of 100 l/sec and are equipped with water-cooled baffles, liquid nitrogen traps and gate valves for isolating the source region. The usual operating pressures are $\sim 2 \times 10^{-5}$ torr in the source and $\sim 5 \times 10^{-7}$ torr in the lens section.

Source

The source arm is shown in Fig. 3. The ion source

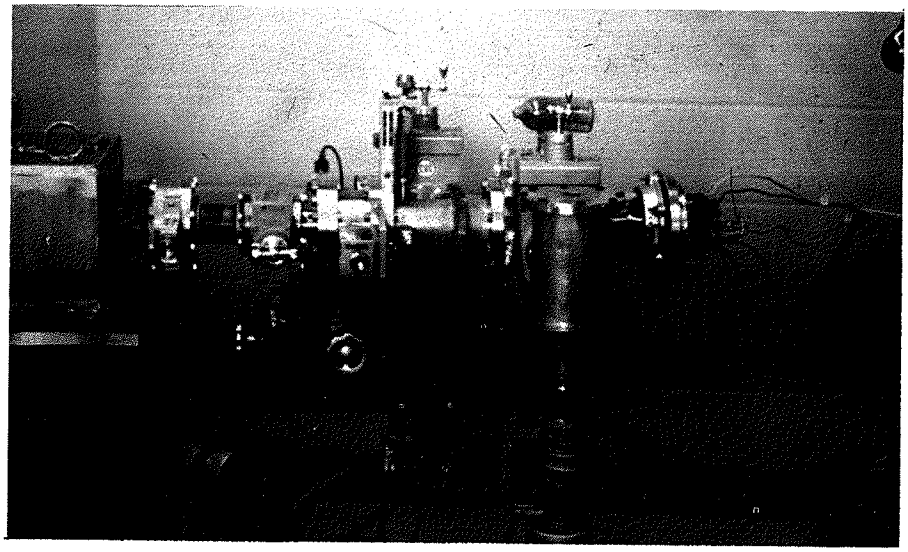

Fig.3 Source arm of instrument.

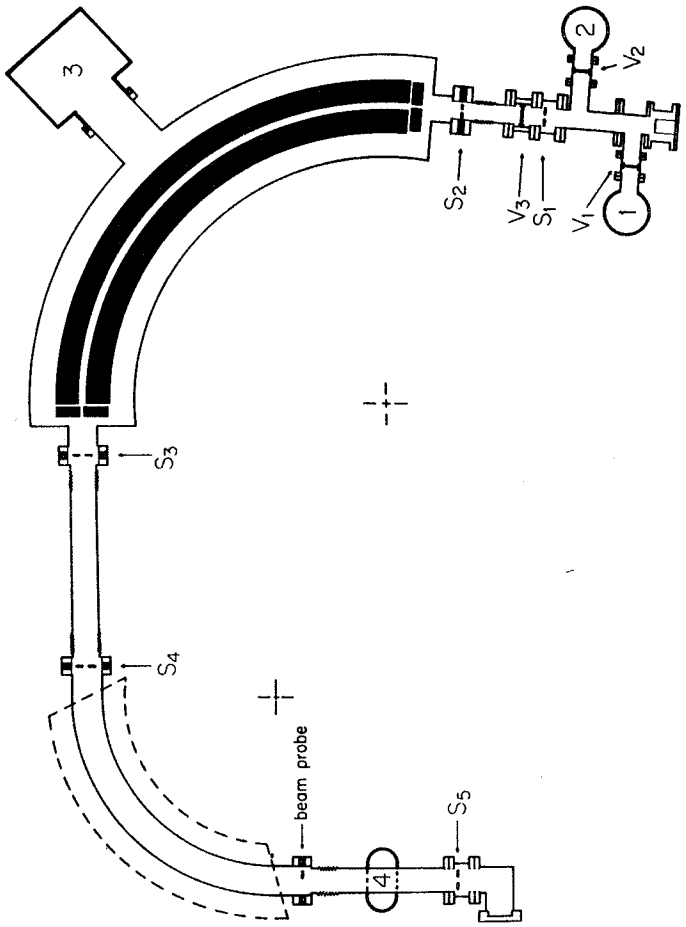

Fig.2 Physical layout of new instrument.

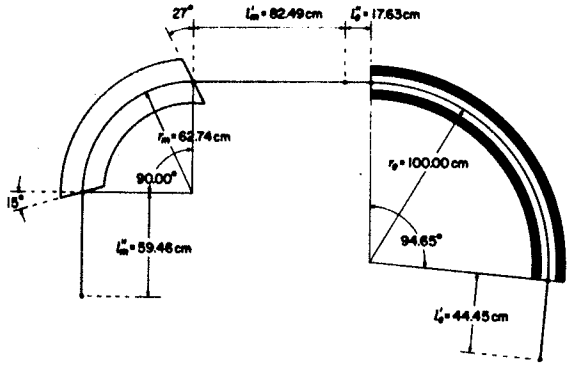

Fig.1 Geometry of second-order double-focusing mass spectrometer.

which was chosen to be 1. 00 metre. The total length of the optic axis is 4. 59 metres and the overall magnification of the instrument is . 50.

Fig. 2 shows the physical layout of the apparatus in somewhat different detail. The principal slit, S_1, is variable in width and orientation and would be 2. 2 microns wide when the instrument is set to give a resolution of 1/200, 000 at the base of the peaks. The angular spread accepted by the instrument is determined by the slit S_2 which is usually set at 1. 2 mm. This value corresponds to $\alpha = \pm 2 \times 10^{-3}$ radians although the maximum value of α (determined by the position of the fringe blocks) is 10^{-2} radians. Slit S_3 is located at the direction focus of the electrostatic analyzer and would be typically set at 3 mm. corresponding to $\beta = \pm 8 \times 10^{-4}$. The height of the beam traversing the magnetic field is limited to ~2 mm. by S_4.

The beam can be monitored by collectors at two locations; one is behind the β slit while the second is a moveable probe at the exit boundary of the magnet.

PART II: A New Second-Order Double-Focussing Mass Spectrometer*

by

R. C. Barber, J. O. Meredith, R. L. Bishop, H. E. Duckworth, M. E. Kettner and P. Van Rookhuyzen

University of Manitoba, Winnipeg, Canada

Following the 1963 Conference on Nuclidic Masses in Vienna, we decided that the next step in atomic mass determinations should be the construction of an instrument which would provide complete double focusing to second order. Preliminary work in this direction began in January 1964 and was followed by the start of construction in the summer of that year. The assembly of the instrument took place at the University of Manitoba from May 1965 onwards.

An extensive study of the second order geometry of mass spectrometers and spectrographs by Hintenberger and Kŏnig (1) led to the proposal by them of a number of instruments which would provide partial or complete second-order double focussing. The instrument which we selected as the most desirable one of this group is a mass spectrometer with deflection in the same sense in both electric and magnetic fields and with straight magnetic field boundaries. The geometrical arrangement is shown in Fig. 1. The considerations in selecting this instrument were the following:

(1) An intermediate direction focus is formed at l''_e This permits the use of the electrostatic analyzer as an energy analyzer with a resolution of about 1 volt.

(2) The total ion path is not unreasonably long. Also the individual distances from source to electrostatic analyzer (l'_e), the separation between the two fields(d), and the image distance (l''_m)are all relatively short.

(3) It is not necessary for the ion beam to cross a curved magnetic field boundary at a prescribed angle.

The scale of the instrument is determined by the mean radius of curvature in the electrostatic analyzer

Reprinted from Proceedings of the
Third International Conference
on Atomic Masses
Winnipeg, 1967

CHAPTER 4

PEAK MATCHING BY COMPUTER

The 1024 channel memory of the signal averager has been split into four quadrants. The reference peak is stored in the first quadrant, while the second peak is shifted near to coincidence by adding voltages ΔV_1, ΔV_2, ΔV_3 to V, and the three corresponding spectra are stored in quadrants two, three and four. The position of the second peak relative to the first is found as a function of Δv and the Δv for a match is determined. The precision obtained is compared to the statistical limit set by the number of ions.

Introduction

As noted in Chapters 2 and 3, the peak matching method of determining a mass difference depends on a theorem due to Bleakney (1936). Thus all voltages should be switched in the ratio $\frac{\Delta M}{M} = \frac{\Delta V}{V}$, i.e. the accelerating voltage, V_a, must be switched by an amount of ΔV_a and strictly speaking, voltages on the quadrupole lens electrodes should also be switched. However, for the narrow doublets reported

here ($\Delta M/M \sim 1/40,000$), the effect of the quadrupole switching voltages on the spacings is negligble and therefore these voltages were not switched.

A brief description of the computer peak matching method has been given by Meredith et al (1971). Here we shall give more details of the voltage supplies and the switching mechanism, as well as a report of the results on two cadmium chloride doublets.

Description of Apparatus

The Fabri-Tek FT1052 signal averager, used originally for the visual null method of peak matching, has been modified by splitting the memory into four sections of 256 channels. During the first quarter of a cycle (1 cycle = a sweep of all 1024 channels) $\Delta V = 0$, and a signal proportional to the reference peak of mass M is stored in the first quadrant. During the second, third and fourth quarters of the cycle, voltages ΔV_1, ΔV_2 and ΔV_3 respectively are added to the ESA voltage, V, and the corresponding signals for the peak of mass M' are stored in the remaining three quadrants. The whole cycle is repeated many times to increase the number of ions collected and to improve the signal to noise ratio (see for instance, Klein and Barton 1963). The accumulated memory contents are shown schematically in Fig. 4-1 with the four quadrants displayed one above the other.

Generally, ΔV_2 is set near the expected value for the doublet while $\Delta V_1 = \Delta V_2 - \delta V$ and $\Delta V_3 = \Delta V_2 + \delta V$ are set 0.1%

to 1.0% below and above ΔV_2. The lateral displacement of the peaks from the matched condition (the D_i) is exaggerated for quadrants two and four. The displacement D_2 is usually very small and is not shown in the figure.

Either M or M' may be used as the reference peak, that is, the lighter member of the doublet may be matched to the heavier, or vice versa. This corresponds to adding or subtracting ΔV. Also, the ion beam may be swept in two different directions across the collector slit. We call these "Sweep forward" (where the lighter member of the doublet is displayed first), and the other is "sweep reverse". Finally, the ΔV staircase may increase (N), or decrease (B), as shown in Fig. 4-2b. Permutation of these three arrangements leads to eight different matching configurations. In order to reduce the possibility of a systematic error due to the matching configuration, all eight are used, and the weighted average is called one run. Fig. 4-1 represents the memory contents for N, Add, Forward, accumulated after several minutes.

The ΔV wave form shown in Fig. 4-2b is derived from the circuit shown in Fig4-2a using a Guildline 9745/4 mechanical chopper. The chopper was selected for low voltage applications because of its very low thermal emfs ($<0.02\mu V$) and very small variation in resistance between the gold contacts. It is driven by a synchronous motor via an "O" ring at an average frequency of 5.67 cps. Separate trigger signals are taken

from the fourth set of contacts, labelled signals A and B. These are used to start the address advance for each quadrant at ∿44 msec intervals. When the Fabri-Tek memory advance reaches address 4 in each quadrant, a trigger signal is sent to the oscilloscope. It starts its sweep, and drives the Helmholtz coils to modulate the ion beam across the collector slit. The actual time interval for the collection of data is 25.6 msec (100 msec/channel), following which there is a dead time of ∿7 msec. Then V and V_a are switched to new values as indicated in the figure; there is a further interval of ∿10 msec for transients to die away, and the process continues. The time base of the oscilloscope sweep is adjusted to coincide with the quadrant sweep. Since the ΔV_a which corresponds to δV is 0.5 to 5 mvolts, ΔV_a need not be stepped exactly to correspond to the three slightly different ΔV's. ΔV_a is set to a precision of ∿0.1 volts at the calculated value for ΔV_2; and is then constant for the last three quarter cycles.

In order to make maximum use of the information available, the peak of interest is adjusted to occupy as many channels as possible in the centre of each quadrant, leaving about 30 channels at each end to establish a base line. The memory contents are read out onto magnetic tape, then the matching configuration is changed, and the process repeated. When all eight configurations have been used, one run is complete.

As many runs as desired may be recorded, usually with minor refocussing of the spectrometer between runs. One tape will hold more than 15 runs, although an average day is about 5 to 10 runs.

Computer Analysis

The seven track tape is carried to the computer centre for analysis on an IBM 360/65. The tape is read, and the binary record is translated to decimal. Each record is then written in EBCDIC on a library tape. and the spectrum is plotted on the line printer for visual inspection.

The points A, B, C and D in Fig. 4-1 are identified by eye and are read into the computer on punched cards. The base line is calculated between A and B and between C and D for each quadrant, and is subtracted from the peak between B and C. The overlap of tails from the peaks has the effect of reducing the calculated separation if all of the peak right down to the base line is used. Stevens and Moreland (1968) have commented on this, their lead has been followed here. Only that part of the peak lying 15% above the base line is used. A further discussion of the effect of the tails will be given in Appendix B.

Instead of using the single highest point as the peak height, the parabolic approximation of Weichert and Russell (1968) is assumed near the local maximum. A seven point

least squares smoothing, developed by Savitzky and Golay (1964) is carried out to obtain a more reliable value of the peak height. Then, starting at point B, the programme searches for three consecutive points lying above the desired 15% level as shown in Fig. 4-1. The first of these three points is labelled B'. In order to treat the leading and trailing edges in a similar fashion, the programme then goes to the point C and searches backwards for three consecutive points lying above the cut-off level. The first of these is called C', the end of the peak.

Now we wish to know the number of ions in the peak between B' and C'. Work by Campbell and Halliday (1965) has shown that the fundamental limit of precision in locating a peak is determined by the number of ions in the peak. The ideal peak is triangular, and the weighted mean, or centroid, is the best method of estimating the location. For a large number of ions, N, the triangle can be approximated by a normal distribution with a standard deviation of $W/\sqrt{24N}$, where W is the full width at the base of the peak. After subtraction of the base line, the peak height is converted to the actual number of ions by multiplying by a previously determined calibration constant.

The centroid and first four moments of the distribution between B' and C' are calculated. From the second moment the standard deviation is calculated; this agrees with the

estimate based on $W/\sqrt{24N}$ to within a few percent when the cut-off level is ∿15%. The third and fourth moments allow more detailed comparison of the peak shape;skewness and sharpness relative to a Gaussian.

After finding the centroid and its standard deviation for the peak in each quadrant, the displacements D_1, D_2 and D_3 are calculated. As shown in Fig. 4-1, D_i is the displacement of the peak in quadrant (i + 1) relative to the reference peak in quadrant one. The error[1] in D_i is d_i where d_i is the r.m.s. combination of the errors in locating the two peaks. A straight line is fitted to the three pairs of points $(D_i \pm d_i, \Delta V_i \pm V_i)$. The iterative least squares fitting developed by Williamson (1968) takes into account the errors in both coordinates. (See also Appendix A.)

The matched condition prescribed by Bleakney's theorem is D = 0; thus the intercept of the fitted line on the ΔV axis is the desired ΔV. The calculated error in the intercept agrees very well with the error expected on the basis of the total number of ions in the match.

A series of experiments was carried out to determine if a linear fit was justified. A series of ten matches were taken, each with ΔV = 0 (that is, a peak is matched to itself), and different δV's applied, spanning the range usually used, ranging from 4 times smaller to 4 times bigger than the normal δV. A straight line, then second and third order polynomials

[1] In this work, 'error' means standard deviation, and the two terms are used interchangeably.

were fitted to the resulting set of about 30 points. This was done for each of the eight matching configurations. In each case the coefficient of the quadratic term was three orders of magnitude smaller than that of the linear term, and had the same sign for both positive and negative slopes. This introduces an error smaller than the errors on the intercept and slope. Moreover, since half of the configurations lead to a positive slope and half to a negative slope, then neglecting the quadratic term gives results slightly too high for fits with positive slope, and slightly too low for those with negative slope. Thus, the small effect cancels over a complete run. If the curve were 's' shaped, there would be little or no error introduced into the determination of the intercept. However, a cubic fit resulted in essentially unchanged lower order coefficients, and the cubic coefficient was four orders of magnitude smaller than the quadratic.

In this matching of a peak to itself it was noted that the peak in quadrant one was shifted by $\sim$0.18 channels with respect to the same peak in the other three quadrants. This is of the same size as the error of locating a single peak, and becomes apparent only after considerable work. The effect of this makes half of the determinations too high and half too low, so that the final result is not systematically changed. However, it results in an unnecessarily larger error in the final result since the values for the eight configurations break

into two groups of four. A correction of 0.18±.02 channels is now applied to the D_i before fitting the straight lines and averaging the eight intercepts.

Results

Three well known doublets in the spectrum of cadmium chloride were studied to test the operation and precision of the new system. Table 4-1 shows the working resolving power (FWHM), the values of ΔM obtained for individual runs, and the 'internal' and 'external' errors as defined by Birge (1932). The value of ΔM in column 3 is the weighted mean of the eight different matching configurations. Since the standard deviation on each match depends on the number of ions, all eight configurations have approximately the same weight. The internal error in column 4 is the error expected on the basis of the errors calculated for each match. The external error in column 5 is calculated from the spread of the eight values about their weighted mean. The Birge ratio (defined as $\sigma_{ext}/\sigma_{int}$) is often about 5. This means that the differences between results from the eight configurations is a factor of five larger than would be expected on the basis of the precision associated with each match. The internal error of $\sim$ 0.5μu at M $\sim$200μ is the lower limit attainable with the number of ions collected and the resolution used. At present, there does not appear to be a systematic variation of the

result which can be associated with the matching configuration. The larger spread of the results is probably due to changes in the spectrometer operation from match to match. Source conditions often change drastically due to sparks or sudden evaporation of a small quantity of the sample. The quadrupole settings often have to be adjusted slightly and the ESA may be moved if refocusing is required. All of these may contribute to the variation in the final answer beyond that expected on statistical grounds alone.

The larger of σ_{int} and σ_{ext} (i.e.σ_{ext}) is then used to calculate the final weighted mean for the 6 or 7 runs on each doublet. In this final calculation the new internal and external errors are the same size to within 5%, indicating that the assignment of an error of 1.5 to 4 μu for a single run is realistic. The reproducibility of the spectrometer from run to run and from day to day is as good as its short term stability from match to match within a given run.

To compare the actual doublet values, Table 4-2 presents determinations made in a number of different laboratories over the last eight years. It is seen that the present work has achieved the same precision as the total of all past work with about two to three hours of machine time, with only one operator in place of the two previously used.

Finally, to show the improvement in precision of this method over that obtained by the visual null method, three histogrammes are shown in Fig. 4-3. The precision for a

doublet is $\delta M/M$, where δM is the standard deviation for the doublet and M is the mass at which the determination was made. This figure is multiplied by $\sqrt{N}$, where N is the number of runs for the given doublet, in order to obtain the precision associated with a single run. The histogrammes are plots of the values of $\delta M\sqrt{N}/M$. The upper two histogrammes are for the visual null method before and after the installation of the vibration mounts. The precision for a single run is 6.6 ± 6μu at mass 200μ. The lower part is the precision achieved with the new computer peak matching. The precision now for one run is 4.6 ± 8μu at mass 200μ.

It is thus seen that there is a significant improvement in precision. Moreover, there is a reduction by a factor of two in man-hours required in instrument operation which is not considered in the above.

References for Chapter 4

Birge, R.T. (1932), Phys. Rev. 40, 207

Bishop, R.L., Barber, R.C., McLatchie, W., Macdougall, J.D., van Rookhuyzen, P. and Duckworth, H.E. (1963) Can. J. Phys. 41, 1532

Bishop, R.L. (1963) M.Sc. Thesis, McMaster University

Bishop, R.L. (1969) Ph.D. Thesis, University of Manitoba

Bleakney, W. (1936) Amer. Phys. Teacher 4, 12

Damerow, R.A., Ries, R.R. and Johnson, W.H. Jr. (1963) Phys. Rev. 132, 1673

Klein, M.R. and Barton, G.W. Jr. (1963) Rev. Sci. Instrum. 34, 754

Macdougall, J.D., McLatchie, W., Whineray, S. and Duckworth, H.E. (1966) Z. Naturforschg. 21a, 63

McLatchie, W. (1966) Ph.D. Thesis, McMaster University

Meredith, J.O., Southon, F.C.G., Barber, R.C. and Duckworth, H.E. (1971) to be published

Savitzky, A. and Golay, M.J.E. (1964) Anal. Chem. 36, 1627

Stevens, C.M. and Moreland, P.E. (1968) Proc. 3rd Int. Conf. on Atomic Masses (R.C. Barber, Ed.) University of Manitoba Press p.673

Weichert, D.H. and Russell, R.D. (1968) Can. J. Phys. 46, 1443

Williamson, J.H. (1968) Can. J. Phys. 46, 1845

TABLE 4-I

CADMIUM DOUBLETS

All Masses in Micro Units

Date	R.P. (FWHM)	ΔM	σ_{int}	σ_{ext}
	$^{116}Cd^{35}Cl$-$^{114}Cd^{37}Cl$			M/ΔM ≈ 34,600
March 18/71	123,000	4343.7	0.89	3.7
March 19	168,000	4351.8	0.60	4.0
March 19	165,000	4350.3	0.65	2.5
March 24	117,000	4345.7	0.85	3.9
March 25	140,000	4351.8	0.57	2.9
March 25	157,000	4347.0	0.57	2.5
	Weighted Mean	4348.7 ±	1.2	
	$^{114}Cd^{35}Cl$-$^{112}Cd^{37}Cl$			M/ΔM ≈ 42,000
March 17	163,000	3553.8	0.54	2.1
March 17	152,000	3547.6	0.25	1.2
March 18	156,000	3546.3	0.28	1.5
March 18	150,000	3545.3	0.27	2.8
March 22	145,000	3551.6	1.13	2.6
March 22	139,000	3549.9	0.71	2.1
March 25	176,000	3547.9	0.57	2.0
	Weighted Mean	3548.5 ±	1.0	
	$^{113}Cd^{35}Cl$-$^{111}Cd^{37}Cl$			M/ΔM ≈ 58,000
March 24	220,000	3175.4	0.96	3.54

TABLE 4-II

CADMIUM DOUBLETS

	Source	ΔM(μu)	Ref.
$^{116}Cd^{35}Cl$-$^{114}Cd^{37}Cl$			
1963	McMaster, Visual	4353 ± 2	(a)
1963	Minnesota	4352 ± 4	(b)
1965	McMaster, Visual	4337 ± 3	(c)
	McMaster, Enhancetron	4344 ± 2	(c)
1966	Aldermaston (t,p)	4383 ± 10	(d)
	McMaster, Nier Network	4346 ± 2	(d)
	Weighted Average 4347.9 ± 1.3 μu		
$^{114}Cd^{35}Cl$-$^{112}Cd^{37}Cl$			
1963	McMaster, Visual	3547 ± 2	(a)
1963	Minnesota	3554 ± 4	(b)
1965	McMaster, Visual	3546 ± 3	(c)
	McMaster, Enhancetron	3547 ± 3	(c)
1966	Aldermaston (t,p)	3548 ± 10	(d)
	McMaster, Nier Network	3548 ± 2	(d)
1967	Manitoba	3547.0± 2.3	(e)
1968	Manitoba	3548.2± 2.1	(e)
	Weighted Average 3547.7 ± .9 μu		
$^{113}Cd^{35}Cl$-$^{111}Cd^{37}Cl$			
1963	McMaster	3174 ± 2	(f)

(a) Bishop, et al (1963)
(b) Damerow, et al (1963)
(c) Macdougall, et al (1966)
(d) McLatchie (1966)
(e) Bishop (1969)
(f) Bishop (1963)

Figure 4-1

Schematic of Memory Contents, for N, Add, Forward. M_R is the reference peak and M_L the lighter member of the doublet is being matched to M_R. Points, A, B, C and D are used for calculating the base line. Points B' and C' are at the 15% level for each peak. An expanded diagram of the parabolic approximation is also shown.

FIGURE 4 - 1

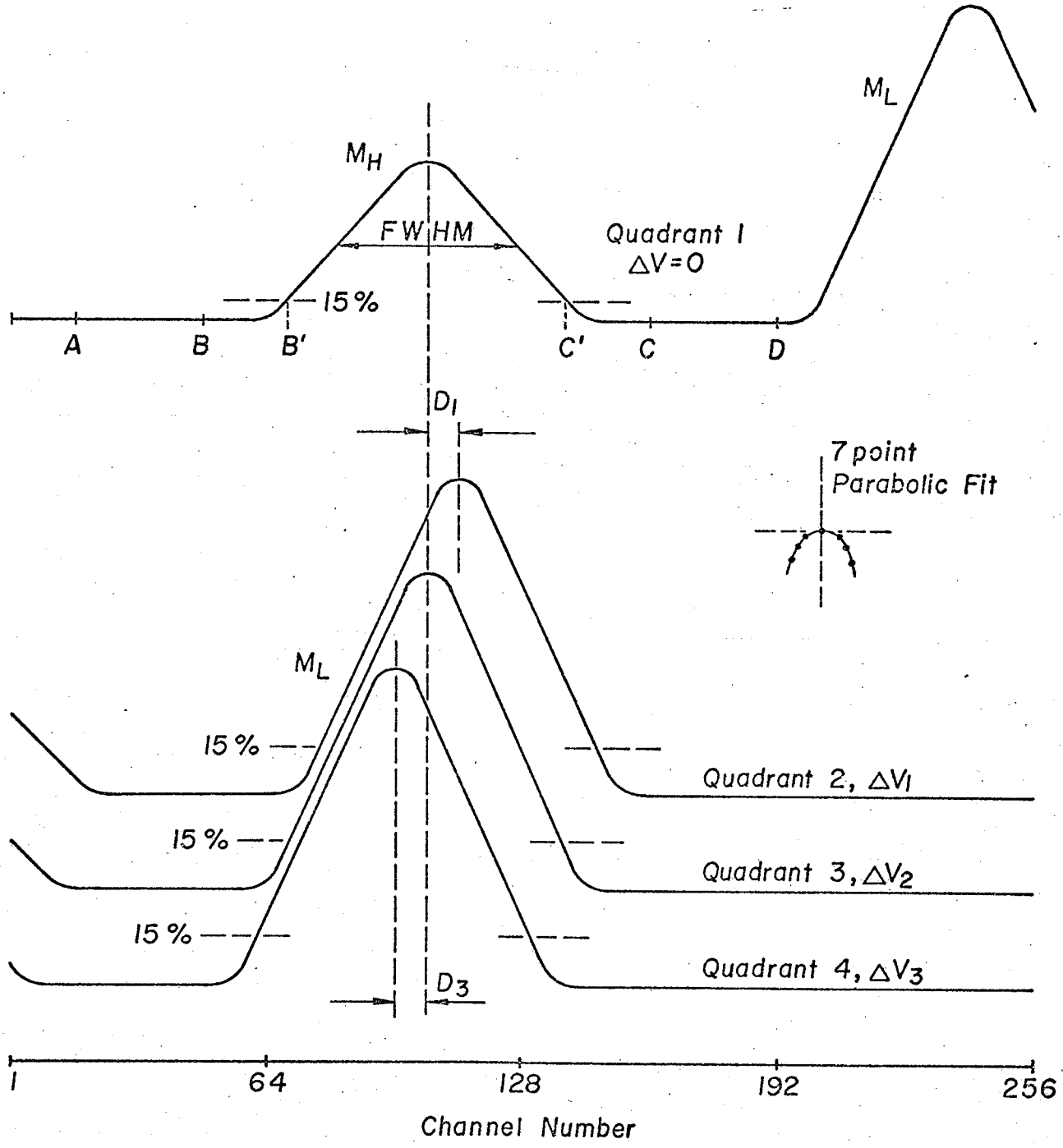
M_L
M_H
FWHM
Quadrant I
ΔV=0
15 %
A
B
B'
C'
C
D
D_1
7 point
Parabolic Fit
M_L
15 %
15 %
15 %
Quadrant 2, ΔV_1
Quadrant 3, ΔV_2
Quadrant 4, ΔV_3
D_3
1
64
128
192
256
Channel Number

Figure 4-2a

Chopper and δV Supply

The δV's are supplied by the 1.5 V battery and the network shown. The supply for ΔV is the same as that for the visual null method. The mechanical chopper is a Guildline 9745/4 with four independently adjustable double pole - double throw contacts.

FIGURE 4 - 2a

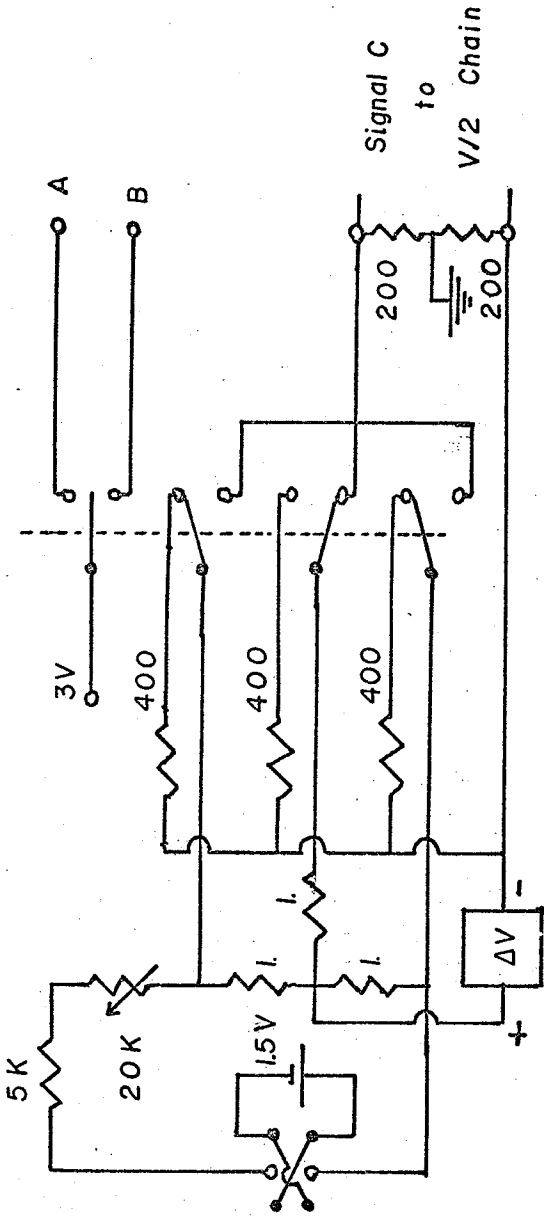

Figure 4-2b

ΔV Wave form and Synchronization

ΔV_a is shown reduced by a factor of 25. The ΔV signal is shown as an increasing staircase(N), or decreasing (B). The heavy part of the trace indicates when the sawtooth modulation is applied and the ions are collected.

FIGURE 4 - 2b

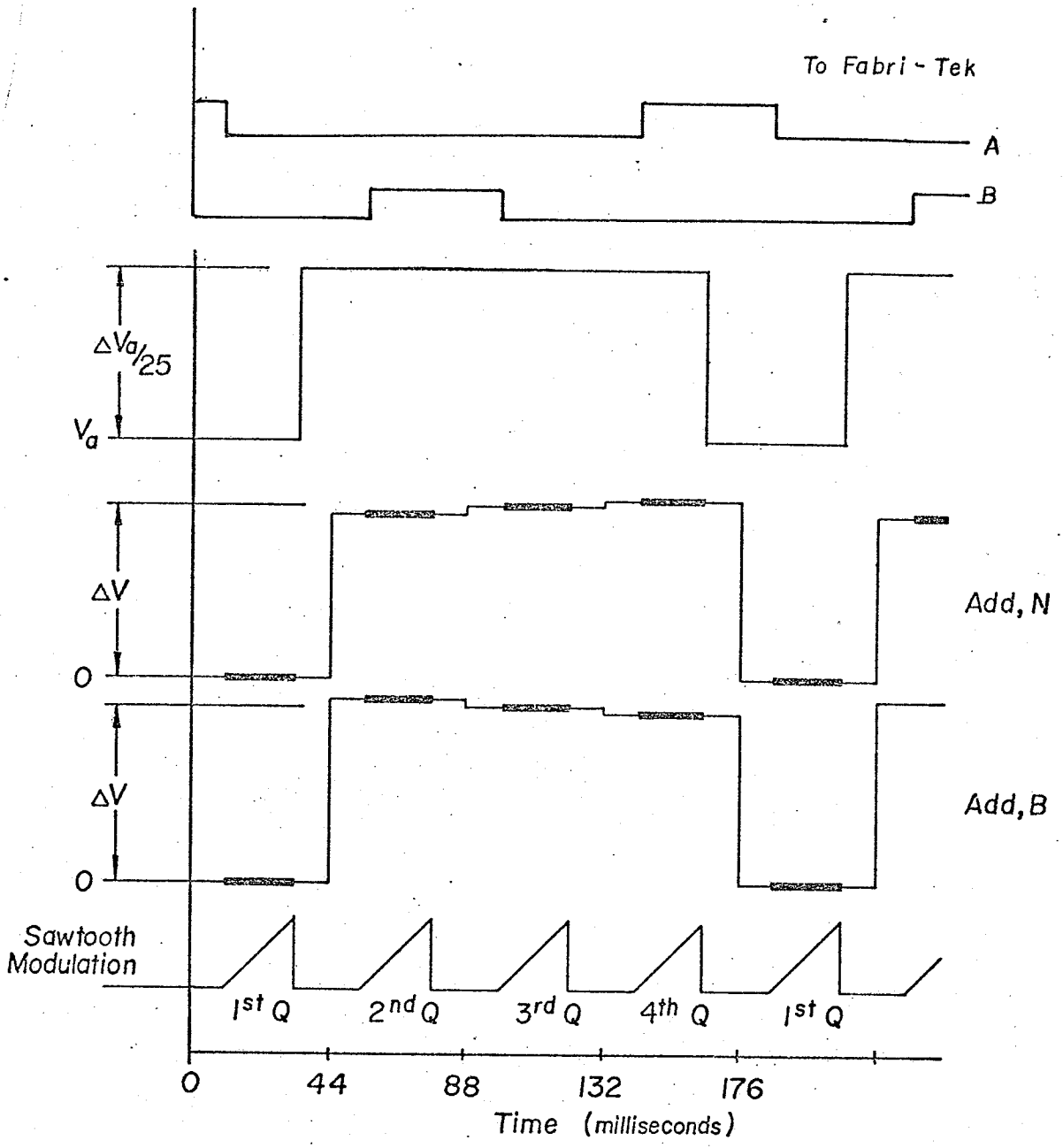
To Fabri - Tek
A
B
ΔVa/25
Va
ΔV
0
Add, N
ΔV
0
Add, B
Sawtooth Modulation
1st Q
2nd Q
3rd Q
4th Q
1st Q
0
44
88
132
176
Time (milliseconds)

Figure 4-3

Comparison of Precision Achieved

There are three histogrammes of precision achieved on the basis of a single run. That is $\Delta M\sqrt{N}/M$ where N was the number of runs used to determine a particular doublet and δM was the standard deviation of the mean for the doublet.

FIGURE 4 - 3

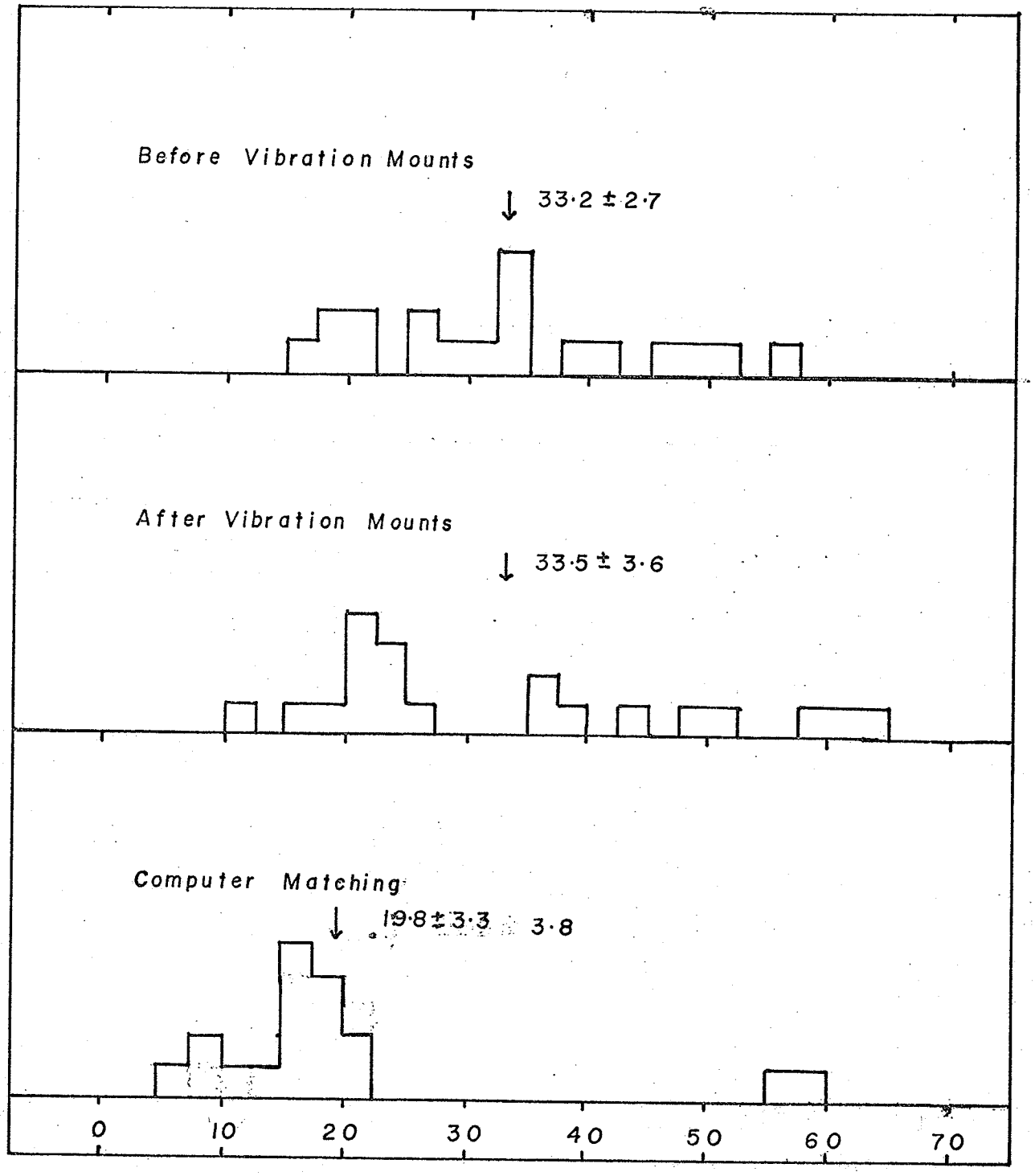
Before Vibration Mounts
33·2 ± 2·7
After Vibration Mounts
33·5 ± 3·6
Computer Matching
19·8 ± 3·3
3·8
0
10
20
30
40
50
60
70
Matching Precision of One Run (parts in 10^9)

CHAPTER 5

EXPERIMENTAL ATOMIC MASS DIFFERENCES

Doublet spacings in the chloride spectra of neodymium, holmium, erbium, thulium and ytterbium are presented. They are compared with other mass spectroscopic data and with the 1964 Mass Table. The values are examined for self consistency and for possible systematic errors.

Introduction

The determinations presented here cover the rare earth region from $^{165}_{67}Ho$ to $^{176}_{70}Yb$, along with three doublets in $NdCl_2$. This is part of a research programme to systematically study the rare-earth nuclides to obtain a better understanding of nuclear binding energies. (See Duckworth et al (1969) for a brief, overall survey of double neutron separation energies for $82 \leq N \leq 126$.) Determinations of mass differences in the region of the onset of nuclear deformation, $88 \leq N \leq 92$ have been presented by Bishop (1969) up to $^{164}_{66}Dy$. A more complete picture of atomic mass differences and energy systematics for $59 \leq Z \leq 69$ has been given in a pair of papers, Barber et al (1971b) and Meredith et al (1971a). Hereafter, these two papers will be referred to as Paper II and Paper III respectively. The

experimental data in this Chapter extends the above work to $68 \leq Z \leq 70$, and in addition provides a redetermination of three doublets in neodymium.

New Mass Differences

In most cases reported here, the doublets were of the form $^{A}X^{35}Cl - {}^{A-2}Y^{37}Cl$, where X and Y may or may not be the same element. Except for $^{154}Sm - {}^{154}Gd$, the rest of the doublets were of the type $^{A}X^{35}Cl_2 - {}^{A-4}Y^{37}Cl_2$. While the latter type of measurement is carried out with the rare-earth dichloride ions, the first type may be done with either the monochloride or dichloride. Often the dichloride ions are produced more abundantly in the ion source, and in addition, the intensity ratio of $X^{35}Cl_2$ to $X^{35}Cl^{37}Cl$ is more favourable. The chlorine isotopes differ in mass excess by 2,952 μu so that most of the doublets studied range between 3800 to 6600 μu. Accordingly, $\Delta M/M \gtrsim 1/40,000$.

The dichloride spectra of erbium and ytterbium are shown schematically in Fig.5-1a and 5-1b, where the relative abundances are shown as a percent of the total. Note that it is a semi-log scale and that the intensity is poorest at the light end. Here ΔM is smallest, and the relative intensities of the pair are very badly mis-matched. By far the most difficult doublet was $^{168}Yb^{35}Cl_2 - {}^{170}Yb^{35}Cl^{37}Cl$, where the intensity was 0.05% to 1.7%, $\Delta M/M = 1/63,000$ and ytterbium chloride has the lowest vapour pressure of any of the rare-earth chlorides.

The twenty-four doublets presented in this work are listed in Table 5-I, along with the code letter which will be used in this chapter. Columns 3 and 4 give the results obtained with the computer matching method or the visual null method respectively. For comparison, values obtained by this group at McMaster University, (Macdougall et al, 1970, and Whineray et al, 1970), are given in column 5. The 'adopted' values of column 6 result from a combination of the values in columns 3, 4 and 5.

When two or more values of the same quantity exist, a weighted average is taken, and the larger of σ_{int} or σ_{ext} is used as the error of the weighted average, (see Birge 1932, and also Appendix A). In addition, there are simple closed loops: F, G, H; I, J, K; L, M, N and V, W, X. In these cases a least squares adjustment of the loops was carried out to obtain the adopted values. The values for A, B and C, marked $^{+}$, are the result of an adjustment of eleven mass differences in neodymium and samarium, measured both here and at McMaster. (See Paper II, Table I, for all of the raw data.) The last column contains other comparisons, generally from the 1964 Mass Table (Mattauch et al, 1965a, b), but also from the Minnesota (Benson and Johnson 1966) and Russian (Demirkhanov, 1968) groups.

Comparison of Results

A visual comparison of columns 3,4 and 5 is given in

Fig. 5-2 a. The solid dots represent 'adopted - McMaster', with the solid error bar indicating the combined error on the difference. The open circles represent 'adopted - Manitoba', and the error bars are broken lines.

Since the errors on the present work are about three times smaller than those on the McMaster work, they are weighted about ten times as much in any adjustment. As a result, the adopted values are very similar to the raw Manitoba values. This is apparent in looking at the open circles in Fig. 5-2a. Deviations are small, most less than 1 μu, all the error bars span the zero line, and the points are randomly above and below.

In contrast, the 13 solid points representing 'adopted - McMaster' are all above the zero line, and only four error bars cross the zero axis, while one just touches it. The points corresponding to McMaster values tend to lie too high by about 5 μu. This suggests that the McMaster doublet determinations were, on the average, 5 μu smaller than the present work.

A comparison with Figure 3 of Paper II shows a similar situation, although it was thought at the time that the data were insufficient to draw firm conclusions. Now, with these two sets of data, plus more doublets in hafnium and lutetium (Southon 1971), there are a total of 25 comparisons to be analysed. The mean difference 'adopted - McMaster' is 4.6 μu,

and the standard deviation of the mean is ± 1.0 μu. When the stated errors on the doublet spacings are used to calculate the self-consistency of the results, the expected error on the difference is also ±1.0 μu. Thus the McMaster work appears to have had the random (or statistical) errors correctly assigned.

Now that there is a significant difference between the adopted values (which are almost the same as the present work) and the McMaster values, which, if either, are 'correct'? Paper III provides an extensive comparison between mass spectroscopic doublets and nuclear reaction and decay Q-values. A set of 30 precise atomic mass determinations and about 150 Q-values are combined in a least squares adjustment of the atomic masses in the region $59 \leq Z \leq 69$. Reference to Table VIII of Paper III shows that, on the average, the mass spectroscopic values change by -0.5 ± 0.4 μu. Of the 39 doublets, 7 are McMaster values alone. If they are excluded, the average difference between the adjusted values and the mass spectroscopic values is +0.04 ± 0.31. Again, the mass spectroscopic input to the adjustment is largely determined by the work here at Manitoba.

Thus we conclude that the new lm. instrument at the University of Manitoba has no significant systematic error for doublets of 2000 to 10,000 μu. Also, it would appear that there was a small systematic error in the work reported by Whineray *et al* (1970) and Macdougall *et al* (1970) at McMaster.

Again, for doublets of 3000 - 10,000 μu, their answers appear on the average to be 4.6 ± 1.0 μu too small. Since this is about the same size as their random errors, it would be very difficult to detect, especially in the absence of a detailed comparison with other accurate data.

For completeness, Fig. 5-2 b presents the comparison between our 'adopted values' and other work, mainly the 1964 Mass Table. Note that the scale has been changed by a factor of 10, and that the error bars are much larger, (from 20 μu to 160μu). The points corresponding to the 1964 Mass Table appear to be randomly high and low. As noted in Paper II, the agreement with Demirkhanov et al (1968) is not good, while the agreement with the more precise work at the University of Minnesota (Benson and Johnson 1966) is very good.

On the basis of these comparisons, the present doublets in neodymium, gadolinium and erbium are in agreement with other precise nuclear reaction and decay Q-values, and the doublets in thulium and ytterbium are self consistent.

References for Chapter 5

Barber, R.C., Bishop, R.L., Meredith, J.O., Southon, F.C.G., Williams, P., Duckworth, H.E. and van Rookhuyzen, P. (1971) to be published.

Benson, J.L. and Johnson, W.H. Jr. (1966) Phys.Rev. 141, 1112

Birge, R.T. (1932) Phys.Rev. 40, 207

Bishop, R.L. (1969) Ph.D. Thesis, University of Manitoba

Demirkhanov, R.A., Dorokhov, V.V. and Dzkuya, M.I. (1968) Proc. 3rd. Int. Conf. Atomic Masses (R.C. Barber, Ed.) University of Manitoba Press, Winnipeg, 864

Duckworth, H.E., Barber, R.C., van Rookhuyzen, P., Macdougall, J.D., McLatchie, W., Whineray, S., Bishop, R.L., Meredith, J.O., Williams, P., Southon, F.C.G., Wong, W., Hogg, B.G. and Kettner, M.E. (1969) Phys.Rev. Lett. 23, 592

Macdougall, J.D., McLatchie, W., Whineray, S. and Duckworth, H.E. (1970) Nucl.Phys. A145, 223

Meredith, J.O., Barber, R.C. and Duckworth, H.E. (1971) to be published

Southon, F.C.G. (1971) Ph.D. Thesis, University of Manitoba

Whineray, S., Macdougall, J.D., McLatchie, W. and Duckworth, H.E. (1970) Nucl.Phys. A151, 377

TABLE 5-I

NEW ATOMIC MASS DIFFERENCES in MICRO UNITS

Code	Doublet	ΔM (This Work) Computer Match	ΔM (This Work) Visual Null	ΔM McMaster	ΔM Adopted	Other	
A	$^{148}Nd^{35}Cl$-$^{146}Nd^{37}Cl$	6720.3±1.9	6722.1±2.7	6721±4 f	6722.2±1.7+	6733± 4	a
						6820±21	b
						6723± 5	d
						6723± 3	e
B	$^{146}Nd^{35}Cl$-$^{144}Nd^{37}Cl$	5977.2±1.7	5981.3±0.9*	5966±4 f	5979.5±2.0+	5997± 4	a
						6030±22	b
						5966± 2	c
						5970± 5	d
						5976± 3	e
C	$^{148}Nd^{35}Cl_2$-$^{144}Nd^{37}Cl_2$	12700.7±1.8	12700.4±1.8	12690±9 f	12701.4±1.7+	12730± 6	a
						12850±21	b
						12699± 4	c
						12693± 7	d
D	^{154}Sm-^{154}Gd		1337.9±3.8		1337.9±3.8	1353±18	a
E	$^{155}Gd^{35}Cl$-$^{153}Eu^{37}Cl$		4344.3±2.4		4344.3±2.4	4392±20	a
F	$^{167}Er^{35}Cl$-$^{165}Ho^{37}Cl$		4678.3±1.1	4666±3 g	4678.8±1.6	4589±35	a
G	$^{169}Tm^{35}Cl$-$^{167}Er^{37}Cl$		5111.9±1.0	5107±3 g	5111.7±1.4	5135±26	a
H	$^{169}Tm^{35}Cl_2$-$^{165}Ho^{37}Cl_2$		9790.6±0.6		9760.6±0.6	9724±44	a
I	$^{171}Yb^{35}Cl$-$^{169}Tm^{37}Cl$	5061.2±1.7		5055±3 g	5060.4±1.5	5135±78	a
J	$^{173}Yb^{35}Cl$-$^{171}Yb^{37}Cl$	4835.0±2.1		4827±4 g	4835.8±1.9	4585±86	a
K	$^{173}Yb^{35}Cl_2$-$^{169}Tm^{37}Cl_2$	9896.4±1.2			9896.4±1.1	9715±78	a
L	$^{160}Gd^{35}Cl$-$^{158}Gd^{37}Cl$		5900 ±7	5899±3 f	5900.1±2.3	5887± 8	a
M	$^{162}Er^{35}Cl$-$^{160}Gd^{37}Cl$		4673.4±1.9		4673.8±1.7	4575±100	a
N	$^{162}Er^{35}Cl_2$-$^{158}Gd^{37}Cl_2$		10574.9±2.5		10574.1±2.1	10462±136	a

Code	Doublet	ΔM (This Work) Computer Match	ΔM (This Work) Visual Null	ΔM McMaster	ΔM Adopted	Other	
O	$^{164}Er^{35}Cl$-$^{162}Er^{37}Cl$		3372.5±1.3		3372.5±1.3	3497±86	a
P	$^{166}Er^{35}Cl$-$^{164}Er^{37}Cl$		4039.9±1.3		4039.9±1.3	3970±47	a
Q	$^{168}Er^{35}Cl$-$^{166}Er^{37}Cl$		5027.6±1.4	5026±3 g	5027.3±1.3	5026±25	a
R	$^{170}Er^{35}Cl$-$^{168}Er^{37}Cl$		6045.4±1.7	6040±3 g	6044.1±2.3	6127±75	a
S	$^{168}Yb^{35}Cl_2$-$^{164}Dy^{37}Cl_2$	10596.3±10.3			10596 ±10	10860±160	a
T	$^{170}Yb^{35}Cl$-$^{168}Yb^{37}Cl$	3801.1±7.7			3801.1±7.7	3812±160	a
U	$^{172}Yb^{35}Cl$-$^{170}Yb^{37}Cl$	4562.0±2.2	4566.1±2.4		4563.9±2.0	4284±86	
V	$^{174}Yb^{35}Cl$-$^{172}Yb^{37}Cl$	5431.6±2.1	5428.6±1.1	5420±4 g	5429.5±1.5	5337±75	a
W	$^{176}Yb^{35}Cl$-$^{174}Yb^{37}Cl$	6657.7±2.1	6654.8±0.9	6652±3 g	6655.1±1.1	6882±75	a
X	$^{176}Yb^{35}Cl_2$-$^{172}Yb^{37}Cl_2$	12087.9±3.4			12084.8±1.9	12220±99	a
Y	$^{175}Lu^{35}Cl$-$^{173}Lu^{37}Cl$	5505.5±3.2		5503±4 g	5504.5±2.5	5531±92	a

\+ Least Squares Adjustment without the computer matches included

* Previously measured by Bishop (1969)

a 1964 Mass Table (Mattauch et al 1965)

b Demirkhanov et al, 1968

c Sum of two doublets, Benson and Johnson 1966

d Least Squares Adjustment, Benson and Johnson 1966

e Measured doublet, Benson and Johnson 1966

f Macdougall et al 1970

g Whineray et al 1970

Figure S-1a

Spectrum of $ExCl_2$

The total intensity has been normalized to 100%, and plotted on a 4-cycle semi-log scale.

Figure S-1b

Spectrum of $YbCl_2$

The total $YbCl_2$ intensity has been normalized to 100%. The $^{169}TmCl_2$ and $^{171}TmCl_2$ peaks are shown there with their approximate relative intensity. Again, a 4-cycle semi-log scale is used.

FIGURE 5 - 1a, b

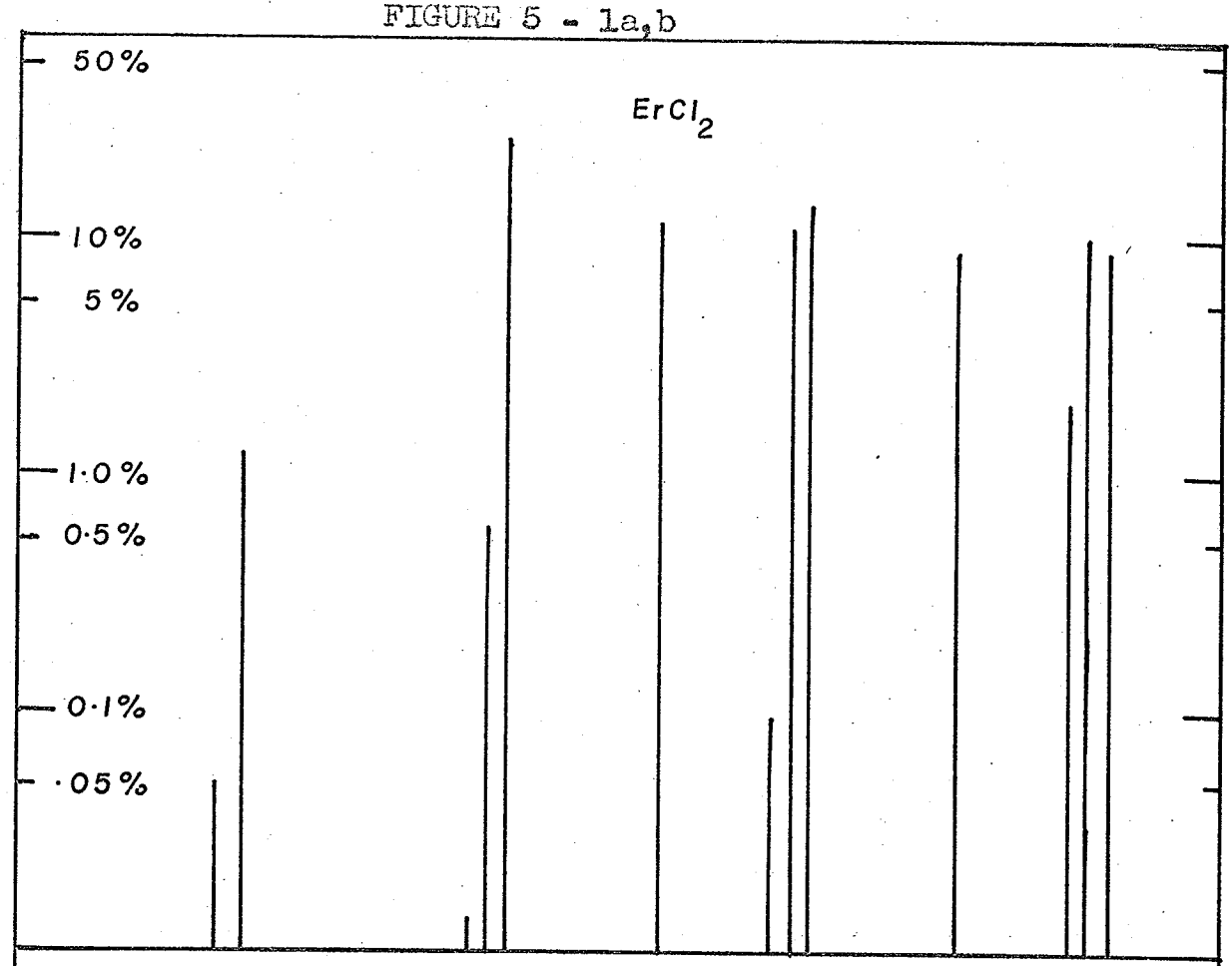
50%
ErCl2
10%
5%
1·0%
0·5%
0·1%
·05%
234
236
237
238
239
240
Mass Number

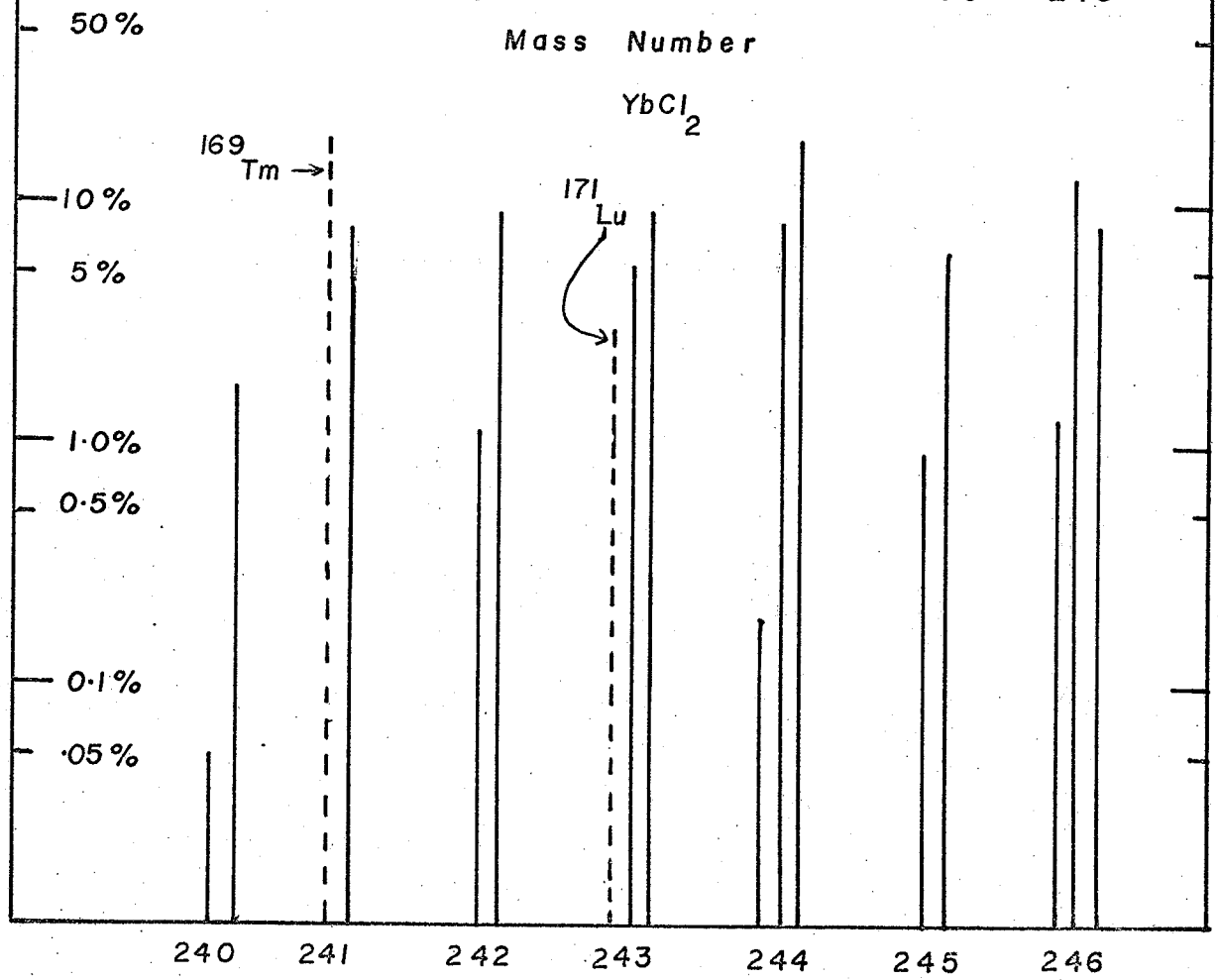
50%
YbCl2
169
Tm
171
Lu
10%
5%
1·0%
0·5%
0·1%
·05%
240
241
242
243
244
245
246

Figure 5-2a

Comparison of Results, Manitoba & McMaster

The open circles with dashed errors bars represent the adopted values of Table 5-I minuss the raw Manitoba results. The solid dots with solid error bars are Adopted-McMaster.

Figure 5-2b

Comparison of Results with Other Data

Note that the scale has changed by a factor of 10. See Table 5-I for the actual data and references.

FIGURE 5 - 2a, b

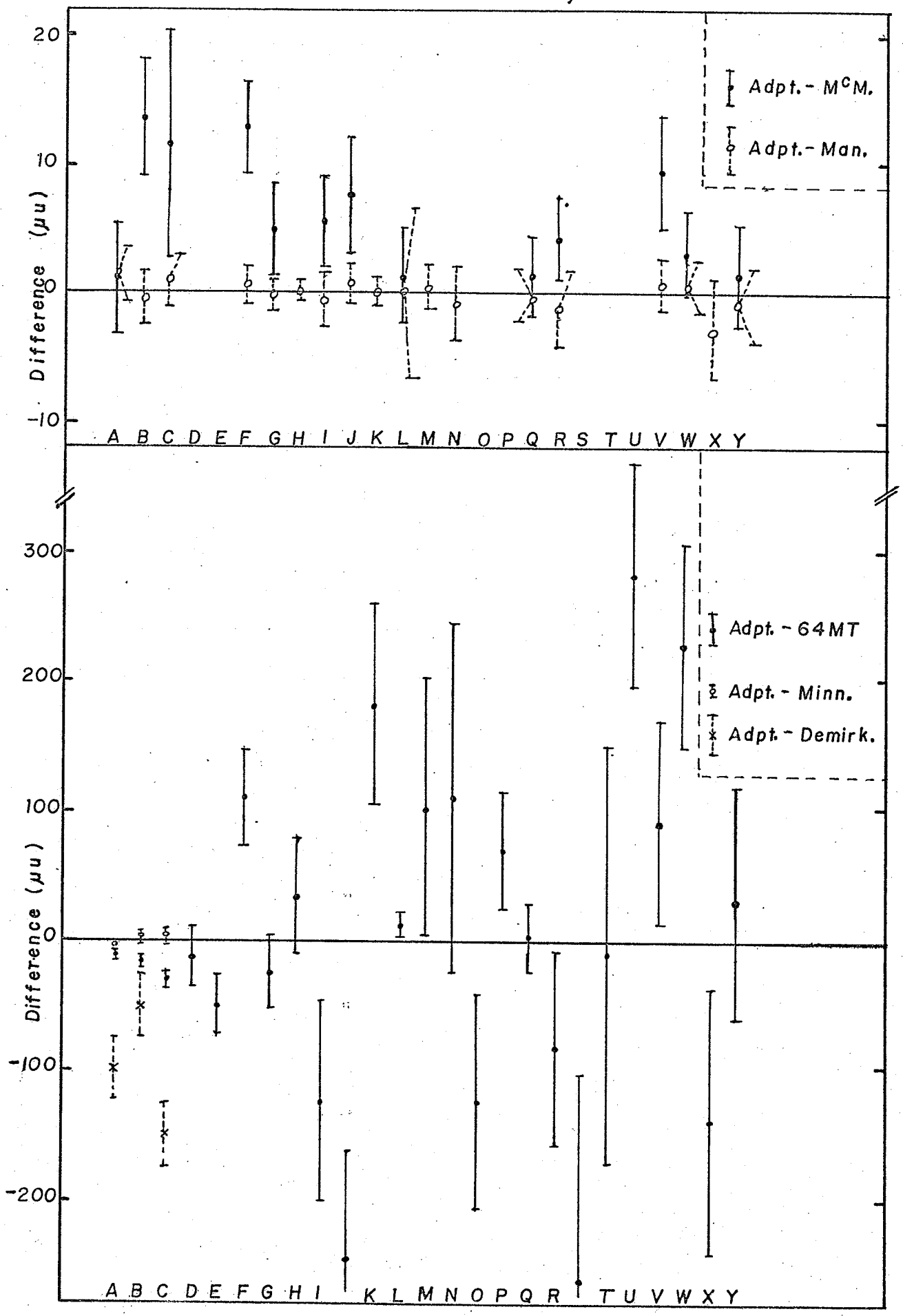
20
10
0
-10
Difference (μu)
Adpt. - M^cM.
Adpt. - Man.
A B C D E F G H I J K L M N O P Q R S T U V W X Y
300
200
100
0
-100
-200
Difference (μu)
Adpt. - 64MT
Adpt. - Minn.
Adpt. - Demirk.
A B C D E F G H I K L M N O P Q R T U V W X Y

CHAPTER 6

LEAST SQUARES ADJUSTMENT OF THE ATOMIC MASSES $68 \leq Z \leq 72$

The precise atomic mass differences reported in the previous chapter are combined with existing nuclear reaction and decay Q-values and atomic mass data in a least squares adjustment of the atomic masses. For nuclides in the region $58 \leq Z \leq 72$ the quantities S_{2n}, S_n, P_n, S_{2p}, S_p, P_p, $Q(\beta^-)$ and $Q(\alpha)$ are calculated where possible.

Introduction

In 1964 (Barber et al, 1964 , Duckworth et al, 1964) a series of precise atomic mass differences involving nuclides in the region $N \sim 90$ were reported by the research group at McMaster University. These data provided an accurate picture of the mass effect associated with the onset of nuclear deformation. This work has been extended (Duckworth et al, 1969) to provide a picture of the variation of the mass surface between the 82 and 126 neutron shells.

Using the second-order double-focusing mass spectrometer (see Paper I, Barber et al, 1971a), we have continued a programme of determining precise atomic mass difference

in the rare-earth region. The results for $59 \leq Z \leq 69$ have been reported in Paper II (Barber et al, 1971b)and have been combined with existing nuclear reaction and decay Q-values in Paper III (Meredith et al, 1971).

In a similar manner, the results of Chapter 5, i.e. $68 \leq Z \leq 71$, plus doublets for $Z = 72$ (Southon, 1971) are combined here with a large, but incomplete, body of Q-values. This allows a comparison and evaluation of the data which derive from different types of experiments, allows the calculation of unknown Q-values and results in 'best' values for both measured and calculated Q-values.

Since many atomic mass differences are overdetermined, we have followed the lead of Mattauch (1960) and his co-workers, and carried out a least squares adjustment of the atomic masses for the region $68 \leq Z \leq 72$.

Details of the Calculation

Method - The general method of least squares has been extensively described, starting with Gauss, and used recently by Taylor et al (1970) for evaluation of the fundamental constants. The method is also presented in Appendix A, using matrix notation for the final result, and there it is in a form for convenient solution by a digital computer. Here, we will simply note that any mass difference, or Q-value can be expressed as the difference of two masses M_i

and M_j. Thus the experimental values may be regarded as a set of N linear combinations of the atomic masses.

$$\sum_{j=1}^{n} A_{Ij} M_j = y_I \qquad I = 1,2, \ldots N \text{ and } j = 1,2, \ldots n.$$

and the coefficients A_{Ij} are in general 0 or ± 1. Each experimental y_I has an associated error σ_I, and to each observational equation above, we assign a weight $\omega_I = 1/\sigma_I^2$. We also define a residual, $r_I = \sum_{j=1}^{n} A_{Ij} M_j^* - y_I$ of the N observational equations, and minimize the sum of the squares of the residuals, multiplied by the appropriate weight, i.e. the solution is that for which $\chi^2 = \sum_{I=1}^{n} \omega_I r_I^2$ is a minimum.

Presentation of Input - In the present work, there are approximately 60 masses in the region $68 \leq Z \leq 72$, with a total of 20 mass spectroscopic differences, 36 β-decays, 33 induced reactions, and 3 alpha decays linking the 60 nuclides.

Figure 6-I shows the nuclides in the region, the links between them, and the label for each mass difference. The mass spectroscopic links are indicated by lower case letters, β-decay Q-values by b_1, b_2, etc., α-decay Q-values by a_1, a_2, a_3 and neutron separation energies by r_1, r_2, etc.

The adopted values of mass spectroscopic differences are shown in Table 6-I. This differs from Table 5-I in that the lower Z mass differences are not present, and four

doublets in HfCl have been included from Southon (1971). The anticipated link '1' is not yet available. Also, the simple closed loops have not been adjusted as they were in the previous Chapter, since all the input to the adjustment of the atomic masses must be linearly independent.

Table 6-II shows the adopted constants needed to reduce the data in Table 6-I and in subsequent tables to the required form for the adjustment.

The adopted values of the mass spectroscopic mass differences are given in Table 6-III in terms of an energy in keV and the neutron rest mass, n. Also given are the output values, the residual, r_I, and the quantity $(r_I/\sigma_I)^2$, i.e. the contribution of each value to χ^2.

Nuclear reaction Q-values which lead to the determination of the neutron separation energy are compiled in Table 6-IV. Where there is more than one measurement of the same mass difference, a weighted mean is calculated and given as the 'input': The error is the larger of σ_{int} or σ_{ext} as defined by Birge (1932). Again, the residuals, and contribution to χ^2 are shown for comparison.

Table 6-V presents β^-, β^+ and e,c, Q-values in a smiliar manner, and α-decay Q-values are given in Table 6-VI.

This adjustment (Fig. 6-1) overlaps the previous one of Paper III. See Fig. 6-2 for comparison. All of erbium is included, as are the few precise data ir holmium.

Thus, the mass of all erbium isotopes will be re-evaluated, (and not change significantly), and the re-evaluation of the mass of thulium isotopes will reflect the precise mass differences in both erbium and ytterbium. In addition, the mass of ^{172}Er can now be calculated. At the other end, the only precise link to tantalum has been used to calculate the mass of ^{182}Hf.

The absolute masses used are ^{162}Er as calculated in Paper III, and ^{168}Yb, calculated from the mass spectroscopic doublet of Chapter 5, and the mass of ^{164}Dy from Paper III. These two masses are given as mass excesses in Table 6-VII.

Discussion of Input - The closed loops formed by the mass spectroscopic differences in Table 6-III have already been shown to be consistent in Chapter 5. Reference to Table 6-VIII will indicate that they are also consistent with all the other reaction and decay Q-values. The average residual, that is, the average amount by which the differences were adjusted is -0.8±0.7 keV and the contribution to χ^2 is 16.1 for 20 values.

In the preliminary adjustment of the differences, the reaction Q-values of Table 6-IV needed further examination. First for r_{26} the average, i.e. 6980 ±65 keV had been used. It was now possible to choose 7072.7±2.0 as the input value and reject 6890.3±2.0 on the assumption that the ground

state transition was not observed. Secondly, the value of 7770±50 for r_{24} was eliminated on similar grounds. Even after these modifications, the contribution to χ^2 was 90.2, very large for 26 values. It was noted that nearly all of this came from the seven data with errors <1.0 keV due to the presence of very precise (n,γ) reactions. These values were changing by 1.0 to 3.0 keV randomly, but since the input errors were 0.3 to 0.7 keV, the $(r_I/\sigma_I)^2$ were 4 to 12 for each. That is, in spite of their very high weight, these data were changed considerably more than their quoted errors. A similar but much smaller effect was commented on in Paper III. In this case, a consistency factor (Appendix A) of 1.4 was applied to this set of seven input values. The increased value of σ_I is noted in Table 6-IV, and the new contribution to χ^2 is 21.2 as in Table 6-VIII.

Of the 36 β-decay Q-values in Table 6-V, only 9 were in the preliminary overdetermined set. Two of these, b_9 and b_{29} changed by very large amounts (i.e. $(r_I/\sigma_I)^2$ >25), and were judged inconsistent. They were not used as input to the final adjustment, but their output values are very similar to those of the original adjustment.

The α-decay Q-values in Table 6-VI are presented for completeness. Only one enters the adjustment, and since b_{29} was not used as input, even a_3 does not form part of the overdetermined set. The mass of ^{175}Hf is determined solely

by the values of a_3 and r_{23}. This point will be discussed more fully when the figures for separation and pairing energies are examined

At this point it is interesting to look at the calibration between nuclear reaction and decay Q-values as determined by measuring the energies of particles against to ^{210}Po α-particle as mentioned in Chapter 2, and by measuring γ-ray energies. A recent paper by Stocker et al (1971) measured the first excited state of ^{24}Mg with inelastic deuteron scattering. The result using the polonium calibration energy is consistent with the γ-ray energy to .5 keV or 0.04%

The position of the mass surface was set for this adjustment by using the previously calculated (Paper III) mass excess for ^{162}Er. Also, the mass difference ^{168}Yb^{37}Cl$_2$ - ^{164}Dy^{35}Cl$_2$ was presented in the previous Chapter. If this is combined with the previously adjusted mass excess for ^{164}Dy (Paper III) and the necessary data in Table 6-II, then the mass excess of ^{168}Yb can also be used in this adjustment.

Effects at each end of the adjustment have been minimized by including precise links to holmium and tantalum, but these do not appear in the output.

Results

The results of the least squares adjustment are presented in Tables 6-IX, 6-X, 6-XI and 6-XII. The output of the ad-

justment of Paper III is given in Tables 6-IX and 6-X, while the similar quantitites for the present adjustment are given in Tables 6-XI and 6-XII. Where quantities are missing for erbium and thulium in the first two Tables, they are given wherever possible in the second two Tables. Where quantities are not calculable in the present adjustment, but were in the first, the second two Tables show the reference 'a'. Errors are to two significant figures for 1.0 to 4.9 and 10 to 49, and to one figure for 5-9 and 50 to 90.

In Tables 6-IX and 6-XI, we give the nucleon separation and pairing energies calculated from the following definitions:

$$S_{2n}(Z,N) = 2n - [M(Z,N) - M(Z, N-2)]$$

$$S_{n}(Z,N) = n - [M(Z,N) - M(Z,N-1)]$$

$$P_{n}(Z,N) = (-1)^{N} \tfrac{1}{2}\{S_{n}(Z,N) - \tfrac{1}{2}[S_{n}(Z,N+1) + S_{n}(Z,N-1)]\}$$

for even Z only.

$$S_{2p}(Z,N) = 2M_{H} - [M(Z,N) - M(Z-2,N)]$$

$$S_{p}(Z,N) = M_{H} - [M(Z,N) - M(Z-1,N)]$$

$$P_{p}(Z,N) = (-1)^{Z} \tfrac{1}{2}\{S_{p}(Z,N) - \tfrac{1}{2}[S_{p}(Z+1,N) + S_{p}(Z-1,N)]\}$$

for even N only.

In Tables 6-X and 6-XII we give the Q-values for β^--decays, α-decays and also the mass excesses in keV and μu. From the mass excesses any other mass differences may be calculated. An upper limit for the error on the difference is found by a rms combination of the errors of the two masses. If the co-variance matrix were available, (see Appendix A), the error would be smaller if the two masses were correlated.

Double-neutron separation energies (S_{2n}) - All of the S_{2n} values in Tables 6-IX and -XI are plotted in Figs. 6-3a and 6-3b for even-N and odd-N respectively.

The features of the even-Z, even-N curves (part of Fig. 6-3a) for N$\sim$90 were published earlier (Barber et al, 1964; Duckworth et al, 1964, Macdougall et al, 1966, and Macdougall et al, 1970) at which time attention was drawn to the major discontinuity in slope at N=88, the apparent charge dependence of the effect, and the suggestion that the slopes for N>92 are similar to those for N<88. The regularity of these even-even curves for 92<N<126 was subsequently commented on (Duckworth et al, 1969, Whineray et al, 1970, McLatchie et al, 1970).

Here the addition of the odd-Z data in Fig. 6-3a emphasizes the regularity for N<88 and N>92. Also several points have been added, extending the curves for each element. On the basis of these regularities, the broken lines in Figs. 6-3a and 3b indicate the probable locations of points with large

errors. The values for $^{148}_{64}Gd$ and $^{152}_{66}Dy$ in Fig. 6-3a are correlated in the manner required, and are largely determined by the Q-value for $^{146}Gd(e.c.)^{146}Eu$. The β-decay systematics suggest that this value might be 500 keV too high; i.e. in agreement with our suggested values. In Fig. 6-3b the points for $^{154}_{65}Tb$ and $^{152}_{65}Tb$ are correlated in the required manner for our suggested values, and if the Q-value for ^{152}Tb $(\beta+)^{152}Gd$ were too large by ∿300 keV (as also indicated by β-decay systematics), the points would fall as indicated. The S_{2n} value for $^{160}_{63}Eu$ is not shown to avoid confusion due to a large error (∿500 keV).

As we have noted previously (Duckworth et al 1969) and Paper III, the energy of deformation for nuclides with N=90 is relatively small for neodymium, and increases in going to samarium and gadolinium. Fig. 6-3a suggests that the point at N=88 for dysprosium is higher than expected, and may already have a ground state deformation. By N=92 all the elements seem to behave similarly, and segments of adjacent curves between any two neutron numbers are almost parallel. It is suggested that the ground state deformation starts after N=88 and is complete by N=92 for Z=60, and the effect of the distortion at N=90 becomes stronger as Z increases, until Z=66, there is some distortion at N=88.

A similar effect is noticed in Fig. 6-3b, as the line segments N=87 to 89 become less steep with increasing Z.

By N=91 all nuclides have reached approximately the same energy of defromation.

Below N=88, the odd-Z curves lie equidistant between the even-Z curves (Fig. 6-3a). After N=92, the odd-Z curves are displaced upwards ∿120 keV relative to the even-Z curves. Thus, nuclei with un-paired protons tend to have a higher energy of deformation. The effect is almost gone by N=96, and has disappeared by N=100.

Between N-106 and 108 both the lutetium and hafnium curves turn upwards slightly, but then from N=108 to 110, the curve resumes its downward trend.

Single Neutron Separation Energies (S_n) - Figs.6-4a and 4b show the variation of S_n as a function of neutron number for even-N and odd-N respectively. The general features have been commented on before, but we shall note here that for even-N (Fig.6-4a), the curves for odd-Z nuclides lie next to the even-even curve Z-1 for N<88, but that with the onset of deformation the curves separate and are more or less equidistant for $92 \leq N \leq 98$. That is, neutron-proton pairing is important before deformation starts and again for N>100. In Fig.6-4b, below N=88, the odd-Z curves lie next to the even-Z curves Z+1. This seems to hold through the onset of deformation and perhaps further. The curve for holmium is the only one that seems to separate from the curve above it (erbium, Z=68).

That is, for odd-odd nuclides, the neutron-proton pairing persists well past the region where deformation is established.

Neutron Pairing Energies (P_n) - The plots of P_n vs. N (Fis. 6-5a,b) are already well known, but there are some differences from Bishop (1969), Duckworth et al (1969), Benson and Johnson (1966) and Whineray (1970). The major feature is the sharp maximum near N=90 for even-N and N=89 for odd-N. Re-evaluation of the input data (Paper III) has resulted in the curve for gadolinium moving upwards to lie close to those for samarium and dysprosium, and the curve for neodymium definitely lying lower for N=88 to 91. Except for the behaviour of neodymium, the neutron pairing energy has little dependence on Z through the region of deformation.

After N=92, the curves, while still decreasing, split apart, and as Z increases, become less steep. Whineray (1970) points out that the curve for hafnium is almost flat, but here we see that it does not appear much different from those of lower Z until N=106. This is due to the choice of r_{27} rather than b_{29} to determine the mass defect of ^{175}Hf. Since r_{27} is very recent work (Alenius, 1971), Whineray had no reason to suspect that b_{29} might be in error.

Proton Separation Energies (S_{2p}, S_p) - These are plotted in Figs. 6-6a,b, - 7a,b. The behaviour of all curves is quite

regular, and indicates (i) no major errors or discrepancies in the data, and (ii) regular behaviour of the proton states while the neutron states are undergoing deformation. The displacement in Figs. 6-7a and 7b of the odd-Z curves towards Z-1 for even-N and towards Z+1 for odd-N is more evidence of neutron-proton pairing.

Proton Pairing Energy (P_p) - When P_p was plotted as a function of Z (as was done for the proton separation energies), no systematic behaviour was noticeable. (See for example, Benson and Johnson 1966). However, when P_p is plotted against N as in Fig.6-8, certain features became apparent. In the region of spherical nuclei, $N<88$, the proton pairing energy is 1.2 - 1.5 MeV. At N=88, there is a sharp decrease which appears the same for all elements. After the transition region, there is again a Z dependence, and the average pairing energy is much lower than that for spherical nuclei.

References for Chapter 6

Ageev, A. (1964) Izv. Akad. Nauk. SSSR 20, 60

Alenius,G., Arnell, S.E., Schale, C., Wallander, E. (1971) Nucl. Phys. A161, 209

Arlt, R., Malek, Z. Musiol, G. Pfrepper, G. and Strusny, M. (1970) Bull. Acad. Sci. USSR Phys. Ser. 33, 1133

Balalaev, V.A., Dzhelepov, B.S., Medvedev, A.I. Ter-Nersesyants, V.E., Uchevatkin, I.F. and Shestopalova, S.A. (1970) Bull. Acad. Sci. USSR, Phys. Ser. 34, 1

Barber, R.C., Duckworth, H.E., Hogg, B.G., Macdougall, J.D., McLatchie, W. and van Rookhuyzen, P. (1964) Phys. Rev. Lett. 12, 597

Barber, R.C., Bishop, R.L., Duckworth, H.E., Meredith, J.O., Southon, F.C.G., van Rookhuyzen, P. and Williams, P. (1971a) Rev. Sci. Instrum. 42, 1. (Paper I)

Barber, R.C., Bishop, R.L., Duckworth, H.E., Meredith, J.O., Southon, F.C.G., van Rookhuyzen, P. and Williams, P. (1971b) Can. J. Phys. (to be published) Paper II

Bartholomew, G.A. (1957) AECL, No. 517

Benson, J.L. and Johnson, W.H. Jr. (1966) Phys. Rev. 141,1112

Berthal, F.H., Rasmussen, J.O. and Hollander, J.M. (1971) Phys. Rev. C3, 1294

Bichard, J.W., Mihelich, J.W. and Harmatz, B. (1959) Phys. Rev. 116, 720

Birge, R.T. (1932) Phys. Rev. 40,207

Bishop, R.L. (1969) Ph.D. Thesis. University of Manitoba

Bollinger, L.M. and Thomas, G.E. (1970) Phys.Rev. C2, 1951

Bondarenko, W., Kramer, N. Prokofjew, P., Manfrass, P. Andreeff, A. and Kastner, R. (1967) Nucl. Phys. A102, 577

Bunch-Osmalovskaya, N.A., Ballund, H., Plochocki, A., Preibisz, K. and Zglinski, A.(1971), Nucl. Phys. A162, 305

Burke, D.G., Zeidman, B., Elbek, B., Herskind, B. and Oleson, M. (1966) M.F.M.D.V.S. 35, No. 2

Charvet, A., Duffait, R., Emsallem, A. and Chery, R. (1970) Nucl. Phys. A156, 276

Dewdney, J.W. and Bainbridge, K. T. (1965) Phys. Rev. 138,8540

Duckworth, H.E., Barber, R.C., Hogg, B .G., Macdougall, J.D., McLatchie, W. and van Rookhuyzen, P. (1964) Congres Int'l. de Physique Nucleaire, Vol. II (Gugenberger, Ed.) Centre National de la Recherche Scientifique, Paris, p. 557

Duckworth, H.E., Barber, R.C., van Rookhuyzen, P. Macdougall, J.D., McLatchie, W., Whineray, S., Bishop, R.L., Meredith, J.O., Williams, P., Southon, F.C.G., Wong, W., Hogg, B.G. and Kettner, M.E. (1969) Phys. Rev. Lett. 23, 592

Erskine, J.R. and Buechner, W.W. (1964) Phys. Rev. 133, B370

Funke, L., Graber, H., Kaun, K.H., Sudan, H. and Werner, L. (1965) Nucl. Phys. 70, 347

Gastebois, J., Barloutaud, M., Laget, J.M. and Quirdort, J. (1966) Phys. Letters 20, 669

Groshev, L.V., Demidov, A.M. Ivanov, V.A. Lutsenki, V.N. and Pelekhov, V.I. (1964) Izv. Akad. Nauk SSSR, Ser. Fiz 28, 1244

Gujrathi, S.C. and D'Auria, J.M. (1971) Nucl. Phys. A161,410

Johansen, H.S. Jørgensen, M. Nielsen, O.B. and Sidenius, G., (1964) Phys. Lett. 8, 61

Katakuse, I., Nakabushi, H. and Ogata, K. (1970) Mass Spectroscopy (Tokyo) 18, 1276

Kuroyanagi, T., Yuta, H., Takahashi, K. and Morinaga, H. (1961) J. Phys. Soc. Jap. 16, 2393

Liukkonen, E. and Kantele, J. (1968) Z. Phys. 208, 208

Macdougall, J.D., McLatchie, W., Whineray, S. and Duckworth, H.E. (1966) Z. Naturforschg. 21a, 63

Macdougall, J.D., McLatchie, W., Whineray, S. and Duckworth, H.E. (1970) Nucl. Phys. A145, 223

Matsuda, H. and Matsuo, T. (1968) J. Phys. Soc. Japan 25, 950

Mattauch, J.H.E. (1960) Proc. Int'l. Conf. on Nuclidic Masses (Duckworth, Ed.) University of Toronto Press, p.3

Mattauch, J.H.E., Thiele, W. and Wapstra, A.H. (1965,a,b,c) Nucl. Phys. 67, 1, 32, 73

McLatchie, W., Whineray, S., Macdougall, J.D. and Duckworth, H.E. (1970) Nucl. Phys. A145, 244

Meredith, J.O., Barber,R.C. and Duckworth, H.E. (1971) to be published (Paper III)

Michaelis, W. private communication to NDS (1967) A5

Minor, M.M., Sheline, R.K. and Jurney, E.T. (1971) Phys. Rev. C3, 766

Namenson, A., Jackson, H.E. and Smither, R.K. (1966) Phys. Rev. 146, 844

Namenson, A.I. and Ritter, J.C. (1969) Phys. Rev. 183, 983

Orth, C.J., Bunker, H.E. and Starner, J.W. (1963) Phys. Rev. 116, 720

Rasmussen, N.C. private communication to NDS (1967) A5

Rickey, F.A. and Sheline, R.K. (1968) Phys. Rev. 170, 1157

Smith, W.G., Robinson, R.L., Hamilton, J.M. and Langer, L.M. (1957) Phys. Rev. 107, 1314

Smith, E.G. (1971) Phys. Rev. C4, 22

Southon, F.C.G. (1971) Ph.D. Thesis, University of Manitoba

Stevens, C.M. and Moreland, P.E. (1970) Recent Developments in Mass Spectroscopy, University of Tokyo Press, p.1296

Stocker, H., Rollefson, A.A. and Hrejsa, A.F. (1971) Phys. Rev. C (to be published)

Struble, G.L. and Sheline, R.K. (1967) Yadern. Fiz. 5, 1205

Swindle, D.L., Ward, T.E. and Kuruda, P.K. (1971) Phys. Rev. C3, 259

Takahashi, K., Kuroyanagi, T., Yuta, H., Kotajima, K., Magatini, K. and Morinaga, H. (1961) J. Phys. Soc. Japan 16, 1664

Tamura, T. (1965) Nucl. Phys. 62, 305

Taylor, B.H., Parker, W.H. and Langenberg, D.N. (1970) The Fundamental Constants and Quantum Electrodynamics, Academic Press, New York

Tjøm, P. and Elbek, B. (1969) M.F.M.D.V.S. 37, 7

Vergnes, M.N. and Sheline, R.K. (1963) Phys. Rev. 132,1736

Whineray, S., Macdougall, J.D., McLatchie, W. and Duckworth, H.E. (1970) Nucl. Phys. A151, 377

Wing, J., Swartz, B.A. and Huizenga, J.R. (1961) Phys. Rev. 121, 1758

Table 6-I

Mass Spectroscopic Mass Differences

Code	Doublet	ΔM(μu) This Work	ΔM(μu) McMaster	Ref.	ΔM(μu) Adopted
a	$^{179}Hf^{35}Cl - ^{177}Hf^{37}Cl$	* 5543.5±0.7	5539±3	a	5543.3±1.0
b	$^{175}Lu^{35}Cl - ^{173}Yb^{37}Cl$	5505.5±3.2	5503±4	a	5504.5±2.5
c	$^{173}Yb^{35}Cl - ^{171}Yb^{37}Cl$	4835.0±2.1	4827±4	a	4835.2±3.3
d	$^{171}Yb^{35}Cl - ^{169}Tm^{37}Cl$	5061.2±1.7	5055±3	a	5059.7±1.7
e	$^{173}Yb^{25}Cl_2 - ^{169}Tm^{37}Cl_2$	9896.8±1.2			9896.8±1.2
f	$^{169}Tm^{35}Cl - ^{167}Er^{37}Cl$	5111.9±1.0	5107±3	b	5111.4±1.2
g	$^{167}Er^{35}Cl - ^{165}Ho^{35}Cl$	4678.3±1.1	4666±3	b	4676.8±4.0
h	$^{169}Tm^{35}Cl_2 - ^{165}Ho^{37}Cl_2$	9790.6±0.6			9790.6±0.6
i	$^{180}Hf^{35}Cl - ^{178}Hf^{37}Cl$	* 5796.8±0.8	5797±3	a	5796.8±0.8
j	$^{178}Hf^{35}Cl - ^{176}Hf^{37}Cl$	* 5237.8±1.1	5236±5	a	5237.7±1.1
k	$^{180}Hf^{35}Cl_2 - ^{176}Hf^{37}Cl_2$	*11033.5±1.8			11033.5±1.8
l	$^{176}Hf^{35}Cl - ^{174}Hf^{37}Cl$				
m	$^{176}Yb^{35}Cl - ^{174}Yb^{37}Cl$	6655.2±1.0	6652±3	a	6654.7±1.2
n	$^{174}Yb^{35}Cl - ^{172}Yb^{37}Cl$	5429.2±1.2	5420±4	a	5428.7±1.7
o	$^{176}Yb^{35}Cl_2 - ^{172}Yb^{37}Cl_2$	12087.9±3.4			12087.9±3.4
p	$^{172}Yb^{35}Cl - ^{170}Yb^{37}Cl$	4563.9±2.0			4563.9±2.0
q	$^{170}Yb^{35}Cl - ^{168}Yb^{37}Cl$	3801.1±1.7			3801.1±7.7
r	$^{170}Er^{35}Cl - ^{168}Er^{37}Cl$	6045.4±1.7	6040±3	b	6044.1±2.3
s	$^{168}Er^{35}Cl - ^{166}Er^{37}Cl$	5027.6±1.4	5026±3	b	5027.3±1.3
t	$^{166}Er^{35}Cl - ^{164}Er^{37}Cl$	4039.9±1.3			4039.9±1.3
u	$^{164}Er^{35}Cl - ^{162}Er^{37}Cl$	3372.5±1.3			3372.5±1.3

* Southon (1971)

a) Whineray et al (1970)

b) Macdougall et al (1970)

TABLE 6-II

Values of Constants

	Experimental		Adopted
$^{37}Cl-^{35}Cl$			
	1.997 048 89	±59 u[a]	
	049 7	±60 u[b]	
	050 59	±42 u[c]	1.99704972 ±9u
	049 711	± 63u[d]	
$^{1}_{1}H$	1.007 825 055	± 40u[c]	
	825 220	± 30u[b]	
	825 190	± 80u[e]	
	825 029	± 5u[d]	1.007825035±14u
	824 990	±140u[h]	
	825 005	± 49u[i]	
$^{4}_{2}He$			4.0026031 ±4u[e]
$^{1}_{0}n$			1.0086652 ±1u[f]
Mass to Energy Conversion			0.931481 ±5 $\frac{keV}{\mu u}$[f]
$S_n(^{2}_{1}H)$			2224.5 ± 0.1 keV[g]
$S_n(^{3}_{1}H)$			6257.4 ± 0.1 keV[g]

a) Dewdney and Bainbridge, 1965

b) Benson and Johnson, 1966

c) Stevens and Moreland, 1970

d) Smith, 1971

e) Mattauch et al, 1965a

f) Taylor et al, 1969

g) Mattauch et al, 1965b

h) Matsuda and Matsuo, 1968

i) Katakuse et al, 1970

TABLE 6-III

Mass Spectroscopic Input

Code	Nuclide	Input (keV)	Output (keV)	r_I (keV)	$(r_I/\sigma_I)^2$
a	^{179}Hf-^{177}Hf	2n-13727.6±0.9	13727.6±0.9	-0.0	0.00
b	^{175}Lu-^{173}Yb	2n-13763.7±2.3	13762.7 2.2	-1.0	0.19
c	^{173}Yb-^{171}Yb	2n-14389.0±3.1	14388.6 1.6	-0.4	0.02
d	^{171}Yb-^{169}Tm	2n-14178.1±1.6	14176.1 1.3	-2.0	1.56
e	^{173}Yb-^{169}Tm	4n-28563.5±1.3	28564.7 1.2	1.2	0.85
f	^{169}Tm-^{167}Er	2n-14129.9±1.1	14128.2 1.0	-1.7	2.39
g	^{167}Er-^{165}Ho	2n-14534.7±3.7	14533.6 1.1	-1.1	0.09
h	^{169}Tm-^{165}Ho	4n-28662.4±0.7	28661.8 0.7	-0.6	0.73
i	^{180}Hf-^{168}Hf	2n-13491.5±0.8	13490.6 0.7	-0.9	1.26
j	^{178}Hf-^{176}Hf	2n-14012.2±1.0	14012.6 0.9	0.4	0.16
k	^{180}Hf-^{176}Hf	4n-27504.6±1.7	27503.2 1.0	-1.4	0.68
l	^{176}Hf-^{174}Hf		14862 22	-	-
m	^{176}Yb-^{174}Yb	2n-12692.3±1.1	12692.0 1.0	-0.2	0.03
n	^{174}Yb-^{172}Yb	2n-13834.3±1.6	13834.0 1.4	-0.3	0.03
o	^{176}Yb-^{172}Yb	4n-26522.5±3.2	26526.0 1.6	3.5	1.20
p	^{172}Yb-^{170}Yb	2n-14639.9±1.9	14638.9 1.7	-1.0	0.28

q	^{170}Yb-^{168}Yb	2n-15350.4±7.2	15338.0±5.6	-12.4	2.97
r	^{170}Er-^{168}Er	2n-13261.1±2.1	13263.7 1.7	2.4	1.53
s	^{168}Er-^{164}Er	2n-14208.2±1.2	14207.6 0.8	-0.6	0.25
t	^{166}Er-^{164}Er	2n-15128.0±1.2	15128.9 1.2	0.9	0.56
u	^{164}Er-^{162}Er	2n-15749.7±1.2	15748.3 1.2	-1.4	1.36

TABLE 6-IV

NEUTRON SEPARATION ENERGY DATA

CODE	NUCLIDE	REACTION	REF	Q-VALUE (keV)	INPUT (keV)	OUTPUT (keV)	r_I (keV)	$(r_I/\sigma_I)^2$
r_1	^{166}Ho	(d,p),(n,γ)	a	--	6243.4±0.9	-	-	-
r_2	^{162}Er	(d,t)	b	9215 ±10	9215 ±10 1.3+	9215 ± 10	0.0	0.00
r_2	^{163}Er	(d,p)	b	6904 ±10	6904 ±10	6901 ± 7	-3.0	0.09
r_4	^{164}Er	(d,t)	b	8851 ±10	8851 ±10	8849 ± 7	+2.0	0.04
r_5	^{165}Er	(d,p)	b	6657 ±10				
		(n,γ)	c	6650.1± 0.7				
					6650.1± 0.7 1.0	6650.8± 1.0	+0.7	0.49
r_6	^{166}Er	(d,t)	a	--	8474.5± 7.1	8477.4± 1.5	+2.9	0.17
r_7	^{167}Er	(d,p),(n,γ)	a	--	6436.2± 0.5	6435.5± 0.7	-0.7	0.77
r_8	^{168}Er	(d,p),(d,t),(n,γ)	a	--	7771.0± 0.7 0.8	7772.1± 0.8	+2.1	4.41
r_9	^{169}Er	(d,p),(d,t),(n,γ)	a	6003.1± 0.3				
		(n,γ)	c	6002.7± 0.8				
					6003.0± 0.3 1.0	6003.2± 0.4	+0.2	0.16
r_{10}	^{170}Er	(d,t)	a	--	7263.4± 9.5 0.5	7259.4± 1.8	-4.0	0.18

TABLE 6-IV cont'd.

CODE	NUCLIDE	REACTION	REF	Q-VALUE (keV)	INPUT (keV)	OUTPUT (keV)	r_I (keV)	$(r_I/\sigma_I)^2$
r_{11}	^{171}Er	(d,p)	a	5678.7± 5.8				
		(n,γ)	d	5681.5± 0.5				
					5681.5± 0.5 0.8	5681.7± 0.7	+0.2	0.06
r_{12}	^{169}Tm	(γ,n)	a	--	8055 ±55	8055 ±55	-	
r_{13}	^{170}Tm	(d,p),(n,γ)	a	--	6595.0± 2.5	6529.9± 2.2	-2.1	0.71
r_{14}	^{168}Yb	(d,t)	e	--	9055 ±12	9055 ±12	-	0.12
r_{15}	^{169}Yb	(d,p)	e	6861 ±12				
		(n,γ)	f	6859 ± 4				
					6859.2± 3.8	6860.5± 3.7	+1.3	0.12
r_{16}	^{170}Yb	(d,t)	e	--	8469 ±12	8479 ± 6	+10.3	0.74
r_{17}	^{171}Yb	(d,t)	e	6617 ±12				
		(d,p)	e	6614 ±12				
					6615.5± 8.5	6177.7± 2.3	+2.2	0.07
r_{18}	^{172}Yb	(d,t)	e	8030 ±12				
		(d,p)	e	8021.5±12				
					8025.8± 8.5	8020.1± 1.7	-5.7	0.45

TABLE 6-IV cont'd.

CODE	NUCLIDE	REACTION	REF	Q-VALUE (keV)	INPUT (keV)	OUTPUT (keV)	r_I (keV)	$(r_I/\sigma_I)^2$
r_{19}	^{173}Yb	(d,t)	e	6372 ±12				
		(d,p)	e	6369.5±12				
		(n,γ)	g	6365 ± 3				
		(n,γ)	d	6367.3± 0.5				
					6367.2± 0.5 0.8	6367.5± 0.7	+0.3	0.14
r_{20}	^{174}Yb	(d,t)	e	7476 ±12				
		(d,p)	e	7463.5±12				
					7469.8± 8.5	7466.4± 1.6	-3.4	0.16
r_{21}	^{175}Yb	(d,p)	e	5820 ±12				
		(n,γ)	h	5822 ± 5				
					5821.7± 4.6	5822.6± 4.0	+0.9	0.04
r_{22}	^{176}Yb	(d,t)	e	--	6879 ±12	6868.5± 4.1	-10.5	0.77
r_{23}	^{177}Yb	(d,p)	i	5565 ±16				
		(d,p)	e	5561.5±12				
					5562.8± 9.6	5565.9± 8.8	+3.1	0.10
r_{24}	^{175}Lu	(γ,n)	j	7770 ±50	*	7670 ±11	-	-

TABLE 6-IV cont'd.

CODE	NUCLIDE	REACTION	REF	Q-VALUE(keV)	INPUT(keV)	OUTPUT(keV)	r_I(keV)	$(r_I/\sigma_I)^2$
r_{25}	^{176}Lu	(d,t)	k	6282 ±15				
		(d,p)	l	6295 ± 8				
		(d,p)	l	6295 ± 8				
		(d,p)	m	6294.5±15				
					6292.6± 6.4	6291 ± 6	-1.5	0.05
r_{26}	^{177}Lu	(d,p)	k	7072.7± 2.0				
		(n,γ)	n	6890.3± 2.0*				
					7072.7± 2.0	7073.7± 1.8	+1.0	0.25
r_{27}	^{175}Hf	(n,γ)	d	--	6708.8± 0.5	6708.8± 0.8	-	-
r_{28}	^{177}Hf	(d,p)	a	--	6374.5± 0.8 7	6387.7± 1.7	+13.2	3.55
r_{29}	^{178}Hf	(n,γ)	p	7623 ± 3				
		(n,γ)	q	7619 ± 5				
		(d,t)	o	7621 ± 9				
					7621.9± 2.5	7624.0± 1.5	+2.1	0.70
r_{30}	^{179}Hf	(d,p)	i	6102 ±14				
		(n,γ)	p	6098 ± 3				
					6098.2± 2.9	6103.5± 1.5	+5.2	3.22

TABLE 6-IV cont'd.

CODE	NUCLIDE	REACTION	REF	Q-VALUE(keV)	INPUT(keV)	OUTPUT(keV)	r_I(keV)	$(r_I/\sigma_I)^2$
r_{31}	^{180}Hf	(n,γ)	p	7383 ± 3				
		(d,t)	o	7381 ± 6				
					7382.6± 2.7	7387.9± 1.6	+5.3	3.85
r_{32}	^{181}Hf	(d,p)	r	5665 ±25				
		(n,γ)	p	5693 ± 3				
		(d,p)	o	5699.5±10				
					5693.2± 2.8	5693.2± 2.8	-	-
r_{33}	^{182}Ta	(n,γ)	s	6060 ± 8				
			t	6056.5± 8				
		average ++		6058.8± 5.6		-	-	-
r_{33}'	^{182}Hf	from r_{32}, b_{33}, b_{34}			6582 ±200	-	-	-

* Excluded on the assumption that ground state transition was not observed.

\+ Where the quoted error of (n,γ) was less than 1.5 keV, it has been multiplied by a consistency factor of 1.40. See text.

++ Average used to calculate r_{33}'.

TABLE 6-IV cont'd.

a. Meredith et al (1971)
b. Tjøm and Elbek (1969)
c. Bollinger and Thomas (1970)
d. Alenius et al (1971)
e. Burke et al (1966)
f. Michaelis (1967)
g. Namenson and Ritter (1969)
h. Bondarenko et al (1967)
i. Vergnes and Sheline (1963)
j. 1964 Mass Table, Mattauch et al (1965)
k. Minor et al (1971)
l. Struble and Sheline (1967)
m. Whineray et al (1970)
n. Rasmussen et al (1967)
o. Rickey and Sheline (1968)
p. Nameson et al (1966)
q. Groshev et al (1964)
r. Gastebois et al (1966)
s. Bartholomew (1957)
t. Erskine and Buechner (1964)

TABLE 6 - $\overline{V}$

BETA DECAY Q-VALUES

CODE	DECAY	REF.	Q-VALUE (keV)	INPUT (keV)	OUTPUT (keV)	r_I (keV)	$(r_I/\sigma_I)^2$
b_1	$^{165}Er(ec)^{165}Ho$	a	-	371 ± 6	-	-	-
b_2	$^{166}Ho(\beta^-)^{166}Er$	a	-	1854 ± 4	-	-	-
b_3	$^{161}Tm(\beta^+)^{161}Er$	a	-	3520 ± 100	3520 ± 100	-	-
b_4	$^{162}Tm(\beta^+)^{162}Er$	a	-	4890 ± 100	4890 ± 100	-	-
b_5	$^{163}Tm(\beta^+)^{163}Er$	a	-	2770 ± 30	2270 ± 30	-	-
b_6	$^{164}Tm(\beta^+)^{164}Er$	a	-	3962 ± 20	3960 ± 20	-	-
b_7	$^{165}Tm(ec)^{165}Er$	a	-	1565 ± 30	1560 ± 30	-	-
b_8	$^{166}Tm(\beta^+)^{166}Er$	a	2980 ± 50				
		b	3035 ± 12				
				3032 ± 12	3031 ± 12	-	-
b_9	$^{169}Er(\beta^-)^{169}Tm$	c	340.0 ± 2.0	*	354.4 ± 1.3	-	-
b_{10}	$^{171}Er(\beta^-)^{171}Tm$	a		1490.0 ± 2.0	1490.8 ± 1.7	+0.8	0.16
b_{11}	$^{172}Er(\beta^-)^{172}Tm$	a	891 ± 10				
		b	889 ± 7				
				889.6 ± 5.7	890 ± 6	-	-
b_{12}	$^{165}Yb(\beta^+)^{165}Tm$	d	2922 ± 10	2922 ± 10	2922 ± 10	-	-
b_{13}	$^{167}Yb(\beta^+)^{167}Tm$	e	1960 ± 20				
		f	2015 ± 70				
		d	1954 +				
				1964 ± 19			

TABLE 6 - $\overline{V}$

BETA DECAY Q-VALUES

CODE	DECAY	REF.	Q-VALUE (keV)	INPUT (keV)	OUTPUT (keV)	r_I (keV)	$(r_I/\sigma_I)^2$
b_{14}	$^{170}Tm(\beta^-)^{170}Yb$	b	967 ± 4	967 ± 4	963.6± 2.6	- 3.4	0.72
b_{15}	$^{171}Tm(\beta^-)^{171}Yb$	g	97 ± 1	97 ± 1	97.1± 1.0	+ 0.1	0.01
b_{16}	$^{172}Tm(\beta^-)^{172}Yb$	b	1869 ± 9	1869 ± 9	1869 ± 9	-	-
b_{17}	$^{173}Tm(\beta^-)^{173}Yb$	h	1320 ± 30	1320 ± 30	1320 ± 30	-	-
b_{18}	$^{174}Tm(\beta^-)^{174}Yb$	b	3040 ± 10	3040 ± 10	3040 ± 10	-	-
b_{19}	$^{176}Tm(\beta^-)^{176}Yb$	i	4200 ± 100	4200 ±100	4200 ±100	-	-
b_{20}	$^{168}Lu(ec)^{168}Yb$	j	4360 ± 80	4360 ± 80	4360 ± 80	-	-
b_{21}	$^{169}Lu(\beta^+)^{169}Yb$	k	2290 ± 70	2290 ± 70	2290 ± 70	-	-
b_{22}	$^{170}Lu(\beta^+)^{170}Yb$	l	3465 ± 20	3465 ± 20	3465 ± 20	-	-
b_{23}	$^{173}Lu(ec)^{173}Yb$	m	690 ± 30	690 ± 30	690 ± 30	-	-
b_{24}	$^{174}Lu(\beta^+)^{174}Yb$	n	1372 ± 11	1372 ± 11	1372 ± 11	-	-
b_{25}	$^{175}Yb(\beta^+)^{175}Lu$	b	467 ± 10	467 ± 10	473.8± 4.5	+ 6.8	0.46
b_{26}	$^{177}Yb(\beta^-)^{177}Lu$	o	1400 ± 20	1400 ± 20	1406 ± 10	+ 6.0	0.09
b_{27}	$^{167}Hf(\beta^+)^{167}Lu$	d	4716 +	-	-	-	-
b_{28}	$^{169}Hf(\beta^+)^{169}Lu$	d	3365 ± 200	3365 ±200	3365 ±200	-	-
b_{29}	$^{175}Hf(ec)^{175}Lu$	p	590 ± 30	*	758 ± 30	-	-
b_{30}	$^{176}Lu(\beta^-)^{176}Hf$	b	1191 ± 5**				
		q	1195 ± 8 1193 ± 5	1193.6±4.2	1185.0± 2.4	- 8.6	4.19

TABLE 6 - $\overline{V}$

BETA DECAY Q-VALUES

CODE	DECAY	REF.	Q-VALUE (keV)	INPUT (keV)	OUTPUT (keV)	r_I(keV)	$(r_I/\sigma_I)^2$
b_{31}	$^{177}Lu(\beta^-)^{177}Hf$	b	497 ± 1	497 ± 1	498.0± 1.0	+1.0	1.00
b_{32}	$^{178}Lu(\beta^-)^{178}Hf$	r	2250 ± 50	2250 ± 50	2250 ± 50	-	-
b_{33}	$^{179}Lu(\beta^-)^{179}Hf$	r	1350 ± 40	1350 ± 40	1350 ± 40	-	-
b_{34}	$^{180}Lu(\beta^-)^{180}Hf$	s	3060 ± 100				
		i	3300 ± 1000				
		t	3100 ± 100				
b_{35}	$^{181}Hf(\beta^-)^{181}Ta$	b	1023 ± 4++	3081 ± 71	3080 ± 70	-	-
b_{36}	$^{182}Hf(\beta^-)^{182}Ta$	u	500 ± 200++		-	-	-
					-	-	-

* Not used in final adjustment because of inconsistency; ground state transition probably not observed.

\+ Not used because no error was quoted.

** Calculated value by Whineray et al, 1970

++ Not used in adjustment, but used to calculate S_n for ^{182}Hf.

a Meredith et al (1971) (Paper III)

b Whineray et al (1970)

c 1964 Mass Table Mottauch et al (1965c)

d Arlt. et al (1970)

e Ageev (1964)

f Tamura (1965)

g Smith et al, (1957)

h Orth et al (1963)

i Takahashi et al (1961)

j Charvet et al (1970)

k Balalaev et al (1970)

l Bunch-Osmolovskaya et al (1971)

m Bichard et al (1959)

n Liukkonen & Kantele (1968)

o Johansen et al (1964)

p Funke et al (1965)

q Bernthal et al (1971)

r Kuroyanagi et al (1961)

s Swindle et al (1971)

t Gujrathi & D'Auria (1971)

u Wing et al (1961)

TABLE 6-VI

ALPHA DECAY Q-VALUES

Code	Decay	Ref	Q-value	Input (keV)	Output (keV)	r_I (keV)	$(r_I/\sigma_I)^2$
a	$^{156}Yb(\alpha)^{152}Er$	a)	4920±100	*	-	-	-
a	$^{157}Yb(\alpha)^{153}Er$	a)	4610±100	*	-	-	-
a	$^{174}Hf(\alpha)^{170}Yb$	b)	2560± 30	2560±30	2560 ± 30	-	-

a) Toth et al (1970)

b) MacFarlane (1961)

* Not part of the adjustment

TABLE 6-VII

MASS EXCESSES

A	Nuclide	Ref	Mass Excess (keV) Input	Output	r_I (keV)	$(r_I/\sigma_I)^2$
162	Er	a)	-66347.0±6.0	-66352.8±5.4	+5.8	0.95
168	Yb	*	-61605 ±11	-61587 ±7.0	-17.8	2.61

*Calculated from mass of ^{164}Dy as in ref. a) and the doublet s.

a) Meredith et al (1971).

TABLE 6-VIII

SUMMARY OF ADJUSTED INPUT DATA [a]

Table No.	Nature of Input	Number of Data	Average r_I (keV)	Contribution to χ^2
6-III	Mass Spectroscopic Differences	20	-0.8 ± 0.7	16.1
6- IV	S_n Q-values	26	-	90.2 b)
			+0.9 ± 0.9	21.2 c)
6- V	Q(β)	7	+0.4 ± 2.0	6.6
6- VI	Q(α)	0	-	-
6-VII	Mass Excess	2	-6.0 ±12.0	3.5

a) Only data involved in the overdetermined set are included.

b) Preliminary adjustment

c) Final adjustment, with errors on (n,γ) measurement of <± 1.5 multiplied by a consistency factor of 1.4

TABLE 6-IX

SEPARATION AND PAIRING ENERGIES IN KEV.

A	EL	Z	S2N	SN	PN	S2P	SP	PP
142	PR	59	*	5843.4+- 0.8	*	*	*	*
	ND	60	*	5808 +- 9		*	7224.4+- 1.9	
	PM	61	*	8610 +-220	*	*	4210 +-100	*
	SM	62	*	*	*	*	5780 +-230	
143	PP	59	13200.6+- 2.9	7357.1+- 2.9		*	*	*
	ND	60	15933 +- 9	6124.8+- 1.5	1344.1+- 2.4	*	7505.7+- 2.0	
	PM	61	19470 +-200	9860 +-100		11483 +- 14	4259 +- 14	1261 +- 11
	SM	62	*	8440 +-130	*	9813 +- 32	5610 +-100	
	EU	63	*	*		8430 +-280	2660 +-240	*
144	PR	59	13112.1+- 3.7	5754.9+- 3.7		*	*	*
	ND	60	13942.3+- 1.6	7817.6+- 0.8	938.3+- 0.8	*	7966.1+- 2.2	
	PM	61	16380 +-110	6524 +- 44		12164 +- 42	4658 +- 42	1192 +- 31
	SM	62	19030 +-120	10592 +- 31	1495 +- 38	10597.4+- 1.8	6339 +- 14	
	EU	63	*	9220 +-200		8040 +-100	3433 +- 43	770 +- 60
145	PR	59	12701 +- 10	6946 +- 11		*	*	*
	ND	60	13574.5+- 1.7	5757.1+- 1.6	967.3+- 1.0	*	7969.2+- 3.4	
	PM	61	14517 +- 14	7993 +- 42		12709.5+- 2.9	4933.4+- 1.9	1322.0+- 3.6
	SM	62	17358 +- 32	6764 +- 8	1365 +- 10	11239 +- 8	6580 +- 42	
	EU	63	19640 +-200	10422 +- 33		9602 +- 20	3263 +- 14	1190 +-100
	GD	64	*	*	*	7770 +-200	4340 +-200	
146	PR	59	12210 +-100	5260 +-100		*	*	*
	ND	60	13322.7+- 1.5	7565.6+- 1.0	1018.9+- 0.9	*	8588 +- 10	
	PM	61	14227 +- 46	6234 +- 20		13279 +- 20	5311 +- 20	1114 +- 15
	SM	62	15167 +- 13	8401 +- 15	920 +- 11	11822 +- 13	6089 +- 13	
	EU	63	17670 +- 34	7248 +- 21		10325 +- 44	3745 +- 17	1138 +- 17
	GD	64	*	11030 +-450	*	8210 +-400	4950 +-400	
147	PR	59	11920 +-150	6660 +-130		*	*	*
	ND	60	12964.4+- 2.2	5298.9+- 2.1	1074.7+- 1.6	*	8630 +-100	
	PM	61	13901.0+- 2.3	7667 +- 20		14000 +- 10	5411.7+- 2.0	1336.9+- 2.8
	SM	62	14754 +- 8	6355 +- 13	958 +- 10	12419.8+- 2.0	7109 +- 20	
	EU	63	15712 +- 17	8464 +- 18		10796 +- 10	3807 +- 16	1357 +- 13
	GD	64	18790 +-200	7760 +-400	1140 +-300	9205 +- 20	5460 +- 24	
148	ND	60	12629.5+- 1.5	7330.8+- 2.3	1074.5+- 3.1	*	*	*
	PM	61	13567 +- 22	5900 +- 10		14640 +-100	8300 +-150	
	SM	62	14495 +- 13	8140.4+- 0.9	1013.0+- 3.4	12994.6+- 1.8	6013 +- 10	1039 +- 26
	EU	63	15269 +- 33	6805 +- 31		11367 +- 36	7582.9+- 1.1	
	GD	64	16820 +-400	9055 +- 21	860 +-100	9859 +- 16	4257 +- 30	1191 +- 23
	TB	65	*	*		9110 +-300	6052 +- 14	
149	ND	60	12396 +- 10	5065 +- 10	1139 +- 8	*	2650 +-300	*
	PM	61	13168.6+- 2.7	7268 +- 10		15250 +-150	*	
	SM	62	14014.5+- 1.7	5874.2+- 1.6	1094.5+- 0.9	13570.0+- 1.9	5950.9+- 2.7	1418 +- 38
	EU	63	*	*		*	7557 +- 10	
	GD	64	15978 +- 21	6923 +- 14	982 +- 12	10427 +- 11	*	*
	TB	65	*	8860 +-300		8508 +- 18	6170 +- 31	1450 +-100
							2454 +- 18	

SEPARATION AND PAIRING ENERGIES IN KEV.

A	EL	Z	S2N	SN	PN	S2P	SP	PP
150	ND	60	12421.2+- 1.7	7356 +- 10	1084 +- 8	*	*	*
	PM	61	12900 +- 60	5630 +- 60	*	*	6510 +- 60	
	SM	62	13960.0+- 1.6	7985.8+- 0.6	1125.2+- 0.9	14225.1+- 1.8	8274.2+- 2.1	*
	EU	63	14063 +- 33	*	*	12463 +- 18	4906 +- 15	1115 +- 12
	GD	64	15643 +- 18	8720 +- 18	1007 +- 14	11007 +- 15	*	
	TB	65	16600 +-300	7737 +- 22	*	9440 +- 34	3270 +- 19	1129 +- 17
	DY	66	*	*		7130 +-400	4680 +-400	
151	ND	60	12647 +- 18	5310 +- 15	1008 +- 14	*	*	
	PM	61	13458 +- 10	7830 +- 50	*	*	6988 +- 10	*
	SM	62	13582.5+- 2.3	5596.7+- 2.3	1263.3+- 1.7	14757 +- 10	8240 +- 60	
	EU	63	*	7970 +- 15	*	13164.4+- 3.0	4690.2+- 2.3	1457.8+- 1.8
	GD	64	15209 +- 15	6488 +- 18	1084 +- 14	11621 +- 10	6715 +- 18	*
	TB	65	16286 +- 18	8549 +- 20	*	*	3099 +- 19	
	DY	66	*	7650 +-400		8156 +- 22	4886 +- 25	
152	ND	60	12607 +- 30	7297 +- 33	*	*	*	*
	PM	61	*	*	*	*	*	
	SM	62	13857.3+- 2.2	8260.6+- 2.8	1264.7+- 1.8	15661.2+- 2.4	8674 +- 10	*
	EU	63	14274 +- 16	6303.6+- 3.4	*	13840 +- 60	5597.1+- 3.4	1084 +- 15
	GD	64	15080 +- 16	8592 +- 10	1111 +- 8	12227.3+- 3.8	7337.1+- 3.7	
	TB	65	15570 +-340	7020 +-340	*	10350 +-340	3630 +-340	1330 +-260
	DY	66	17420 +-400	9468 +- 29	970 +-100	8904 +- 27	5805 +- 25	*
	HO	67	*	*	*	7200 +-300	2310 +-300	
153	PM	61	13520 +-100	*	*	*	*	*
	SM	62	14126.3+- 2.8	5865.7+- 0.4	1126.1+- 1.0	16216 +- 15	7900 +-100	
	EU	63	14363.4+- 2.9	8559.8+- 4.0	*	14570 +- 10	*	1125.5+- 3.3
	GD	64	14842 +- 12	6251 +- 7	1247 +- 6	12891 +- 8	5896.3+- 2.8	*
	TB	65	*	*	*	*	7284 +- 8	
	DY	66	16566 +- 23	7098 +- 26	1159 +- 24	9514 +- 17	*	1470 +-100
	HO	67	*	9340 +-310	*	7991 +- 27	5880 +-340	
154	SM	62	13841.0+- 3.0	7975.3+- 3.0	1069.6+- 2.8	16895 +- 30	2186 +- 33	*
	EU	63	14081 +- 6	6421.7+- 4.5	*	*	8990 +-100	
	GD	64	15147.3+- 1.9	8897 +- 7	1275 +- 5	13517.4+- 3.1	6452.3+- 4.9	1120 +- 38
	TB	65	15770 +-340	*	*	11840 +- 50	7621.0+- 2.9	
	DY	66	16460 +- 60	9360 +- 50	1201 +- 41	10250 +- 50	4560 +- 50	1220 +- 80
	HO	67	17160 +-300	7824 +- 30	*	8790 +-340	*	
	ER	68	*	*		6620 +-400	2911 +- 21	
155	SM	62	13782 +- 9	5807 +- 8	901 +- 8	*	4440 +-400	
	EU	63	14599.0+- 3.6	8177 +- 5	*	15650 +-100	*	*
	GD	64	15339 +- 8	6441.9+- 2.5	1136.8+- 2.5	14093.5+- 2.9	6654.3+- 4.3	920 +- 25
	TB	65	*	9190 +- 50	*	12465 +- 13	7641.2+- 4.5	*
	DY	66	16189 +- 17	6830 +- 50	1288 +- 40	10860 +- 13	4844 +- 12	1123 +- 9
	HO	67	*	*	*	*	6300 +- 50	
	ER	68	*	8200 +-400		7720 +- 25	*	*
156	SM	62	13047 +- 17	7241 +- 18	*	*	4808 +- 27	
	EU	63	14504 +- 15	6327 +- 15	*	*	*	
	GD	64	14976.2+- 1.3	8534.3+- 2.3	1065.8+- 1.9	14652.5+- 3.1	7175 +- 16	*
	TB	65	*	*	*	*	7998.2+- 3.7	
	DY	66	16260 +- 50	9439 +- 10	1271 +- 15	11402.3+- 4.5	*	*
	HO	67	*	*	*	*	6558 +- 12	
	ER	68	*	*		*	*	*

TABLE 6-IX

SEPARATION AND PAIRING ENERGIES IN KEV.

A	EL	Z	S2N	SN	PN	S2P	SP	PP
157	EU	63	13880 +- 50	7550 +- 50				
	GD	64	14887.8+- 2.3	6363.5+- 1.7	935.9+- 1.3	15209 +- 9	7480 +- 50	
	TB	65	15650 +- 13			13516 +- 6	8035 +- 14	
	DY	66	16405 +- 12	6967 +- 7	1140 +- 6	11927 +- 8	5518 +- 5	973.0+- 4.1
	HO	67						
	ER	68						
158	EU	63	13250 +-200	5700 +-210				
	GD	64	14299.7+- 1.4	7936.2+- 1.0	887.7+- 1.6	15905 +- 17	8420 +- 50	
	TB	65		6767 +- 10		13956 +- 17	5922 +- 9	795 +- 7
	DY	66	16022.3+- 3.0	9056 +- 7	1079 +- 6	12448.4+- 3.1	6930 +- 6	
	HO	67					4224 +- 30	
	ER	68						
159	EU	63	12860 +-210	7160 +-280				
	GD	64	13894 +- 5	5958 +- 5	865.9+- 3.8		8680 +-200	
	TB	65	14919 +- 5	8153 +- 9		14560 +- 50	6137.9+- 1.4	893 +- 13
	DY	66	15882 +- 10	6827 +- 7	998 +- 5	12912 +- 7	6990 +- 11	
	HO	67						
	ER	68						
160	EU	63	13300 +-500	6100 +-500				
	GD	64	13401.2+- 1.7	7443 +- 5	822.9+- 4.5		8960 +-200	
	TB	65	14529 +- 9	6376.6+- 1.9		15230 +-200	6557 +- 5	770 +- 50
	DY	66	15415.1+- 2.2	8588 +- 7	973 +- 5	13563.7+- 1.7	7425.8+- 1.6	
	HO	67	16160 +- 60			11500 +- 50	4510 +- 50	1022 +- 38
	ER	68						
161	GD	64	13080 +- 11	5637 +- 10				
	TB	65	14081 +- 5	7704 +- 5			8500 +-500	
	DY	66	15046 +- 7	6457.9+- 1.5	966.6+- 2.0	15780 +-200	6917 +- 5	830 +- 50
	HO	67		8890 +- 70		14064 +- 5	7507.1+- 2.1	
	ER	68				12240 +- 50	4810 +- 50	1058 +- 38
	TM	69				10619 +- 12	6110 +- 50	
162	GD	64						
	TB	65	13960 +- 60	6260 +- 60				
	DY	66	14652.1+- 1.0	8194.2+- 1.4	913.3+- 1.3	15900 +-500	7440 +- 60	400 +-130
	HO	67	15790 +- 60	6900 +- 60		14814.7+- 1.2	7997 +- 5	
	ER	68		9214 +- 10		12759 +- 30	5251 +- 30	860 +- 23
	TM	69		7840 +-140		11244.3+- 1.7	6430 +- 50	
						9650 +-110	3540 +-100	
163	TB	65	13380 +- 50	7120 +- 70				
	DY	66	14471.3+- 1.0	6277.1+- 1.3	823.7+- 1.2	15455 +- 10	8010 +- 60	
	HO	67	15320 +- 50	8428 +- 30		13482 +- 6	5485.0+- 3.1	971.2+- 2.7
	ER	68	16116 +- 11	6902 +- 5	1064.7+- 4.5	11688 +- 5	6437 +- 30	
	TM	69	17370 +-110	9520 +-100		10280 +- 60	3849 +- 30	
164	TB	65	13290 +-130	6170 +-130				
	DY	66	13932.0+- 1.0	7654.9+- 1.4	829.7+- 1.1		8550 +- 50	
	HO	67	15062 +- 37	6635 +- 21		13860 +- 60	5843 +- 21	803 +- 21
	ER	68	15750.6+- 1.3	8849 +- 5	1033.8+- 3.9	12342.8+- 2.1	6857.7+- 3.5	
	TM	69	16680 +-100	7156 +- 36		10540 +- 36	4103 +- 21	

TABLE 6-IX

SEPARATION AND PAIRING ENERGIES IN KEV.

A	EL	Z	S2N	SN	PN	S2P	SP	PP
165	DY	66	13369.7+- 2.0	5713.9+- 1.4	820.6+- 1.7	*	8090 +-120	
	HO	67	14671.8+- 3.7	8037 +- 21		14780 +- 50	6224.9+- 2.5	854 +- 13
	ER	68	15509 +- 7	6660.4+- 4.3	998.8+- 3.4	12726.1+- 4.7	6884 +- 21	
	TM	69	16214 +- 43	9058 +- 36		11170 +- 30	4312 +- 30	*
166	DY	66	12769 +- 6	7055 +- 6	*	*	*	
	HO	67	14291 +- 21	6244.1+- 0.9		14850 +-120	6755.1+- 3.0	522 +- 30
	ER	68	15127.6+- 1.2	8467.2+- 4.2	959.2+- 3.2	13538.4+- 2.4	7313.5+- 1.4	
	TM	69	16110 +- 50	7050 +- 60		11590 +- 50	4710 +- 50	*
167	HO	67	13562 +- 20	7318 +- 20		*	7017 +- 21	*
	ER	68	14904.1+- 4.2	6437.0+- 0.5	841.4+- 1.1	14261.5+- 2.8	7506.3+- 1.6	
	TM	69	*	*		*	*	*
168	HO	67	12760 +-100	5440 +-100		*	*	*
	ER	68	14209.2+- 0.7	7772.3+- 0.7	775.9+- 0.4	14978 +- 5	7961 +- 20	
	TM	69	15490 +- 70	*		12790 +- 60	5290 +- 60	*
169	HO	67	12650 +-100	7200 +-140		*	*	*
	ER	68	13776.1+- 0.7	6003.8+- 0.3	755.6+- 0.6	*	8520 +-100	
	TM	69	*	8060 +- 60		13532 +- 20	5571.3+- 1.2	*
170	HO	67	12360 +-140	5160 +-140		*	*	*
	ER	68	13261.7+- 2.1	7257.8+- 2.2	708.3+- 1.8	*	8580 +-100	
	TM	69	14650 +- 60	6595.5+- 2.5		14680 +-100	6163.0+- 2.8	*
171	ER	68	12936 +- 6	5678 +- 6	*	*	9100 +-100	
	TM	69	14077 +- 7	7481 +- 7		14960 +-100	6385 +- 6	*

A	EL	Z	Q(B-) KEV	Q(ALPHA) KEV	MASS EXCESS KEV	MASS EXCESS MICRO U
141	PR	59	-1801 +- 9	*	-86002.6+- 3.9	-92328.9+- 4.1
	ND	60	-3620 +-200	*	-84201 +- 10	-90395 +- 10
	PM	61	*	*	-80580 +-200	-86510 +-210
142	PR	59	2163.4+- 1.8	*	-83774.6+- 3.8	-89937.0+- 4.1
	ND	60	-4820 +-100	*	-85938.0+- 3.5	-92259.5+- 3.8
	PM	61	-2050 +- 70	*	-81120 +-100	-87090 +-110
	SM	62	*	*	-79070 +-120	-84880 +-130
143	PR	59	931.0+- 2.0	*	-83060.3+- 3.9	-89170.1+- 4.2
	ND	60	-1084 +- 14	*	-83991.3+- 3.4	-90169.6+- 3.6
	PM	61	-3471 +- 28	*	-82908 +- 14	-89006 +- 15
	SM	62	-5000 +-200	*	-79436 +- 31	-85280 +- 33
	EU	63	*	*	-74440 +-200	-79910 +-220
144	PR	59	2993.6+- 3.0	*	-80743.8+- 4.5	-86683.2+- 4.8
	ND	60	-2377 +- 42	*	-83737.4+- 3.3	-89897.1+- 3.6
	PM	61	597 +- 42	*	-81361 +- 42	-87345 +- 45
	SM	62	-6377 +- 30	*	-81957.4+- 3.4	-87986.1+- 3.7
	EU	63	*	*	-75581 +- 30	-81140 +- 32
145	PR	59	1805 +- 10	*	-79618 +- 11	-85475 +- 11
	ND	60	-141.2+- 1.0	*	-81423.1+- 3.4	-87412.5+- 3.7
	PM	61	-630 +- 8	2296.0+- 2.8	-81281.9+- 3.6	-87260.9+- 3.8
	SM	62	-2721 +- 12	1125 +- 12	-80652 +- 8	-86585 +- 9
	EU	63	-5300 +-200	230 +-200	-77931 +- 14	-83664 +- 15
	GD	64	*	*	-72630 +-200	-77970 +-220
146	PR	59	4110 +-100	*	-76810 +-100	-82460 +-110
	ND	60	-1473 +- 20	*	-80917.3+- 3.4	-86869.4+- 3.6
	PM	61	1537 +- 15	1905 +- 20	-79445 +- 20	-85288 +- 22
	SM	62	-3874 +- 8	2532 +- 13	-80982 +- 13	-86939 +- 14
	EU	63	-1520 +-400	1590 +-100	-77108 +- 16	-82780 +- 17
	GD	64	*	1050 +-420	-75590 +-400	-81150 +-430
147	PR	59	2750 +-150	*	-75390 +-150	-80940 +-160
	ND	60	895.4+- 0.8	*	-78144.6+- 3.8	-83892.8+- 4.0
	PM	61	224.9+- 0.6	1595.6+- 2.9	-79040.0+- 3.7	-84854.1+- 4.0
	SM	62	-1765 +- 10	2301.7+- 2.0	-79264.9+- 3.6	-85095.5+- 3.9
	EU	63	-2221 +- 15	2983 +- 10	-77500 +- 11	-83201 +- 11
	GD	64	*	1733 +- 33	-75279 +- 18	-80816 +- 20
148	ND	60	-535 +- 10	*	-77403.9+- 3.5	-83097.6+- 3.8
	PM	61	2465 +- 10	1450 +- 11	-76869 +- 11	-82523 +- 11
	SM	62	-3101 +- 30	1978.8+- 1.8	-79333.9+- 3.6	-85169.6+- 3.9
	EU	63	29 +- 31	2703 +- 30	-76233 +- 30	-81841 +- 32
	GD	64	-5620 +-300	3270 +- 10	-76263 +- 11	-81873 +- 11
	TB	65	*	2510 +-300	-70640 +-300	-75840 +-320
149	ND	60	1668 +- 10	*	-74397 +- 11	-79870 +- 11
	PM	61	1070.9+- 2.0	1128 +- 10	-76065.8+- 4.2	-81661.1+- 4.5
	SM	62	*	1861.7+- 2.0	-77136.6+- 3.6	-82810.7+- 3.9
	EU	63	*	*	*	*
	GD	64	-3684 +- 14	3113 +- 7	-75114 +- 11	-80640 +- 12
	TB	65	*	4076.3+- 4.0	-71430 +- 15	-76685 +- 16

A	EL	Z	Q(B-) KEV	Q(ALPHA) KEV	MASS EXCESS KEV	MASS EXCESS MICRO U
150	ND	60	-60 +- 60	*	-73682.2+- 3.6	-79102.2+- 3.9
	PM	61	3430 +-60	760 +-120	-73620 +- 60	-79040 +- 60
	SM	62	-2297 +- 15	1441.5+- 1.8	-77051.0+- 3.6	-82718.8+- 3.9
	EU	63	1009.3+- 4.0	2266 +- 18	-74754 +- 16	-80252 +- 17
	GD	64	-4667 +- 13	2794 +- 9	-75763 +- 15	-81336 +- 16
	TB	65	-2280 +-400	3587.2+- 5.0	-71096 +- 16	-76325 +- 18
	DY	66	*	4348 +- 17	-68820 +-400	-73880 +-430
151	ND	60	2460 +- 18	*	-70921 +- 15	-76138 +- 16
	PM	61	1196 +- 10	-410 +-150	-73381 +- 11	-78779 +- 12
	SM	62	75.9+- 0.6	1143.6+- 3.0	-74576.3+- 4.3	-80062.0+- 4.6
	EU	63	-472 +- 10	1963.1+- 2.8	-74652.2+- 4.3	-80143.5+- 4.6
	GD	64	-2607 +- 15	2660 +- 10	-74180 +- 11	-79637 +- 11
	TB	65	-2981 +- 17	3502 +- 5	-71573 +- 12	-76838 +- 13
	DY	66	*	4162 +- 6	-68692 +- 19	-73745 +- 21
152	ND	60	*	*	-70147 +- 30	-75307 +- 32
	PM	61	*	*	*	*
	SM	62	-1881.0+- 3.9	213.8+- 2.8	-74765.4+- 4.3	-80265.0+- 4.6
	EU	63	1815.9+- 4.3	1560 +- 11	-72884 +- 5	-78246 +- 6
	GD	64	-4180 +-340	2208.8+- 4.1	-74700 +- 5	-80195 +- 6
	TB	65	-430 +-340	3290 +-340	-70520 +-340	-75710 +-360
	DY	66	-6370 +-300	3749 +- 20	-70089 +- 23	-75245 +- 24
	HO	67	*	4500 +- 50	-63720 +-300	-68400 +-330
153	PM	61	1800 +-100	*	-70760 +-100	-75970 +-110
	SM	62	813.1+- 2.8	-587 +- 10	-72559.6+- 4.3	-77897.0+- 4.6
	EU	63	-493 +- 8	268.3+- 3.6	-73372.7+- 4.7	-78770 +- 5
	GD	64	*	1832 +- 8	-72879 +- 9	-78240 +- 9
	TB	65	*	*	*	*
	DY	66	-4130 +- 26	3574 +- 8	-69116 +- 14	-74200 +- 15
	HO	67	*	4020 +- 20	-64986 +- 25	-69766 +- 27
154	SM	62	-740.6+- 4.9	-1206.1+- 3.6	-72464 +- 5	-77794 +- 5
	EU	63	1981.8+- 4.2	-530 +- 60	-71723 +- 6	-76999 +- 7
	GD	64	-3560 +- 50	921.5+- 3.5	-73705 +- 5	-79126 +- 5
	TB	65	260 +- 70	2180 +- 50	-70150 +- 50	-75310 +- 50
	DY	66	-5670 +- 50	2930 +- 50	-70410 +- 50	-75590 +- 60
	HO	67	-2610 +-400	3933 +- 5	-64738 +- 17	-69500 +- 18
	ER	68	*	4260 +- 20	-62130 +-400	-66700 +-430
155	SM	62	1630 +- 8	-1702 +- 17	-70199 +- 9	-75362 +- 10
	EU	63	246.4+- 2.9	-873 +- 11	-71829 +- 6	-77112 +- 6
	GD	64	-815 +- 13	76.3+- 3.2	-72075.2+- 4.8	-77377 +- 5
	TB	65	-2098 +- 6	968 +- 13	-71260 +- 13	-76502 +- 14
	DY	66	*	2593 +- 15	-69162 +- 12	-74249 +- 13
	HO	67	*	*	*	*
	ER	68	*	4010 +- 10	-62258 +- 22	-66837 +- 23
156	SM	62	716 +- 13	-1646 +- 34	-69368 +- 17	-74471 +- 18
	EU	63	2454 +- 14	*	-70084 +- 15	-75240 +- 16
	GD	64	*	-197.4+- 3.2	-72538 +- 5	-77874 +- 5
	TB	65	*	*	*	*
	DY	66	*	1746.5+- 4.8	-70529 +- 6	-75717 +- 7
	HO	67	*	*	*	*
	ER	68	*	*	*	*

A	EL	Z	Q(B-) KEV	Q(ALPHA) KEV	MASS EXCESS KEV	MASS EXCESS MICRO U
157	EU	63	1270 +- 50	-1230 +-110	-69560 +- 50	-74680 +- 50
	GD	64	-63 +- 5	-695.3+- 3.3	-70830 +- 5	-76040 +- 5
	TB	65	-1343 +- 9	181 +- 6	-70767 +- 7	-75973 +- 8
	DY	66	*	1030 +- 11	-69424 +- 9	-74531 +- 10
	HO	67	*	*	*	*
	ER	68	*	*	*	*
158	EU	63	3500 +-200	*	-67190 +-200	-72140 +-210
	GD	64	-1232 +- 9	-656.1+- 3.3	-70695 +- 5	-75895 +- 5
	TB	65	946 +- 8	-165 +- 10	-69463 +- 10	-74572 +- 11
	DY	66	-4049 +- 29	871.6+- 3.3	-70408 +- 6	-75588 +- 6
	HO	67	*	1360 +- 60	-66359 +- 30	-71241 +- 32
	ER	68	*	*	*	*
159	EU	63	2300 +-200	*	-66280 +-200	-71160 +-210
	GD	64	962 +- 5	-808 +- 10	-68581 +- 7	-73626 +- 8
	TB	65	-380 +- 7	-139.8+- 3.8	-69544 +- 5	-74659 +- 6
	DY	66	*	487 +- 7	-69164 +- 9	-74251 +- 9
	HO	67	*	*	*	*
	ER	68	*	*	*	*
160	EU	63	3600 +-500	*	-64400 +-500	-69100 +-500
	GD	64	-104.2+- 2.5	-1010 +- 17	-67953 +- 5	-72952 +- 6
	TB	65	1831.6+- 2.5	-190 +- 14	-67849 +- 6	-72840 +- 6
	DY	66	-3300 +- 50	432.7+- 2.2	-69681 +- 5	-74806 +- 6
	HO	67	*	*	-66380 +- 50	-71260 +- 50
	ER	68	*	*	*	*
161	GD	64	1963 +- 11	*	-65519 +- 11	-70338 +- 12
	TB	65	585.5+- 5.0	-340 +- 50	-67482 +- 7	-72446 +- 8
	DY	66	-860 +- 50	338.3+- 1.3	-68067 +- 5	-73074 +- 6
	HO	67	-2000 +- 50	1140 +- 50	-67200 +- 50	-72150 +- 60
	ER	68	-3520 +-100	1795 +- 13	-65204 +- 11	-70001 +- 12
	TM	69	*	*	-61680 +-100	-66220 +-110
162	GD	64	*	*	*	*
	TB	65	2520 +- 60	-900 +-210	-65670 +- 60	-70500 +- 60
	DY	66	-2160 +- 30	80.3+- 1.8	-68190 +- 5	-73206 +- 6
	HO	67	317 +- 30	1008 +- 31	-66030 +- 30	-70887 +- 33
	ER	68	-4890 +-100	1636.8+- 2.7	-66347 +- 6	-71227 +- 6
	TM	69	*	2480 +-100	-61460 +-100	-65980 +-110
163	TB	65	1680 +- 50	-860 +-210	-64720 +- 50	-69480 +- 50
	DY	66	-10 +- 10	-239 +- 5	-66396 +- 5	-71280 +- 6
	HO	67	-1208.5+- 4.8	733.1+- 3.1	-66386 +- 6	-71269 +- 6
	ER	68	-2271 +- 30	1562 +- 8	-65177 +- 7	-69972 +- 8
	TM	69	*	*	-62907 +- 31	-67534 +- 33
164	TB	65	3160 +-120	-900 +-500	-62820 +-120	-67440 +-130
	DY	66	-1030 +- 21	-450.6+- 1.5	-65979 +- 5	-70832 +- 6
	HO	67	1006 +- 21	475 +- 21	-64949 +- 22	-69727 +- 23
	ER	68	-3963 +- 20	1301.2+- 2.0	-65955 +- 6	-70806 +- 6
	TM	69	*	1960 +- 50	-61991 +- 21	-66552 +- 22

DECAY ENERGIES AND MASSES

A	EL	Z	Q(B-) KEV	Q(ALPHA) KEV	MASS EXCESS KEV	MASS EXCESS MICRO U
165	DY	66	1293.5+- 2.9	-528 +- 10	-63621 +- 6	-68301 +- 6
	HO	67	-371.2+- 4.2	142 +- 6	-64915 +- 6	-69690 +- 6
	ER	68	-1566 +- 30	1098.7+- 4.8	-64544 +- 7	-69291 +- 8
	TM	69	*	1800 +- 60	-62978 +- 31	-67610 +- 33
166	DY	66	492 +- 5	*	-62605 +- 8	-67211 +- 8
	HO	67	1851.8+- 1.6	160 +- 60	-63088 +- 6	-67728 +- 6
	ER	68	-2980 +- 50	825.8+- 2.3	-64939 +- 6	-69716 +- 6
	TM	69	*	1640 +- 60	-61960 +- 50	-66520 +- 50
167	HO	67	971 +- 20	-40 +- 50	-62334 +- 21	-66919 +- 22
	ER	68	*	665.9+- 2.4	-63305 +- 6	-67962 +- 6
	TM	69	*	*	*	*
168	HO	67	3300 +-100	690 +-160	-59710 +-100	-64100 +-110
	ER	68	-1700 +- 60	548.5+- 2.5	-63006 +- 6	-67640 +- 6
	TM	69	*	1220 +- 60	-61300 +- 60	-65810 +- 60
169	HO	67	2100 +-100	*	-58840 +-100	-63170 +-110
	ER	68	349.9+- 1.2	258.6+- 2.9	-60938 +- 6	-65421 +- 6
	TM	69	*	1202.1+- 1.8	-61288 +- 6	-65796 +- 6
170	HO	67	4200 +-100	*	-55920 +-100	-60040 +-110
	ER	68	-312.4+- 3.5	56 +- 6	-60125 +- 6	-64547 +- 7
	TM	69	*	850.7+- 3.2	-59812 +- 6	-64212 +- 7
171	ER	68	1490.4+- 2.0	*	-57732 +- 8	-61978 +- 9
	TM	69	*	687 +- 21	-59222 +- 9	-63578 +- 9

TABLE 6-XI

SEPARATION AND PAIRING ENERGIES (keV)

A	EL	S_{2n}	S_n	P_n	S_{2p}	S_p	P_p
162	Er	*	9216 ± 10	*	a	a	1050 ± 39
	Tm	*	7850 ±140	--	a	3540 ±100	--
163	Er	16117 ± 12	6901 ± 7	1065 ± 6	a	a	--
	Tm	17370 ±110	9520 ±100	--	a	3848 ± 30	*
164	Er	15748.3±1.2	8847 ± 7	1036 ± 5	a	a	980 ± 8
	Tm	16680 ±102	7155.9±37	--	a	4104 ± 21	--
165	Er	15499 ± 7	6651.5±1.0	1005.4±1.9	a	a	--
	Tm	16204 ± 43	9048 ± 36	--	a	4305 ± 31	*
	Yb	*	*	*	945 ± 33	5344 ± 38	*
166	Er	15128.9±1.2	8477.3 ± 1.5	966.5±0.9	a	a	873 ± 25
	Tm	16059 ± 23	7011 ± 32	--	a	4664 ± 14	--
	Yb	*	*	*	*	*	*
167	Er	14914.3±1.6	6437.0±0.6	843.5±0.6	a	a	--
	Tm	15735.4±38	8724 ± 26	--	12229 ± 25	4911 ± 25	950 ± 35
	Yb	16695 ± 12	*	*	10644 ± 15	5980 ± 19	--
168	Er	14207.6±0.8	7770.6±0.8	775.3±0.5	a	a	833 ± 15
	Tm	15540 ± 60	6820 ± 60	--	a	5291 ± 55	--
	Yb	*	9054.6±1.2	*	11221 ± 9	6310 ± 25	980 ±100
	Lu	*	*	*	9895 ± 80	3915 ± 80	--
169	Er	13773.8±0.9	6003.2±0.4	756.5±0.5	*	a	--
	Tm	14872 ± 23	8055 ± 55	--	a	5575 ± 8	897 ± 23
	Yb	15913 ± 12	6858.8±3.7	954.0±4.2	11643 ± 10	6352 ± 10	--
	Lu	*	8930 ±110	*	10102 ± 74	3787 ± 90	*
	Hf	*	*	*	8694 ±210	4779 ±220	--

TABLE 6-XI cont'd.

170	Er	13263.7±1.7	7260.5±1.7	709.0±0.9	*	a	*
	Tm	14650 ± 55	6595.0±2.2	--	a	6167 ± 8	--
	Yb	15338 ± 6	8479.2±6.3	870.6±3.7	12351 ± 8	6776 ± 8	*
	Lu	16235 ± 80	7305 ± 70	--	10580 ± 60	4232 ± 13	--
171	Er	12942.4±1.8	5681.9±0.7	687.0±2.7	*	*	--
	Tm	14078.9±1.5	7483.9±2.6	--	a	6390 ± 8	784 ±100
	Yb	15097 ± 7	6617.4±2.3	816.5±2.2	12965 ± 8	6798 ± 8	--
172	Er	12533 ± 11	6851 ± 11	*	*	*	*
	Tm	13734 ± 9	6250 ± 9	--	16067 ±100	6958 ± 13	--
	Yb	14638.9±1.7	8021.5±1.7	764.7±1.4	13726 ± 8	7336 ± 13	847 ± 34
173	Er	13166 ± 30	6916 ± 31	--	*	7023 ± 33	*
	Yb	14388.6±1.6	6367.0±0.7	688.6±0.8	14412 ± 8	7454 ± 14	--
	Lu	*	*	--	12231 ± 31	4895 ± 31	937 ± 50
174	Tm	12663 ± 13	5747 ± 32	--	*	*	--
	Yb	13834.0±1.4	7466.9±1.6	686.2±1.4	15028 ± 14	8005 ± 31	869 ± 46
	Lu	*	6785 ± 32	--	12766 ± 17	5312 ± 14	--
	Hf	*	*	*	11097 ± 31	6202 ± 44	*
175	Tm	*	*	*	*	*	*
	Yb	13288.9±4.2	5822.0±4.0	673.3±3.0	*	8079 ± 14	--
	Lu	14453 ± 30	7668 ± 11	--	13044 ± 31	5513 ± 8	918 ± 34
	Hf	*	6710.4±0.7	*	11440 ± 31	6128 ± 33	--
176	Tm	11530 ±100	*	--	*	*	*
	Yb	12692.1±1.0	6870.1±4.1	588.6±3.7	*	*	*
	Lu	13960 ± 13	6292 ± 6	--	14062 ± 15	5509 ± 11	--
	Hf	14945 ± 31	8235 ± 31	843 ± 15	12207 ± 11	6694 ± 11	*
177	Yb	12434 ± 10	5564 ± 9	*	*	8980 ±100	--
	Lu	13367 ± 6	7074.7±1.8	--	*	6188 ± 11	*
	Hf	14622 ± 31	6387.7±1.7	771 ± 8	12773 ± 11	6790 ± 13	--

TABLE 6-XI cont'd.

178	Lu	12950 ± 50	5870 ± 50	--	15478 ±110	6498 ± 50	--
	Hf	14012.6±0.9	7624.9±1.5	689.8±1.5	13528 ± 11	7340 ± 13	*
179	Lu	12875 ± 40	7000 ± 60	--	*	*	*
	Hf	13727.6±0.9	6102.7±1.5	701.8±1.5	14067 ± 14	7569 ± 50	--
180	Lu	12660 ± 90	5660 ± 80	--	*	*	--
	Hf	13490.6±0.7	7387.8±1.6	745.1±1.3	*	7956 ± 42	*
181	Hf	13080.4±3.2	5692.5±2.8	646 ± 50	*	7987 ± 70	--
182	Hf	12280 ±200	6580 ±200	*	*	*	*

a) Calculated in Meredith et al (1971) and presented in Table 6-IX

TABLE 6-XII

DECAY ENERGIES AND MASSES

A	EL	Z	Q(β^-) (keV)	Q(α) (keV)	Mass Excess (keV)	(μu)
161	Er	68	-3520 ± 100	a	-65208 ± 11	-70005 ± 12
	Tm	69	*	*	-61690 ±100	-66230 ±110
162	Er	68	-4890 ± 100	a	-66353 ± 5	-71234 ± 5
	Tm	69	*	a	-61463 ±100	-65980 ±110
163	Er	68	-2270 ± 30	a	-65182 ± 9	-69977 ± 10
	Tm	69	*	*	-62912 ± 31	-67540 ± 33
164	Er	68	-3960 ± 20	a	-65958 ± 5.5	-70810 ± 6
	Tm	69	*	a	-61997 ± 21	-66557 ± 23
165	Er	68	-1560 ± 30	a	-64538 ± 6	-69285 ± 6
	Tm	69	-2922 ± 10	a	-62974 ± 31	-67606 ± 33
	Yb	70	*		-60052 ± 32	-64469 ± 34
166	Er	68	-3031 ± 12	a	-64944 ± 6	-69721 ± 6
	Tm	69	*	a	-61913 ± 13	-66467 ± 14
	Yb	70	*		*	
167	Er	68	- 744 ± 23	a	-63310 ± 6	-67967 ± 6
	Tm	69	-1962 ± 19		-62566 ± 24	-67168 ± 26
	Yb	70	*		-60604 ± 14	-65062 ± 15
168	Er	68	-1700 ± 55	a	-63009 ± 6	-67644 ± 6
	Tm	69	275 ± 55	a	-61312 ± 55	-65822 ± 60
	Yb	70	-4360 ± 80	1946 ± 9	-61587 ± 7	-66117 ± 8
	Lu	71	*	2340 ± 80	-57230 ± 80	-61440 ± 90

TABLE 6-XII cont'd.

169 Er 68	354.4 ± 1.3	a	-60941 ± 6	-65424 ± 6	
Tm 69	- 921 ± 7	a	-61295 ± 6	-65804 ± 6	
Yb 70	-2290 ± 70	1738 ± 10	-60375 ± 8	-64816 ± 9	
Lu 71	-3360 ±200	2460 ± 80	-58090 ± 70	-62360 ± 80	
Hf 72	*	2900 ±210	-54720 ±210	-58750 ±230	
170 Er 68	-311.1 ± 2.8	a	-60130 ± 6	-64553 ± 6	
Tm 69	963.6 ± 2.6	a	-59819 ± 6	-64219 ± 6	
Yb 70	-3465 ± 10	1737 ± 8	-60782 ± 6	-65253 ± 6	
Lu 71	*	2170 ± 16	-57318 ± 12	-61534 ± 13	
171 Er 68	1490.8 ± 1.7	*	-57740 ± 6	-61987 ± 6	
Tm 69	97.1 ± 1.0	a	-59231 ± 6	-63588 ± 6	
Yb 70	*	1557 ± 8	-59328 ± 6	-63692 ± 6	
Lu 71	*		*	*	
172 Er 68	890 ± 6	*	-56520 ± 12	-60678 ± 13	
Tm 69	1869 ± 9	-120 ±100	-57409 ± 11	-61632 ± 12	
Yb 70	*	1285 ± 8	-59278 ± 6	-63638 ± 6	
Lu 71	*		*	*	
173 Tm 69	1320 ± 30	160 ±100	-56254 ± 31	-60392 ± 33	
Yb 70	- 690 ± 30	942 ± 8	-57574 ± 6	-61809 ± 6	
Lu 71	*	1986 ± 31	-56884 ± 31	-61068 ± 33	
174 Tm 69	3040 ± 10	-430 ±100	-53930 ± 12	-57897 ± 13	
Yb 70	-1372 ± 11	735 ± 8	-56970 ± 6	-61161 ± 6	
Lu 71	200 ± 32	1797 ± 14	-55597 ± 13	-59687 ± 14	
Hf 72	*	2560 ± 30	-55797 ± 31	-59901 ± 33	
175 Tm 69	*		*	*	
Yb 70	473.8 ± 4.5	595 ± 8	-54720 ± 7	-58745 ± 8	
Lu 71	- 758 ± 30	1612 ± 8	-55194 ± 6	-59254 ± 6	
Hf 72	*	2467 ± 31	-54436 ± 31	-58440 ± 33	

TABLE 6-XII cont'd.

176	Tm 69	4200 ±100	*	-49320 ±100	-52950 ±110
	Yb 70	- 105 ± 7	576 ± 14	-53519 ± 6	-57456 ± 6
	Lu 71	1185.0 ± 2.4	1570 ± 14	-53414 ± 9	-57343 ± 10
	Hf 72	*	2254 ± 11	-54599 ± 9	-58615 ± 10
177	Yb 70	1406 ± 10	*	-51011 ± 11	-54763 ± 12
	Lu 71	498.0 ± 1.0	1411 ± 32	-52418 ± 9	-56274 ± 10
	Hf 72	*	2234 ± 11	-52915 ± 9	-56807 ± 10
178	Lu 71	2250 ± 50	1285 ± 50	-50220 ± 50	-53915 ± 50
	Hf 72	*	2076 ± 11	-52469 ± 9	-56329 ± 10
179	Lu 71	1350 ± 40	*	-49150 ± 41	-52765 ± 44
	Hf 72	*	1795 ± 11	-50500 ± 9	
180	Lu 71	3080 ± 70	155 ±120	-46740 ± 70	-50178 ± 70
	Hf 72	*	1277 ± 11	-49817 ± 9	-53481 ± 10
181	Hf 72	*	1148 ± 14	-47438 ± 9	-50927 ± 10
182	Hf 72	*	*	-45950 ±200	-49330 ±210

a) Calculated in Meredith et al (1971) and presented in Table 6-X

Figure 6-1

Chart of the Nuclides $68 \leq Z \leq 72$

The mass spectroscopic links of Table 6-3 are shown in blue, and labelled a,b,c...

ß-decay Q-values: b1, b2,...

α-decay Q-values: a1, a2, a3.

Reactions, leading to S_n values: r1, r2,...

The two masses used as input are underlined in blue.

FIGURE 6 - 1

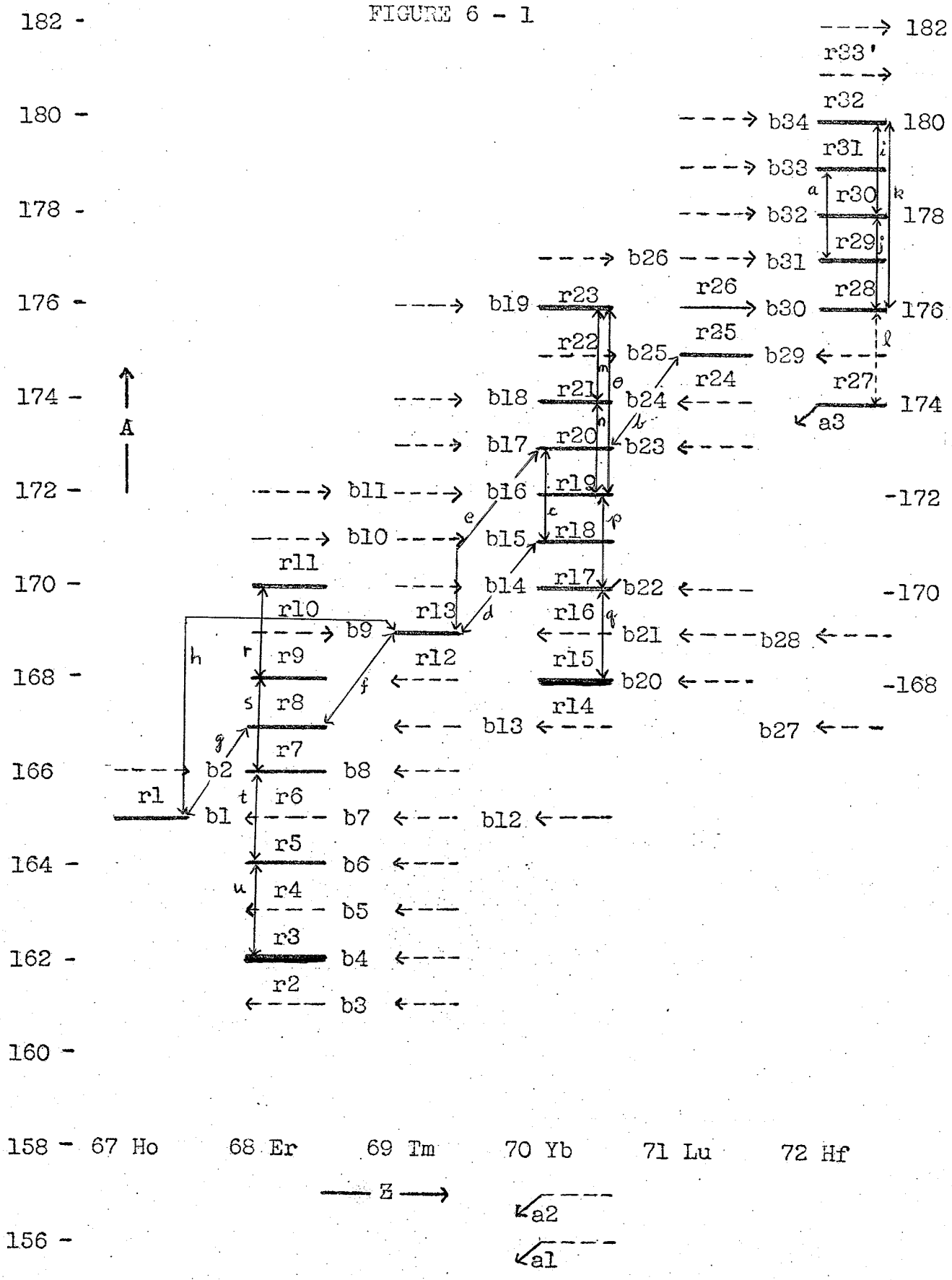
182
180
178
176
174
172
170
168
166
164
162
160
158
156
A
Z
67 Ho
68 Er
69 Tm
70 Yb
71 Lu
72 Hf
r33'
r32
r31
r30
r29
r28
r27
r26
r25
r24
r23
r22
r21
r20
r19
r18
r17
r16
r15
r14
r13
r12
r11
r10
r9
r8
r7
r6
r5
r4
r3
r2
r1
b34
b33
b32
b31
b30
b29
b28
b27
b26
b25
b24
b23
b22
b21
b20
b19
b18
b17
b16
b15
b14
b13
b12
b11
b10
b9
b8
b7
b6
b5
b4
b3
b2
b1
a3
a2
a1

Figure 6-2

Chart of the Nuclides $59 \leq Z \leq 69$

The reaction and decay data compiled in Paper III are shown here to provide a picture of the nuclides in the region. Mass Spectroscopic links presented in Paper II are not shown in this Figure.

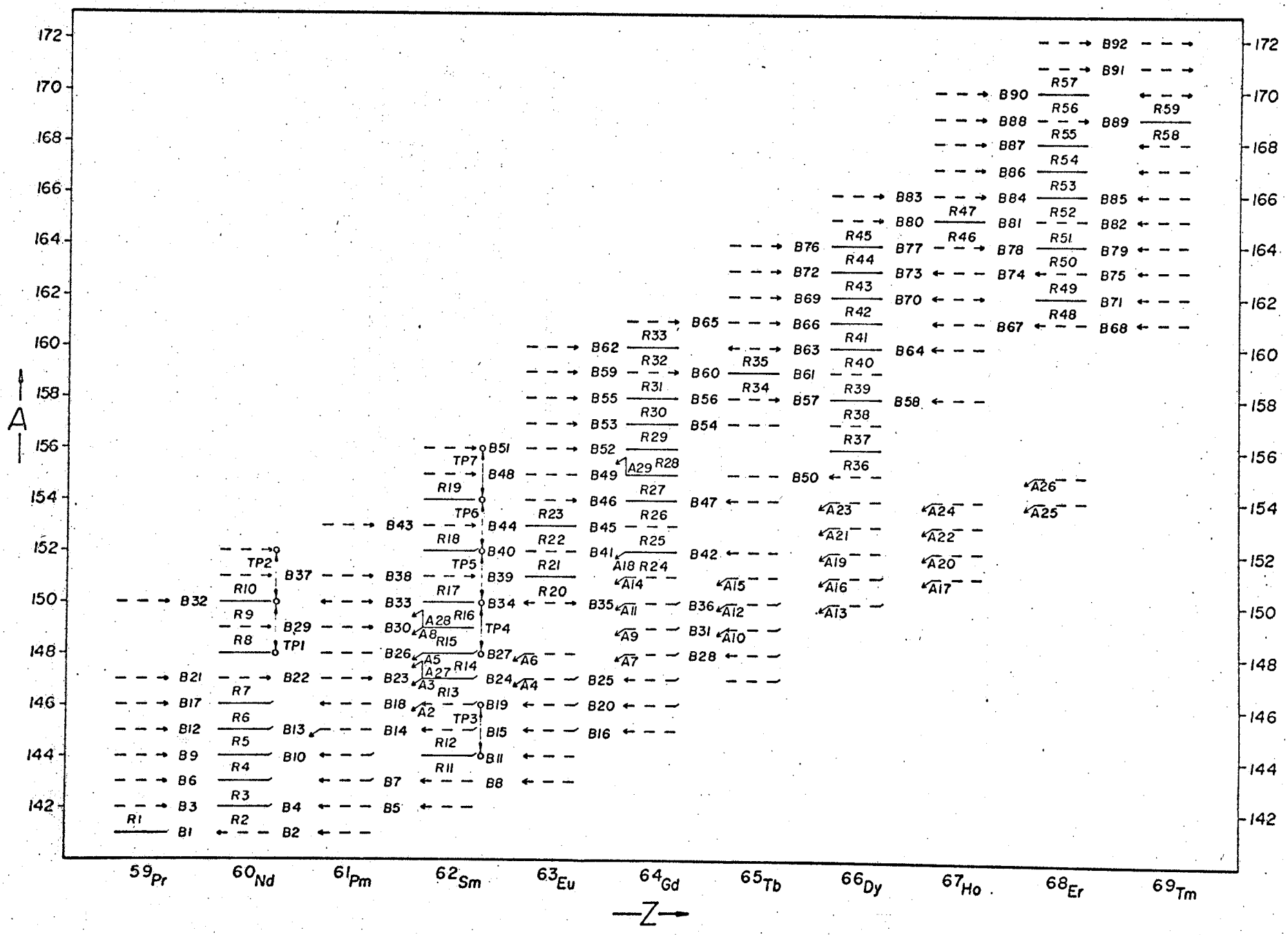
A
Z
59Pr
60Nd
61Pm
62Sm
63Eu
64Gd
65Tb
66Dy
67Ho
68Er
69Tm
172
170
168
166
164
162
160
158
156
154
152
150
148
146
144
142
B1
B2
B3
B4
B5
B6
B7
B8
B9
B10
B11
B12
B13
B14
B15
B16
B17
B18
B19
B20
B21
B22
B23
B24
B25
B26
B27
B28
B29
B30
B31
B32
B33
B34
B35
B36
B37
B38
B39
B40
B41
B42
B43
B44
B45
B46
B47
B48
B49
B50
B51
B52
B53
B54
B55
B56
B57
B58
B59
B60
B61
B62
B63
B64
B65
B66
B67
B68
B69
B70
B71
B72
B73
B74
B75
B76
B77
B78
B79
B80
B81
B82
B83
B84
B85
B86
B87
B88
B89
B90
B91
B92
R1
R2
R3
R4
R5
R6
R7
R8
R9
R10
R11
R12
R13
R14
R15
R16
R17
R18
R19
R20
R21
R22
R23
R24
R25
R26
R27
R28
R29
R30
R31
R32
R33
R34
R35
R36
R37
R38
R39
R40
R41
R42
R43
R44
R45
R46
R47
R48
R49
R50
R51
R52
R53
R54
R55
R56
R57
R58
R59
TP1
TP2
TP3
TP4
TP5
TP6
TP7
A2
A3
A4
A5
A6
A7
A8
A9
A10
A11
A12
A13
A14
A15
A16
A17
A18
A19
A20
A21
A22
A23
A24
A25
A26
A27
A28
A29

FIGURE 6.1

Figure 6-3a

Double Neutron Separation Energies, N-even
Dashed lines are drawn to follow the systematics.
See text.

FIGURE 6 - 3a

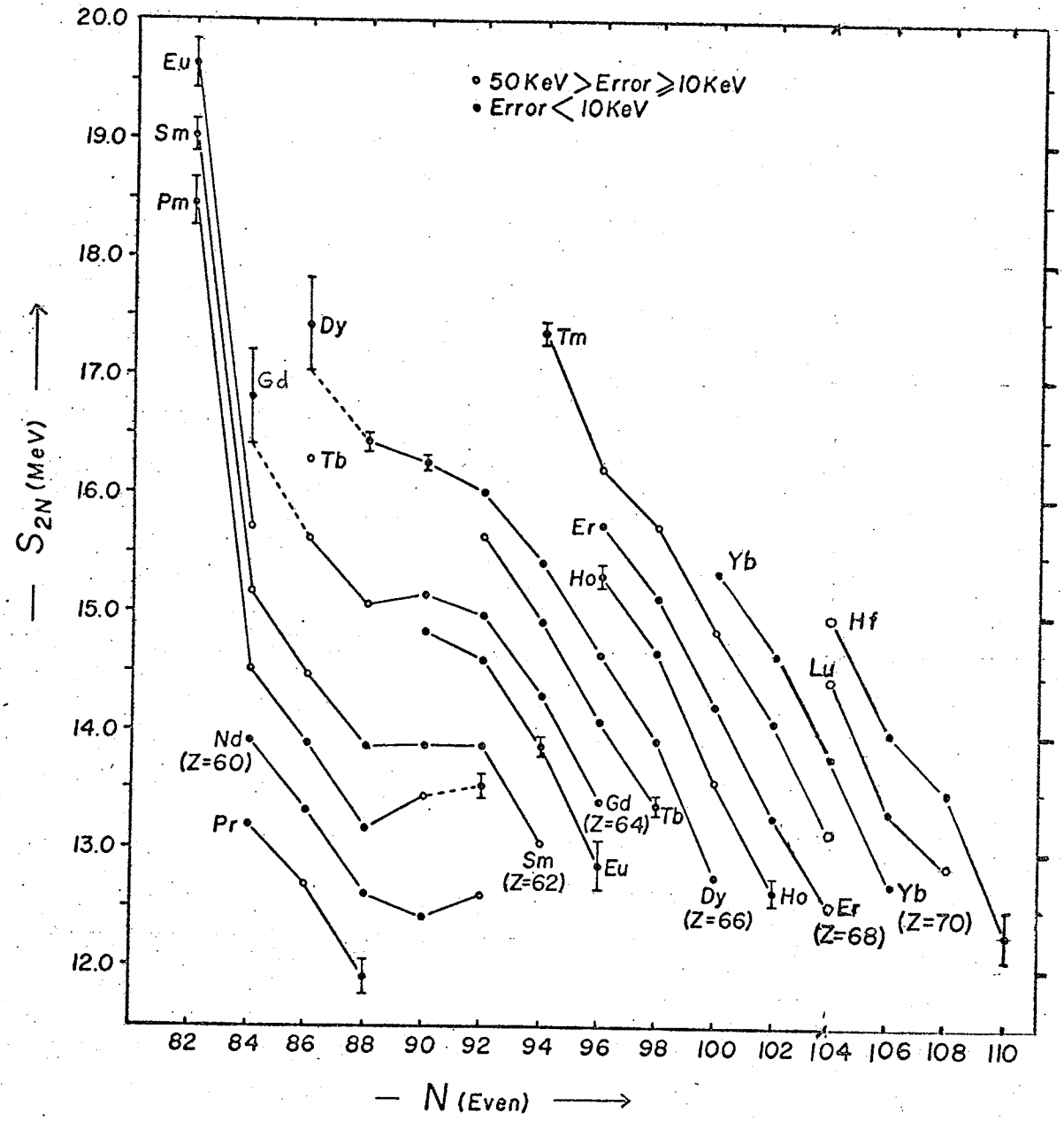
20.0
19.0
18.0
17.0
16.0
15.0
14.0
13.0
12.0
S_{2N} (MeV)
82
84
86
88
90
92
94
96
98
100
102
104
106
108
110
N (Even)
° 50 KeV > Error ≥ 10 KeV
• Error < 10 KeV
Eu
Sm
Pm
Dy
Gd
Tb
Tm
Er
Ho
Yb
Hf
Lu
Nd
(Z=60)
Pr
Gd
(Z=64)
Tb
Sm
(Z=62)
Eu
Dy
(Z=66)
Ho
Er
(Z=68)
Yb
(Z=70)

Figure 6-3b

Double Neutron Separation Energies, N-odd
Dashed lines are drawn to follow the systematics.
See text.

FIGURE 6 - 3b

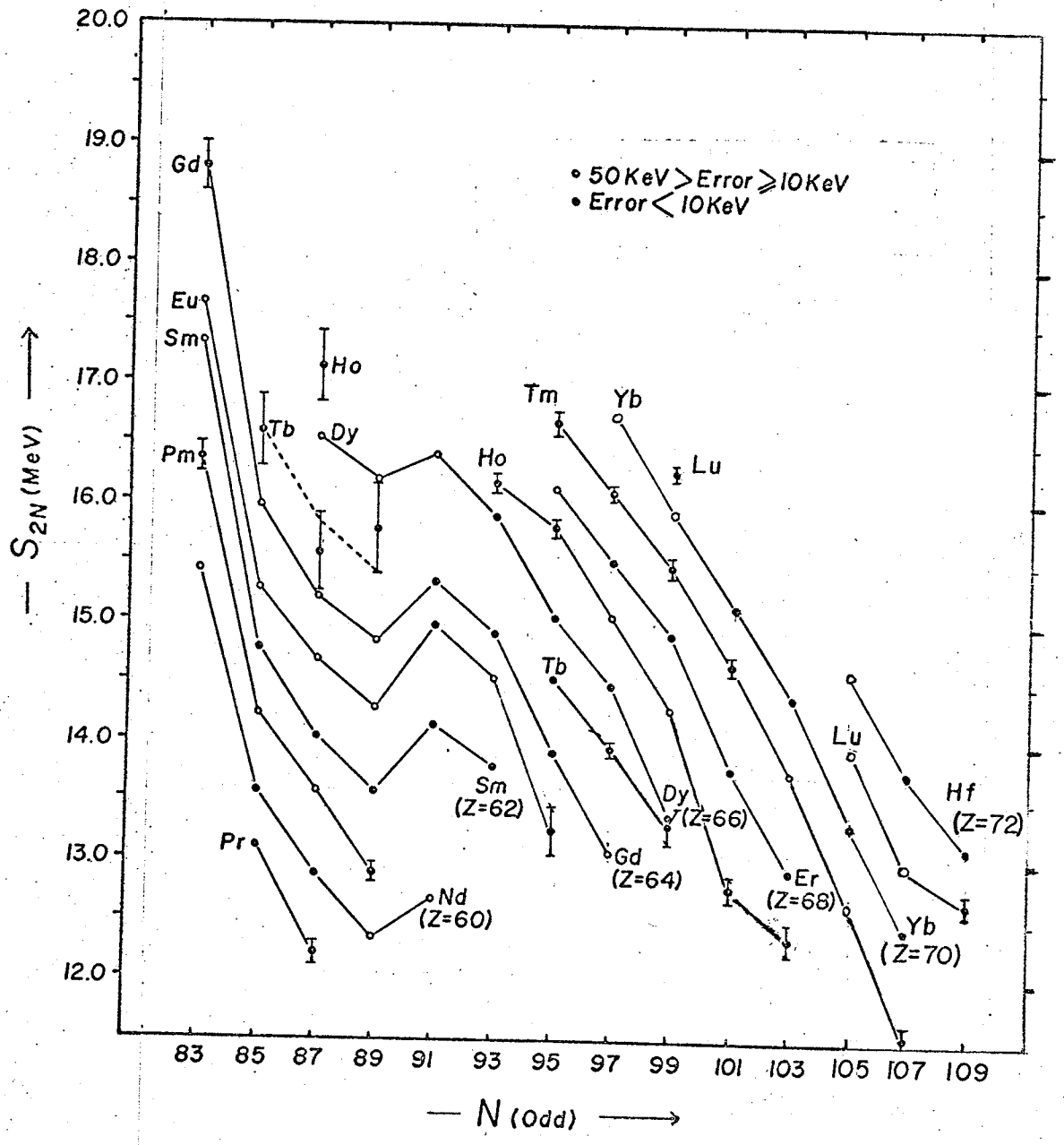
20.0
19.0
18.0
17.0
16.0
15.0
14.0
13.0
12.0
— S_{2N} (MeV) ⟶
83 85 87 89 91 93 95 97 99 101 103 105 107 109
— N (Odd) ⟶
• 50 KeV > Error ≥ 10 KeV
• Error < 10 KeV
Gd
Eu
Sm
Pm
Pr
Nd (Z=60)
Sm (Z=62)
Gd (Z=64)
Tb
Dy
Ho
Dy (Z=66)
Er (Z=68)
Tm
Yb
Lu
Yb (Z=70)
Lu
Hf (Z=72)

Figure 6-4a

Single Neutron Separation Energies, N-even

FIGURE 6 - 4a

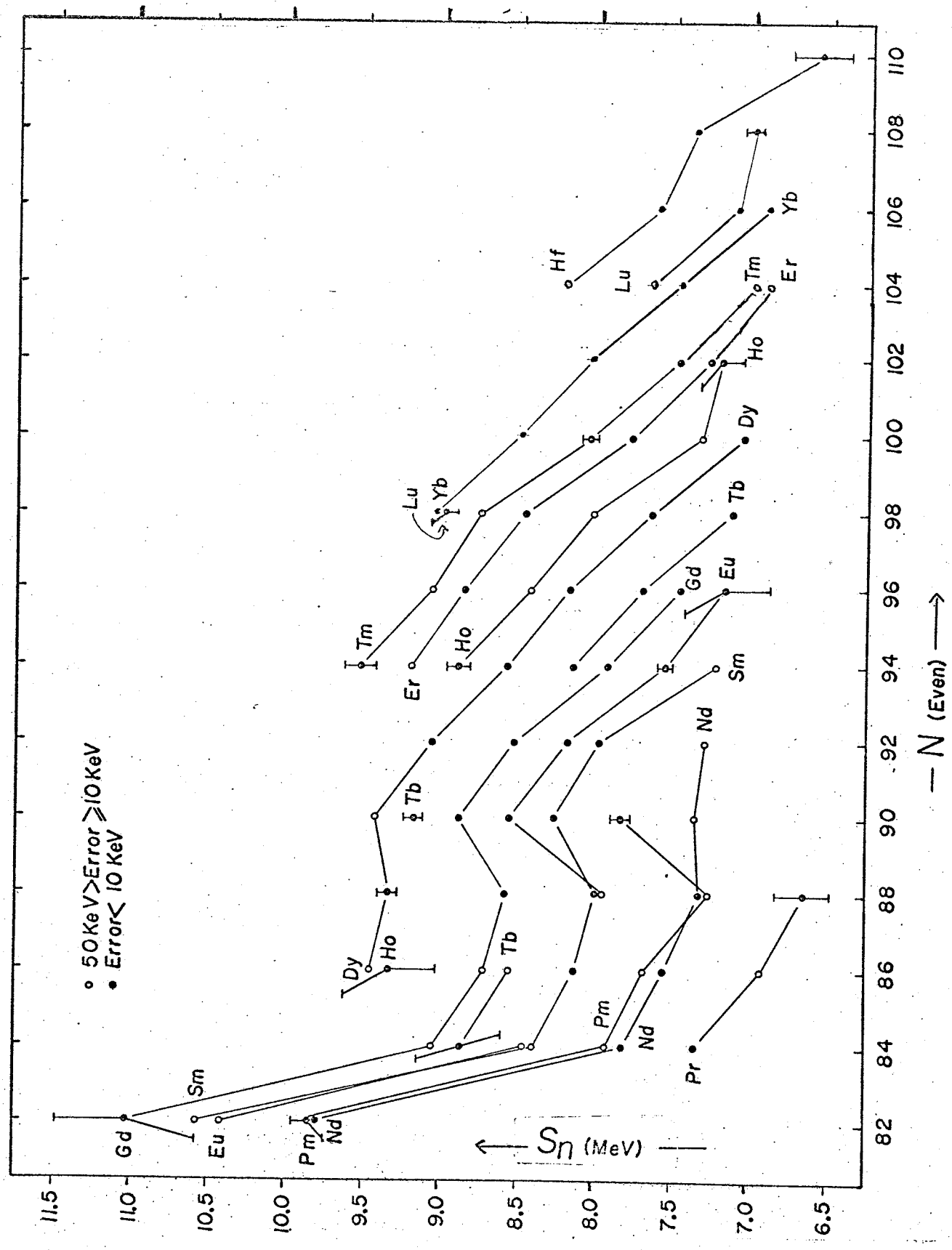
• 50 KeV > Error ≥ 10 KeV
• Error < 10 KeV
← Sη (MeV) —
— N (Even) →
Gd
Sm
Eu
Pm
Nd
Dy
Ho
Tb
Tm
Er
Lu
Yb
Hf
Pr
Nd
Pm
Tb
Dy
Ho
Er
Tm
Yb
Lu
Hf
Sm
Eu
Gd
Tb
Dy
Ho
Er
Tm
Yb
Lu
11.5
11.0
10.5
10.0
9.5
9.0
8.5
8.0
7.5
7.0
6.5
82
84
86
88
90
92
94
96
98
100
102
104
106
108
110

Figure 6-4b

Single Neutron Separation Energies, N-odd

FIGURE 6 - 4b

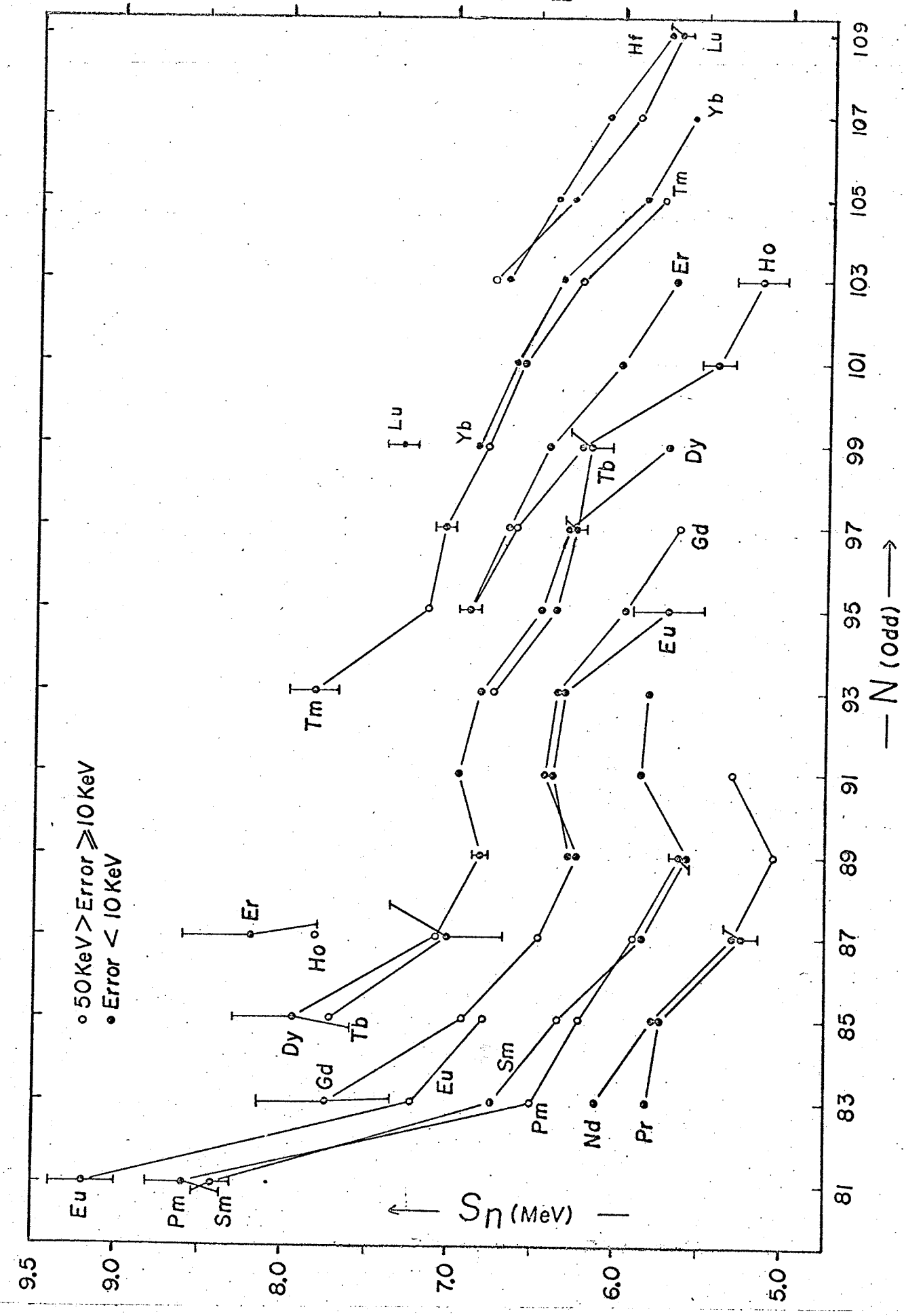
Sη (MeV)
N (Odd)
9.5
9.0
8.0
7.0
6.0
5.0
81
83
85
87
89
91
93
95
97
99
101
103
105
107
109
Eu
Pm
Sm
Nd
Pr
Pm
Sm
Eu
Gd
Dy
Tb
Ho
Er
Tm
Yb
Lu
Hf
Lu
Yb
Tm
Tb
Dy
Er
Ho
Eu
Gd
○ 50 KeV > Error ≥ 10 KeV
● Error < 10 KeV

Figure 6-5a

Neutron Pairing Energies, N-even

FIGURE 6 - 5a

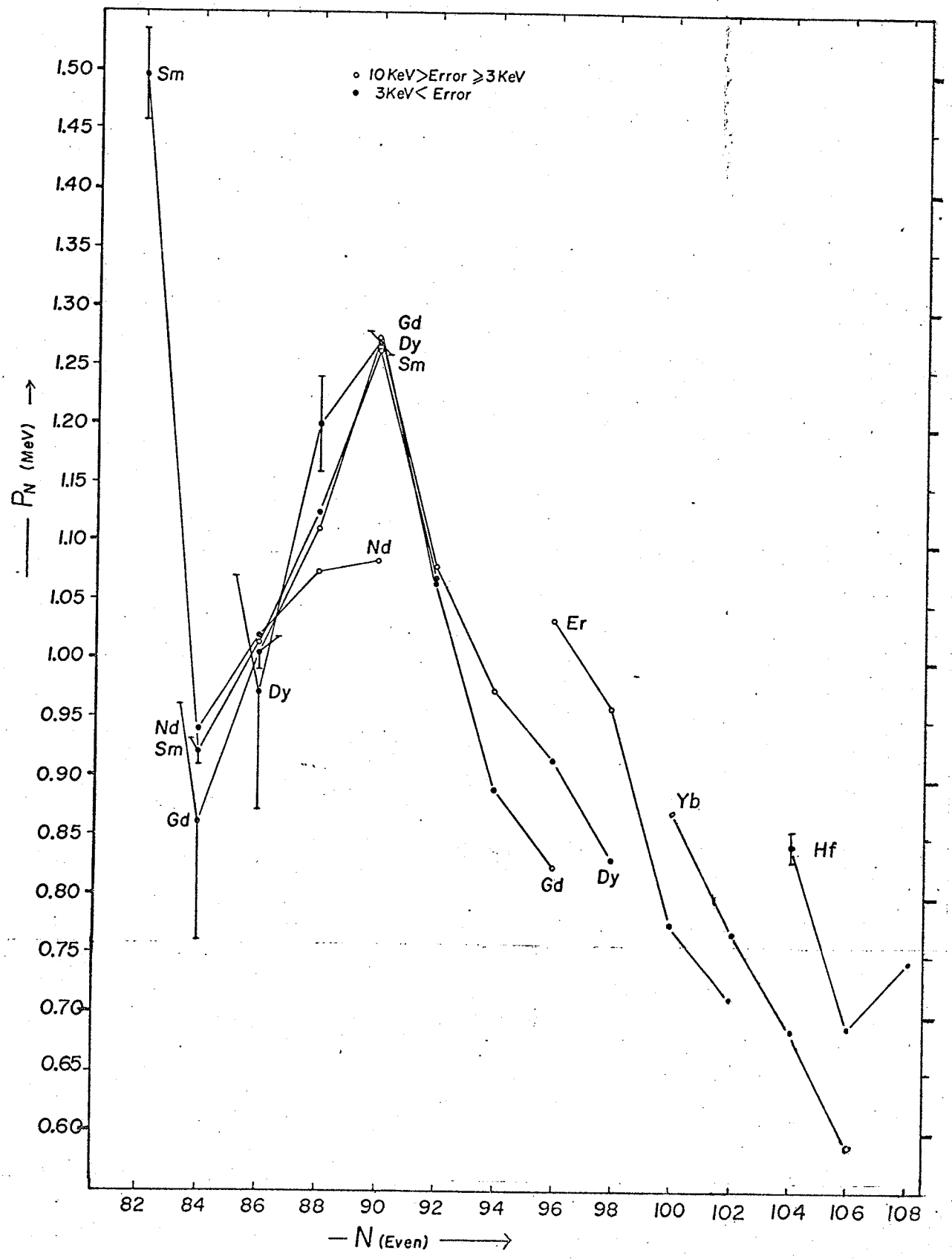
○ 10KeV>Error ≥3KeV
● 3KeV< Error
Sm
Gd
Dy
Sm
Nd
Nd
Sm
Dy
Gd
Er
Gd
Dy
Yb
Hf
1.50
1.45
1.40
1.35
1.30
1.25
1.20
1.15
1.10
1.05
1.00
0.95
0.90
0.85
0.80
0.75
0.70
0.65
0.60
— P_N (MeV) →
82
84
86
88
90
92
94
96
98
100
102
104
106
108
— N (Even) ⟶

Figure 6-5b

Neutron Pairing Energies, N-odd

FIGURE 6 - 5b

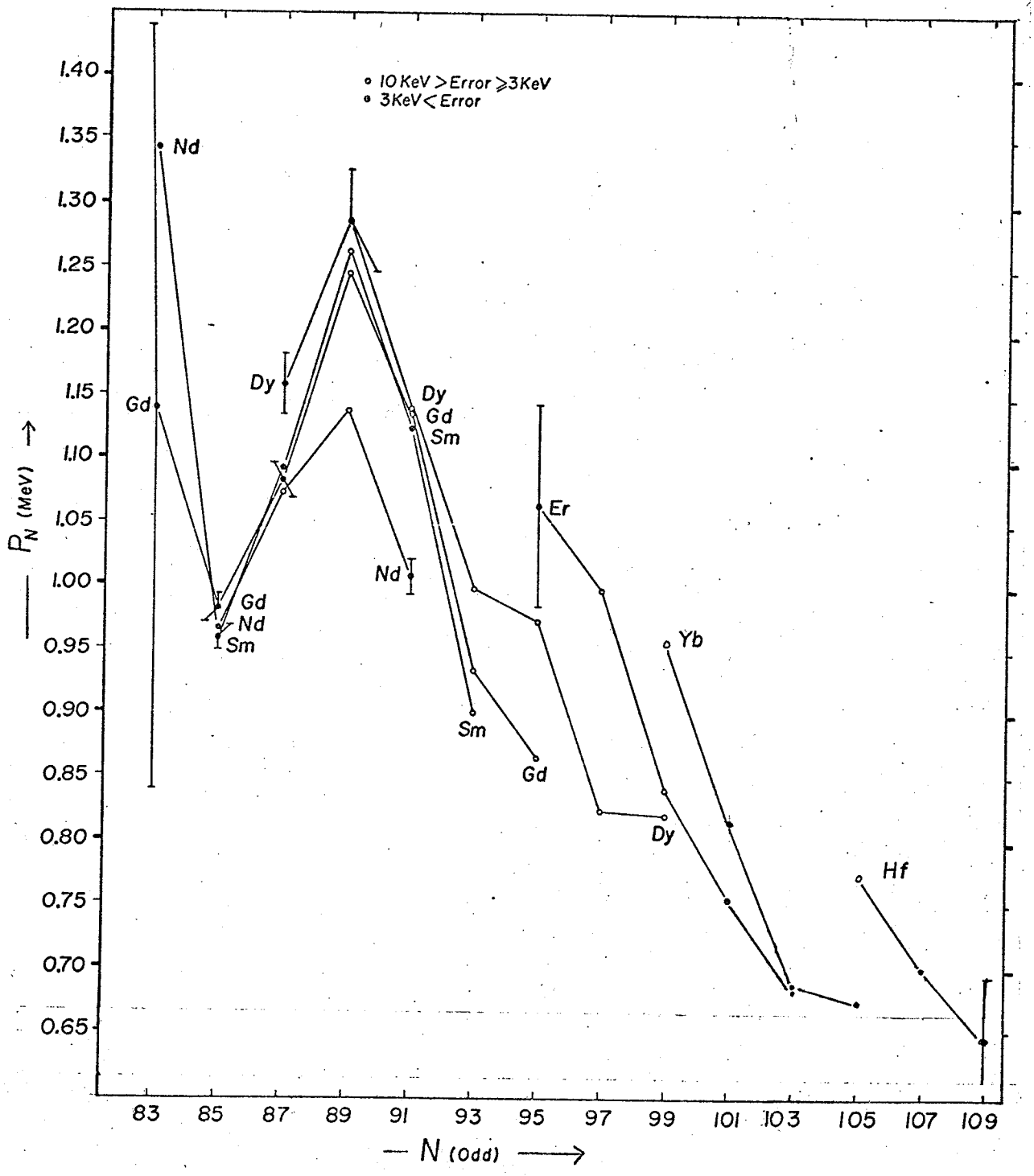
○ 10 KeV > Error ≥ 3 KeV
● 3 KeV < Error
1.40
1.35
1.30
1.25
1.20
1.15
1.10
1.05
1.00
0.95
0.90
0.85
0.80
0.75
0.70
0.65
P_N (MeV) →
Nd
Gd
Dy
Dy
Gd
Sm
Gd
Nd
Sm
Nd
Er
Yb
Sm
Gd
Dy
Hf
83
85
87
89
91
93
95
97
99
101
103
105
107
109
N (Odd) →

Figure 6-6a

Double Proton Separation Energies, $\mathcal{B}$-even

FIGURE 6 - 6a

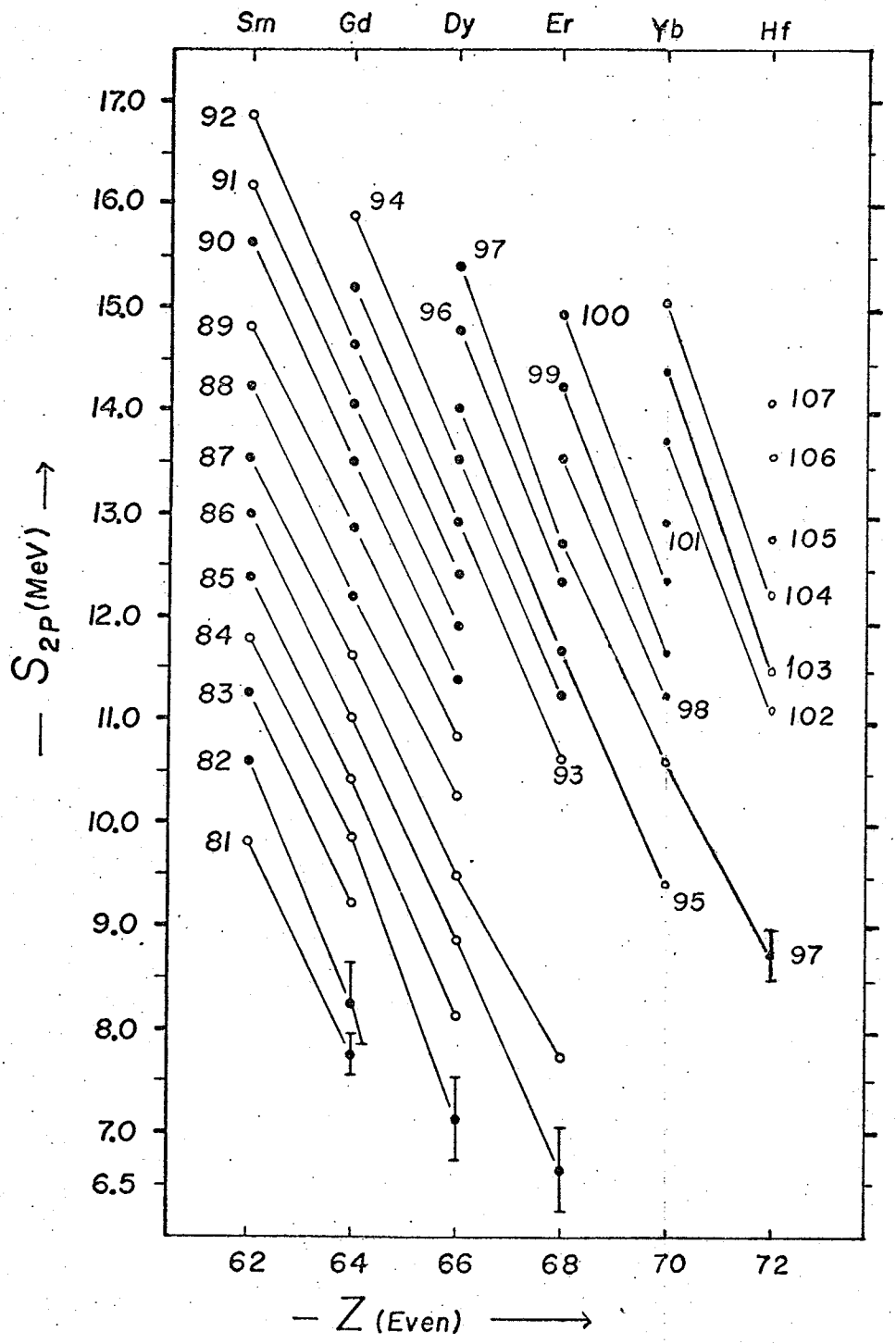
Sm
Gd
Dy
Er
Yb
Hf
17.0
16.0
15.0
14.0
13.0
12.0
11.0
10.0
9.0
8.0
7.0
6.5
92
91
90
89
88
87
86
85
84
83
82
81
94
97
96
100
99
101
98
95
93
107
106
105
104
103
102
97
62
64
66
68
70
72
— S_{2p} (MeV) →
— Z (Even) →

Figure 6-6b

Double Proton Separation Energies, Z-odd

FIGURE 6 - 6b

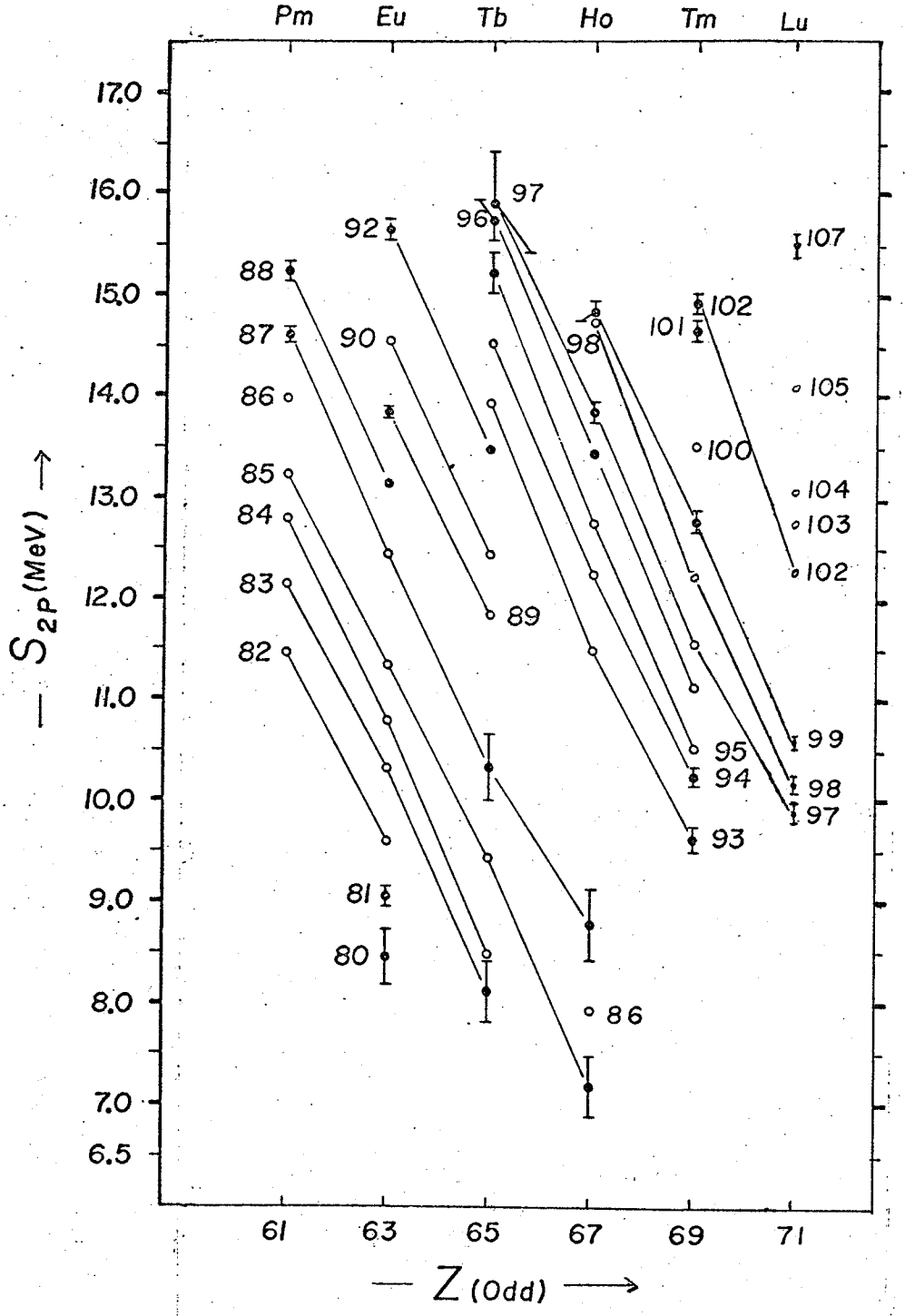
Pm
Eu
Tb
Ho
Tm
Lu
17.0
16.0
15.0
14.0
13.0
12.0
11.0
10.0
9.0
8.0
7.0
6.5
S_{2p}(MeV) ⟶
61
63
65
67
69
71
Z (Odd) ⟶
88
87
86
85
84
83
82
81
80
92
90
89
97
96
98
86
107
102
101
105
100
104
103
102
99
98
97
95
94
93

Figure 6-7a

Single Proton Separation Energies, S-even

FIGURE 6 - 7a

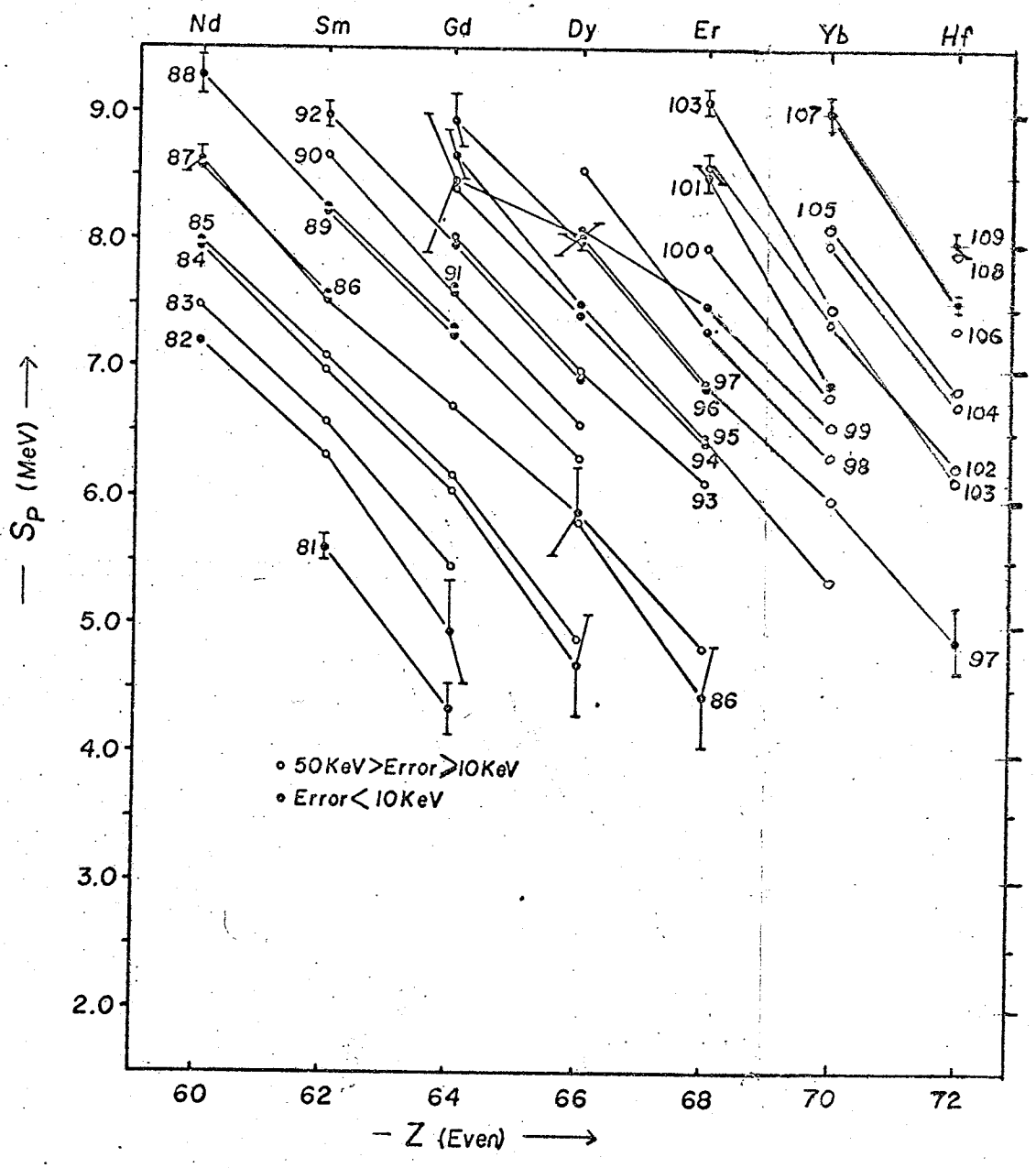
Nd
Sm
Gd
Dy
Er
Yb
Hf
88
92
87
90
85
89
84
86
83
91
82
81
103
107
101
105
100
109
108
106
97
96
104
95
99
94
98
102
93
103
97
86
9.0
8.0
7.0
6.0
5.0
4.0
3.0
2.0
— Sp (MeV) ⟶
60
62
64
66
68
70
72
— Z (Even) ⟶
∘ 50KeV>Error≥10KeV
∘ Error<10KeV

Figure 6-7b

Single Proton Separation Energies, Z-odd

FIGURE 6 - 7b

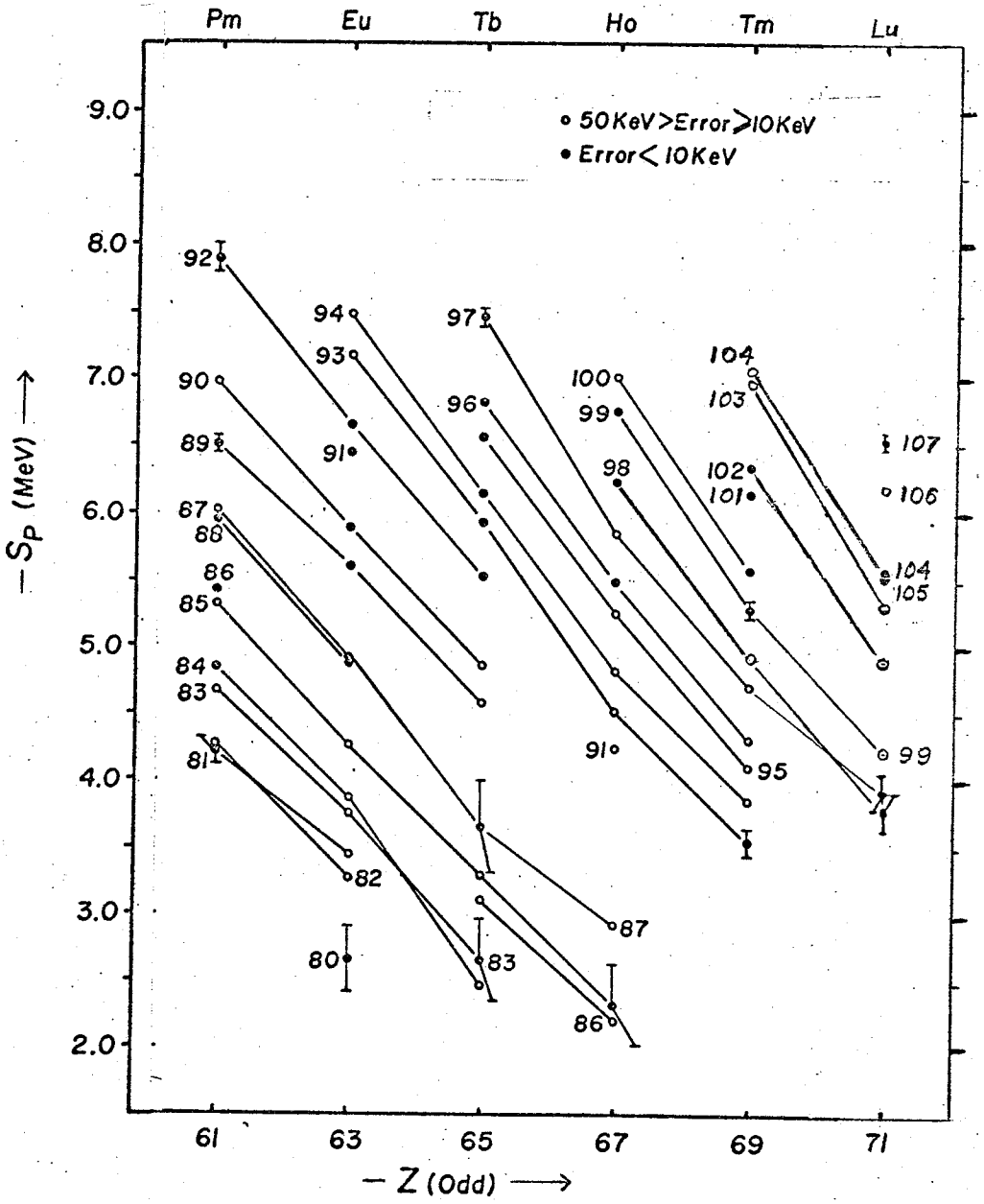
Pm
Eu
Tb
Ho
Tm
Lu
9.0
8.0
7.0
6.0
5.0
4.0
3.0
2.0
$-S_p$ (MeV) ⟶
○ 50KeV>Error≥10KeV
● Error<10KeV
92
94
93
97
90
96
100
99
104
103
89
91
98
102
101
107
106
67
68
86
85
84
83
81
82
80
87
83
86
91
95
104
105
99
61
63
65
67
69
71
− Z (Odd) ⟶

Figure 6-8

Proton Pairing Energies

These are plotted vs N, rather than Z, and are defined for even N only. Points for the same element are joined and Z is shown.

FIGURE 6 - 8

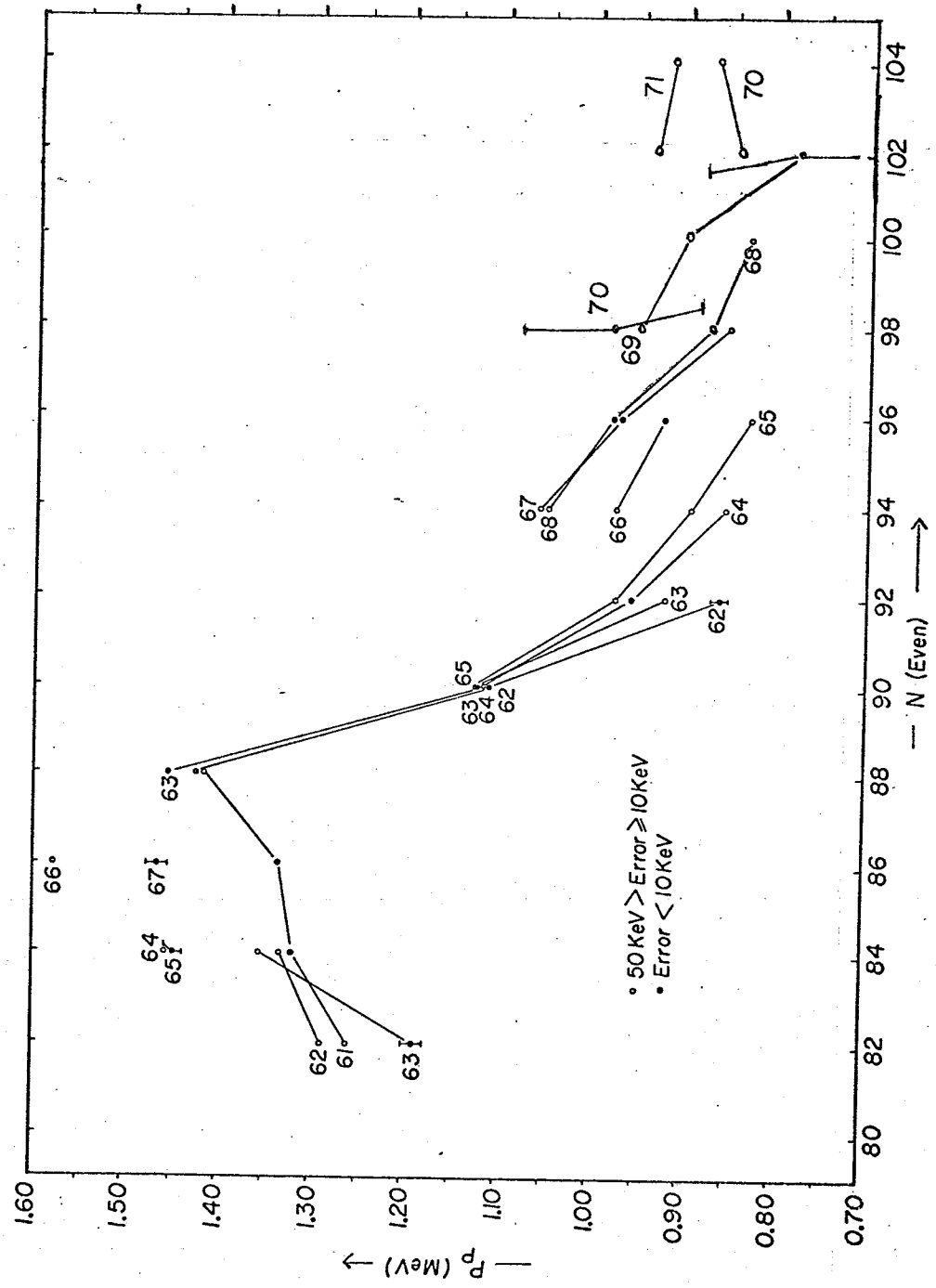
1.60
1.50
1.40
1.30
1.20
1.10
1.00
0.90
0.80
0.70
— P_p (MeV) →
80
82
84
86
88
90
92
94
96
98
100
102
104
— N (Even) →
° 50 KeV > Error ≥ 10 KeV
• Error < 10 KeV

SUMMARY

The second-order double-focusing mass spectrometer has been used to determine some twenty-six close doublets in the rare-earth chlorides from Z = 62 to 70. These provide connections between all stable odd-Z nuclides and between all stable even-Z nuclides accurate to a few keV. There are many overdetermined loops, and the measurements are internally consistent. There is generally agreement with other precise mass spectroscopic data from McMaster University and the University of Minnesota.

A new method of peak matching has been developed making use of a 1024 channel signal averager and the University of Manitoba IBM 360/65 computer. The doublet determinations reported here are as precise as by the previous visual null method, and are achieved in about one quarter of the time, employing only one operator rather than two. The matching precision is $\sim 7 \times 10^{-9}$ since the typical error on each doublet was not reduced below 1 to 2 μu.

The new peak matching method also revealed that while the precision achieved by a single match may be 1 μu, that changes in the spectrometer operations between matches results in a set of eight matches, i.e. one run having a spread of 1.5 to 4 μu, rather than the expected statistical error of $\sim$.3 μu. Now that such matching precision can be achieved

further work is necessary to better understand the behaviour of the instrument.

The new doublet determinations have been combined with previous work and with nuclear reaction and decay Q-values in two overlapping least squares adjustments of the atomic masses for $59 \leq Z \leq 72$. This reveals that there are no significant systematic errors in the mass determinations made with the new spectrometer. Also, a more detailed and extended and precise study of nucleon separation energies can be made. Included are separation and pairing energies for even-N, even-Z nuclides, as before, and in addition, even-N-odd Z, and all odd N nuclides as well. The resulting systematics show in more detail the onset of nuclear deformation, and the behaviour of neutron-neutron, proton-proton and neutron-proton pairing energies for $84 \leq N \leq 108$.

APPENDIX A

Propagation of Errors and Statistics

(1) General

Suppose we have a quantity of Q defined as a function of N variables $v_i \pm \sigma_i$, i = 1, 2, ... N where the variables v_i may or may not be independent. Then, the variance of Q is ε^2, given by

$$\varepsilon^2 = \left(\sum_{i=1}^{N} \frac{\partial Q}{\partial v_i} \sigma_i \right)^2 \qquad (1)$$

$$\varepsilon^2 = \sum_{i=1}^{I} \left(\frac{\partial Q}{\partial v_i} \sigma_i \right)^2 + \sum_{j=1}^{N} \sum_{i=1}^{N} \frac{\partial Q}{\partial v_i} \sigma_i \frac{\partial Q}{\partial v_j} \sigma_j \qquad (2)$$

If all the v_i are independent, σ_i and σ_j are equally likely to be positive or negative and the second term averages to zero. (see, for instance, Taylor, Parker and Langenberg 1969).

(2) Weighted Average

In this case, we have a set of measurements $x_i \pm \sigma_i$, all of the same quantity, and we wish to compute a 'best value'. If we assign a weight

$$\omega_i = 1/\sigma_i^2 \qquad (3)$$

to each experimental value, we define a weighted average as

$$\bar{X} = \frac{\sum_{i=1}^{N} \omega_i x_i}{\sum \omega_i} \tag{4}$$

It is possible to calculate two different errors for the mean in this case (Birge 1932).

$$\sigma_{int} = \sqrt{1/\left(\sum_{i=1}^{N} \frac{1}{\sigma_i^2}\right)}. \tag{5}$$

This is equivalent to saying that the weight of the mean,

$$\omega = \sum_{i=1}^{N} \omega_i \tag{5a}$$

$$\sigma_{ext} = \sqrt{\frac{\sum_{i=1}^{N} \omega_i (x_i - \bar{X})^2}{(N-1)\Sigma\omega_i}} \tag{6}$$

Usually, the larger of the two is used as the final error. The Birge ratio is defined as $R = \sigma_{ext}/\sigma_{int}$. If R is significantly greater than unity; one or more values of x_i may be noticeably inconsistent with the rest. It may be eliminated, a new $\bar{X}$ and σ_{int} and σ_{ext} are calculated.

(3) Centroid of a Peak (or Distribution)

This is a special case of an average. Let the height

of the distribution at any point x_i be n_i, $i = 1,2,\ldots I$.

The summation convention $\Sigma = \sum_{i=1}^{I}$ is used.

The centroid is $\overline{X} = \dfrac{\Sigma n_i x_i}{\Sigma n_i}$ (7)

For convenience, let

$$a = \Sigma n_i x_i \text{ and } b = \Sigma n_i \qquad (8a,b)$$

Then $\overline{X} = f = a/b$ (9)

$$\varepsilon_x^2 = \left(\frac{\partial f}{\partial a}\sigma_a\right)^2 + \left(\frac{\partial f}{\partial b}\sigma_b\right)^2 + 2\frac{\partial f}{\partial a}\frac{\partial f}{\partial b}\sigma_a\sigma_b$$
$$= \frac{1}{b^2}(\sigma_a)^2 + \frac{a^2}{b^4}(\sigma_b)^2 - \frac{2a}{b^3}\sigma_a\sigma_b$$

Now, the only assumption will be that we are dealing with counting the ions arriving, so that at any position x_i, the number of counts n_i obey Poisson statistics. That is, the standard deviation of n_i is $\sqrt{n_i}$, and each n_i is independent.

From equations 8a,b and using $\sigma_i = \sqrt{n_i}$, we derive

$$(\sigma_a)^2 = \Sigma x_i^2 \sigma_i^2 \qquad (11a)$$

$$(\sigma_b)^2 = \Sigma \sigma_i^2 \qquad (11b)$$

Thus $\varepsilon_x^2 = \dfrac{1}{(\Sigma n_i)^2}\left[\Sigma n_i x_i^2 + \dfrac{(\Sigma n_i x_i)^2}{(\Sigma n_i)^2}\Sigma n_i - \dfrac{2\Sigma n_i x_i}{\Sigma n_i}\Sigma x_i\sigma_i\Sigma\sigma_i\right]$ (12)

Let $\Sigma n_i = N$, (13)

$$\varepsilon_{\bar{X}}^2 = \frac{1}{N^2}\left(\Sigma n_i x_i^2 + \frac{\Sigma n_i x_i}{\Sigma n_i}\; n_i x_i - \frac{2\Sigma n_i x_i}{\Sigma n_i}\; \Sigma x_i n_i\right) \tag{14}$$

$$= \frac{1}{N^2}\left(\Sigma n_i x_i^2 - N\bar{x}^2\right) \tag{14a}$$

Suppose we normalize the peak area and use a set of numbers f_i to describe the peak shape so $n_i = f_i \cdot N$ (15)

$$\varepsilon_{\bar{x}}^2 = \frac{1}{N^2}\left(N\Sigma f_i x_i^2 - N\bar{x}^2\right) \tag{16}$$

$$\varepsilon_{\bar{x}} = \frac{1}{\sqrt{N}}\left(\Sigma f_i x_i^2 - \bar{x}^2\right)^{\frac{1}{2}} \tag{17}$$

If the peak shape is roughly Gaussian, or the distribution can be approximated by the normal distribution, the normal definition of the standard deviation of the mean gives:

$$\sigma_{\bar{x}}^2 = \frac{\Sigma n_i (x_i - \bar{x})^2}{N(N-1)} \tag{18}$$

Again, letting f_i represent the shape of the normalized peak,

$$\sigma_{\bar{x}}^2 = \frac{1}{N}\left(\Sigma f_i (x_i - \bar{x}^2)\right) \tag{19}$$

This can be changed into another familiar form for calculating.

$$\sigma_{\bar{x}} = \frac{1}{\sqrt{N}}\left(\Sigma f_i x_i^2 - \bar{x}^2\right)^{\frac{1}{2}} \tag{20}$$

exactly the same as equation 17.

(4) Least Squares Solution of Linear Equations

The experimental values for the mass differences, whether derived from mass spectroscopy or from nuclear energy determinations, may be regarded as a set of N measured values, $Y_I \pm \sigma_I$, each of which is a linear combination of the n atomic masses, M_j. We may express this for the $I^{\underline{th}}$ measured value in the following way:[1)]

$$\sum_{j=1}^{n} A_{Ij} M_j = Y_I \pm \sigma_I \qquad (21)$$

where I = 1,2,..., N and j = 1,2,...,n and the coefficients A_{Ij} are, in general, either 0 or ±1.

This set of N linear equations in the n unknown atomic masses is overdetermined since N>n, and the method of least squares is therefore appropriate to the calculation of best values for the masses (Mattauch, 1960, Bearden and Thompson 1957, Taylor et al, 1970).

To each of the observational equations (21) a weight

$$\omega_I = \frac{1}{\sigma_I^2} \qquad (22)$$

is assigned. Also we define a residual, r_I, for each of the N observational equations (21), viz.,

$$r_I = \sum_{j=1}^{n} A_{Ij} M_j^* - Y_I \qquad (23)$$

where the M_j^* are the desired adjusted masses. The desired least squares solution of the N linear equations (21) for

---

1) Lower case subscripts go from 1 to n, and capital subscripts go from 1 to N.

the n unknown masses is that which minimizes the sum of the weighted squares of the residuals: i.e.,

$$X^2 = \sum_{I=1}^{N} \omega_I r_I^2 \tag{24}$$

is a minimum.

Differentiation of this sum with respect to each of the n variables M_j^* leads to the "normal equations":

$$\frac{\partial}{\partial M_j^*} \left(\sum_{I=1}^{N} \omega_I r_I^2 \right) = 0 \tag{25}$$

where j = 1,2...,n. These n equations may then be solved uniquely for the n values M_j^*.

Each of these n equations (25) may be combined with (23) to yield the result

$$\begin{aligned} \sum_{I=j}^{N} \omega_j A_{Ij} Y_j &= \sum_{I=1}^{N} \omega_j A_{Ij} \sum_{k=1}^{n} A_{Ik} M_k^* \\ &= \sum_{k=1}^{n} \sum_{I=1}^{N} \omega_I A_{Ij} A_{Ik} M_k^* \end{aligned} \tag{26}$$

for each j = 1,2,...,n.

Equation (26) may be written in matrix form by defining

$$\underset{\sim}{G} = \{g_{jk}\} \quad \text{where } g_{jk} = \sum_{I=1}^{N} \omega_I A_{Ij} A_{Ik} \tag{27}$$

$$\underline{D} = \{d_j\} \quad \text{where } d_j = \sum_{I=1}^{N} \omega_I A_{Ij} Y_j \tag{28}$$

$$\underline{M} = \{M_k^*\} \tag{29}$$

so that

$$\underset{\sim}{G}\underline{M} = \underline{D} \tag{30}$$

Here we note that G is a square nxn, symmetric matrix.

Thus the desired solution is

$$\underline{M} = \underset{\sim}{G}^{-1} \underline{D} \tag{31}$$

where

$$\underset{\sim}{G}^{-1} = \{v_{ij}\} \tag{32}$$

is the inverse of G.

The error associated with a particular adjusted mass, M_j^*, is taken to be

$$\varepsilon_j = \sqrt{v_{jj}}. \tag{33}$$

The elements v_{ij} involve only the coefficients A_{Ij} and the weights ω_I. In each case the ε_j corresponds to the σ_{int} defined by Birge (1932).

For a certain mass difference (Q-value) $M_i^* - M_j^*$ the error is

$$\varepsilon_{i,j} = \sqrt{v_{ii} + v_{jj} - 2v_{ij}} \tag{34}$$

The generalized Birge ratio which is defined (Taylor et al 1970) as

$$\sqrt{\frac{X^2}{f}} \tag{35}$$

(where f is the number of degrees of freedom) may be calculated for the adjustment and compared with its expected value,

$$1 \pm \sqrt{\frac{1}{2f}} \tag{36}$$

If the Birge ratio is significantly larger than its expected value, the input data must be examined for inconsistencies.

The generalized Birge ratio (equation 35) is sometimes known as the 'consistency factor' (C.F.). That is, if all input errors σ_I were multiplied by the C.F., and the adjustment were re-calculated, all the adjusted values would remain unchanged, the new ε_J would be the same as the old ones, now multiplied by C.F. and the new Birge ratio would be unity. However, this method increases the errors on all the input data, even if most of them are consistent.

Sometimes, a group of data may be identified as causing a large contribution to χ^2, and the consistency of this group may be evaluated. It may occur that the errors quoted on this sub set of measurements are slightly too small for overall consistency, and that multiplying the input errors of this group only by an appropriate consistency factor will result in the new adjustment having a generalized Birge ratio near unity.

In other cases, a single datum or a few isolated data may be identified as grossly inconsistent. These data may then be evaluated. Since there is no way of determining a consistency factor for an isolated value, it is difficult to arbitrarily increase the error, and so the value may be eliminated from the adjustment.

Solution by Computer

If the equations 26 through 30 are examined, it may be seen that $G = \{g_{jk}\}$ may be written

$$G = (1/\sigma\underset{\sim}{A}^T)\ (1/\sigma\underset{\sim}{A}) \qquad (31)$$

and that $D = \{dj\}$ may be written

$$D = (1/\sigma\underset{\sim}{A}^T)\ (1/\sigma\underset{\sim}{y}) \qquad (32)$$

Thus, if the Nxn matrix A is set up, to describe the system of equations, and with weights $(1/\sigma_I)^2$ then the final equations to be solved are

$$(1/\sigma)\underset{\sim}{A}^T(1/\sigma)\underset{\sim}{A}\ \underline{M} = (1/\sigma)\underset{\sim}{A}^T(1/\sigma)\underline{y} \qquad (33)$$

and the matrix $\underset{\sim}{G} = (1/\sigma)\underset{\sim}{A}^T(1/\sigma)\underset{\sim}{A}$ is to be inverted

$\underline{M} = G^{-1}D$ as before

This premultiplication by $(1/\sigma)\underset{\sim}{A}^T(1/\sigma)$ on both sides of the non-square matrix equation is an easy computer operation. $(1/\sigma)\underset{\sim}{A}^T(1/\sigma)\underset{\sim}{A}$ is a square nxn matrix, and $(1/\sigma)$ multiplied in twice supplies appropriate weights.

An interesting comment is supplied by Cohen (1971), who derives the same matrix equation without even talking about 'least-squares' and 'quadratic forms', and minimizing anything. Starting with the idea that the best estimates is the mean, and generalizing to a weighted mean and then to a multi-variable linear system, he derives the desired result by demanding the invariance of the solution either to the basis vectors of the variable space or to the form in which the observational data may be expressed.

(5) Least Squares Fitting of a Straight Line

The method outlined above could easily be applied to the fitting of a straight line

$$a_o + a_1 x_I = y_I, \quad I = 1,2,\ldots N.$$

Here N is the number of pairs of points and the unknown quantities to be solved for are a_o and a_1. If N>2 the problem is overdetermined, and we want a least squares solution. The matrix method of sec 4 is cumbersome, so we look for other methods. There are many versions of the standard formula available, most of them assuming no errors in either x_I or y_I. However, implicit in the formulation is that x_I are correct, and all the variation is due to y_I. This is discussed by York (1966), and methods are reviewed for explicitly handling errors in either x_I or in y_I. He also suggests a way to include errors in both x_I and y_I.

A much better solution is provided by Williamson (1968). The major difficulty is that when there are errors in both coordinates, the expression for the weight of each point (w_I), the quantity a_1 appears.

$$w_I(x_I,y_I) = 1/(1/\sigma_Y{}^2 + a_1{}^2/\sigma_x{}^2)$$

The way out is to use an iterative technique. If we first use $a_1 = 0$, and solve the normal equations, the solution corresponds to that for no error in x_I. Then, using this first approximation for a_1, the equations are solved again. The process is repeated as often as required.

The computer programme developed here differs from Williamson (1968) in three ways: (i) the initial guess for the slope is always zero, (ii) there is a built in limit to the number of iterations, and (iii) the iteration ceases when the change in a_1 from one stage to the next is significantly smaller than the error in a_1.

References for Appendix A

Beardon, J.A. and Thompson, J.S. (1957) Nuova Cimento, Suppl. 5, 326

Birge, R.T. (1930) Phys. Rev. 40, 207

Cohen, E.R. (1971) to be published

Mattauch, J.H.E. (1960) Proc. Int'l. Conf. on Nuclidic Masses (Duckworth, Ed.) University of Toronto Press, p.3

Taylor, B.N., Parker, W.H. and Langenberg, D.N. (1970) The Fundamental Constants and Quantum Electrodynamics Academic Press, New York

Williamson, J.H. (1968) Can. J. Phys. 46, 1845

York, D. (1966) Can. J. Phys. 44, 1079

```
$JOB  LIST
      SUBROUTINE WTFIT2 ( N,X,EX,Y,EY,A,B,EA,EB,IWR,LNPRNT )
      DIMENSION X(1),EX(1),Y(1),EY(1),
     2          U(100),V(100),W(100)
C         ROUTINE FITS A STRAIGHT LINE TO THE SET OF PAIRS OF POINTS
C         Y(I) , X(I) WHEN THERE IS ERROR IN BOTH COORDINATES .
C
C                                  Y(I) = A + B * X(I)
C
C         B      THE SLOPE OF THE FITTED LINE .
C         VB     THE VARIANCE OF B .
C         A      THE INTERCEPT OF THE FITTED LINE .
C         VA     THE VARIANCE OF A .
      DO 10 I=1,N
      U(I) = EX(I)*EX(I)
   10 V(I) = EY(I)*EY(I)
      IT = 0
      B=1.
   11 IT = IT + 1
      BO = B
      SW = 0.
      SWX = 0.
      SWY = 0.
      DO 12 I=1,N
      W(I) = 1. / ( V(I) + B*B*U(I) )
      SW = SW + W(I)
      SWX = SWX + W(I)*X(I)
   12 SWY = SWY + W(I)*Y(I)
      XBAR = SWX / SW
      YBAR = SWY / SW
      SL = 0.
      SWZ = 0.
      SWZX = 0.
      SWZY = 0.
      SWZZ = 0.
      SWXY = 0.
      DO 13 I=1,N
      XP = X(I) - XBAR
      YP = Y(I) - YBAR
      WZ = W(I) * W(I) *( V(I)*XP + B*U(I)*YP )
      SL = SL + W(I)*W(I) * ( XP*XP*V(I) + YP*YP*U(I) )
      SWXY = SWXY + W(I) * XP * YP
      SWZ = SWZ + WZ
      SWZX = SWZX + WZ * XP
      SWZY = SWZY + WZ * YP
   13 SWZZ = SWZZ + WZ*WZ/W(I)
      B = SWZY / SWZX
      IF ( IT .GT. 30 )          GO TO 15
      A = YBAR - B * XBAR
      ZBAR = SWZ / SW
      Q = SWXY/B + 4.*( SWZZ-SWZ*ZBAR-SWZX )
      VB = SL / (Q*Q)
      IF ( ABS(B-BO) .GT. .01*VB )     GO TO 11
      XZ = XBAR + 2.*ZBAR
      VA = ( VB*XZ + 2.*ZBAR/Q )*XZ + 1./SW
```

```
      XSQ = 0.
      DO 14 I=1,N
      F = A + B*X(I)
      ERR = Y(I) - F
   14 XSQ = XSQ + ERR*ERR*W(I)
   15 CONTINUE
      EA = SQRT( VA )
      EB = SQRT( VB )
      IF ( IWR .EQ. 1 )   WRITE (LNPRNT,101) A,EA,B,EB,XSQ,IT
  101 FORMAT ('0  INTERCEPT = ' F10.2,' +-' F8.2,'     SLOPE = ' F10.2
     2' +-'F8.2,'    CHI-SQUARE =' F12.2,' , NO. OF ITERATIONS' I6 )
      RETURN
      END
//
```

APPENDIX B

TAILS ON PEAKS

(1) Possible Causes

If a beam of ions passes through a smooth, parallel object slit and the subsequent focused image is modulated linearly across a collector slit of the same width as the image, the resulting peak shape is triangular. Tails may be caused by (i) image aberrations, (ii) gas scattering (elastic or inelastic), or (iii) slit irregularities. Since our mass spectrometer is second-order double focusing, with very small measured coefficients (Barber et al, 1971) factor (i) will be neglected although the aberrations probably contribute slightly to the tails.

In considering gas scattering by residual molecules along the ion path, we will consider elastic only scattering, since inelastic events will likely not be brought to focus near the peak. The case for atoms of mass $\sim$200 scattered elastically in air at $\sim$30 keV energy has been studied by Menat (1964) in an isotope separator. In our case, the scattering angle is very small since the collector slit is $\sim 2\mu$ wide, and most scattering takes place 1 to 3 m away, i.e. $\theta \sim 10^{-6}$ radians. Thus we are well below the classicial limit of

$$\theta_c \sim \lambda/2\pi\, a_o Z^{1/3} \sim 10^{-2}$$

for a simple Rutherford scattering by a Coulomb potential (Everhart et al 1955). Thus we must use the quantum mechanical Born approximation.

Schiff (1949) presents the Born approximation for scattering by a screened Coulomb potential when the equations are integrated to find the fraction of the total beam scattered one peak width to the side, the answer is about 10^{-6}, and constant over the region we are considering. The magnitude of this result may be wrong by a factor of ±10 since it is based on differential scattering cross-sections and effective screening lengths measured at much larger angles of $\sim 10^{-3}$ radians. Classical solutions lead to very large cross sections at small angles, increasing to infinity as θ goes to zero. Thus the result of Reudenauer (1970) is entirely fortuitus when applied to our instrument. His curves are not valid below $\Delta M/M \sim 10^{-3}$, but extrapolation to $\Delta M/M \sim 10^{-5}$ produces a scattered fraction of 2%. This is about the size of the tails one slit width away from the centre of the peak, but the quantum mechanical approach required here leads to too small a cross section for gas scattering at 10^{-8} to 10^{-7} Torr. to be considered as the major cause of the tails.

The most likely cause of tails is irregularity in the slit jaws, especially the principal slit which is subjected to ion currents of ~1-10 μa.

If there are irregularities (mainly widenings due to wear) of the order of .1μ, the peak width would be broadened by 2% at a resolving power of 100,000. If these irregularities amount to a few percent of the total usable height of the slit (~20μ in 1 mm height) then the height of the peak at the nominal edge will be increased by a few percent.

Previous tool steel slits could be ground very smooth and gave excellent resolution for a few days, but deteriorated over a few weeks to the point where they had to be replaced. The current tantalum slits do not achieve as high an initial sharpness, but maintain reasonable performance (i.e. tails of a few percent at one peak width from the centre) for several months.

(2) Effects on Peak Separation

The overlap of tails has the effect of reducing the apparent peak separation. This is true for visual matching, the visual null method, or computer matching. However, it is likely that the operator compensates to some extent in the first two methods. The computer cannot do this, and a specific method must be used to eliminate the effects of the tails. We have followed the general lead of Stevens and Moreland (1968) and have used only the part of the peak lying 15% or more of the peak height above the base line.

The effect on the separation of two peaks as they are moved together is shown in Fig. B-1. A singlet was recorded at a typical operating resolution (∿1/100,000). The computer then constructed a well resolved doublet by duplicating the peak a known distance away. Then the regular programme proceeded and the separation was calculated. The difference between the nominal separation and the calculated separation is plotted vs. the separation of the peaks for cut off levels of 3%, 6%, 9% and 15%.

The effect is much more noticeable if the two peaks are not the same intensity. In general, the intensity ratios are 2:1 to 5:1 and occasionally as bad as 30:1. In these cases, the tail of the larger peak makes a significant contribution to the nearer side of the smaller peak. For the bias to be .0002 peak widths or less, with a separation of 1.5 to 2.0 peak widths, a 15% cut-off level was chosen.

The effect on the doubletsreported in Chapter 4 are shown in Fig.B-2. The change of the doublet spacing from its known value is plotted vs. various cut-off levels. Notice the effects of the different intensity ratios.

References for Appendix B

Barber, R.C., Bishop, R.L., Duckworth, H.E., Meredith, J.O., Southon, F.C.G., van Rookhuyzen, P. and Williams, P. (1971) Rev. Sci. Instrum. 42, 1

Everhart, E., Stone, G. and Carbone, R.J. (1955) Phys. Rev. 99, 1287

Menat, M. (1964) Can. J. Phys. 42, 164

Reudenauer, F.G. (1970) Rev. Sci. Instrum. 41, 1487

Schiff, L.I. (1949) Quantum Mechanics (McGraw Hill) p.161

Stevens, C.M. and Moreland, P.E. (1968) Proc. 3rd Int'l. Conf. on Atomic Masses (Barber,Ed.) University of Manitoba Press p.673

Figure B-1

Change in Doublet Spacing vs Peak Separation
Curves are shown for 3%, 6%, 9% and 15% cut-off levels when the intensity ratio is 1:1.
There are two scales, one in channels and one in fraction of a peak width.

FIGURE B - 1

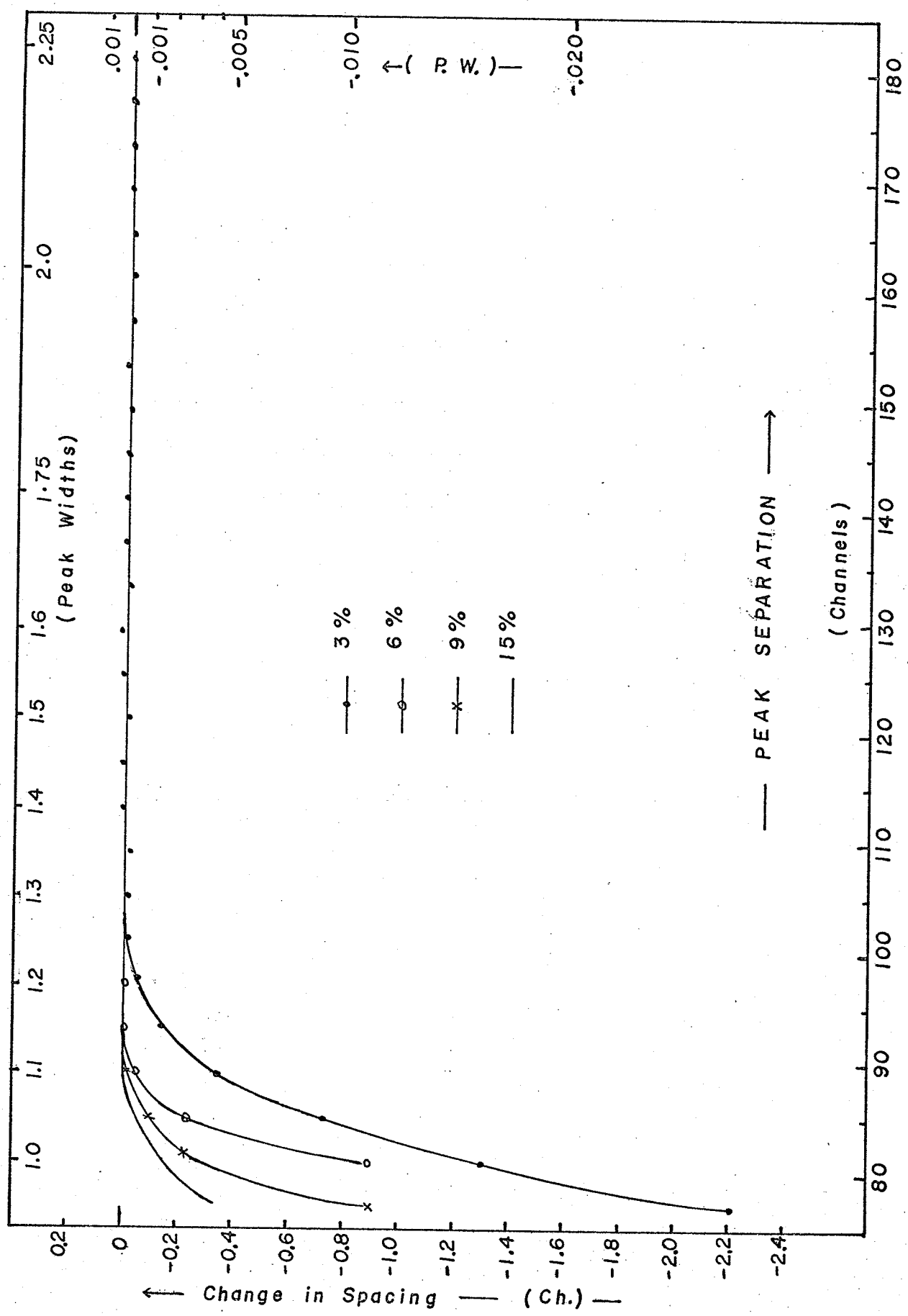
.001
-.001
-.005
-.010
-.020
← (P. W.) —
2.25
2.0
1.75
1.6
1.5
1.4
1.3
1.2
1.1
1.0
(Peak Widths)
3 %
6 %
9 %
15 %
— PEAK SEPARATION —→
(Channels)
180
170
160
150
140
130
120
110
100
90
80
0.2
0
-0.2
-0.4
-0.6
-0.8
-1.0
-1.2
-1.4
-1.6
-1.8
-2.0
-2.2
-2.4
← Change in Spacing — (Ch.) —

FIGURE B - 2

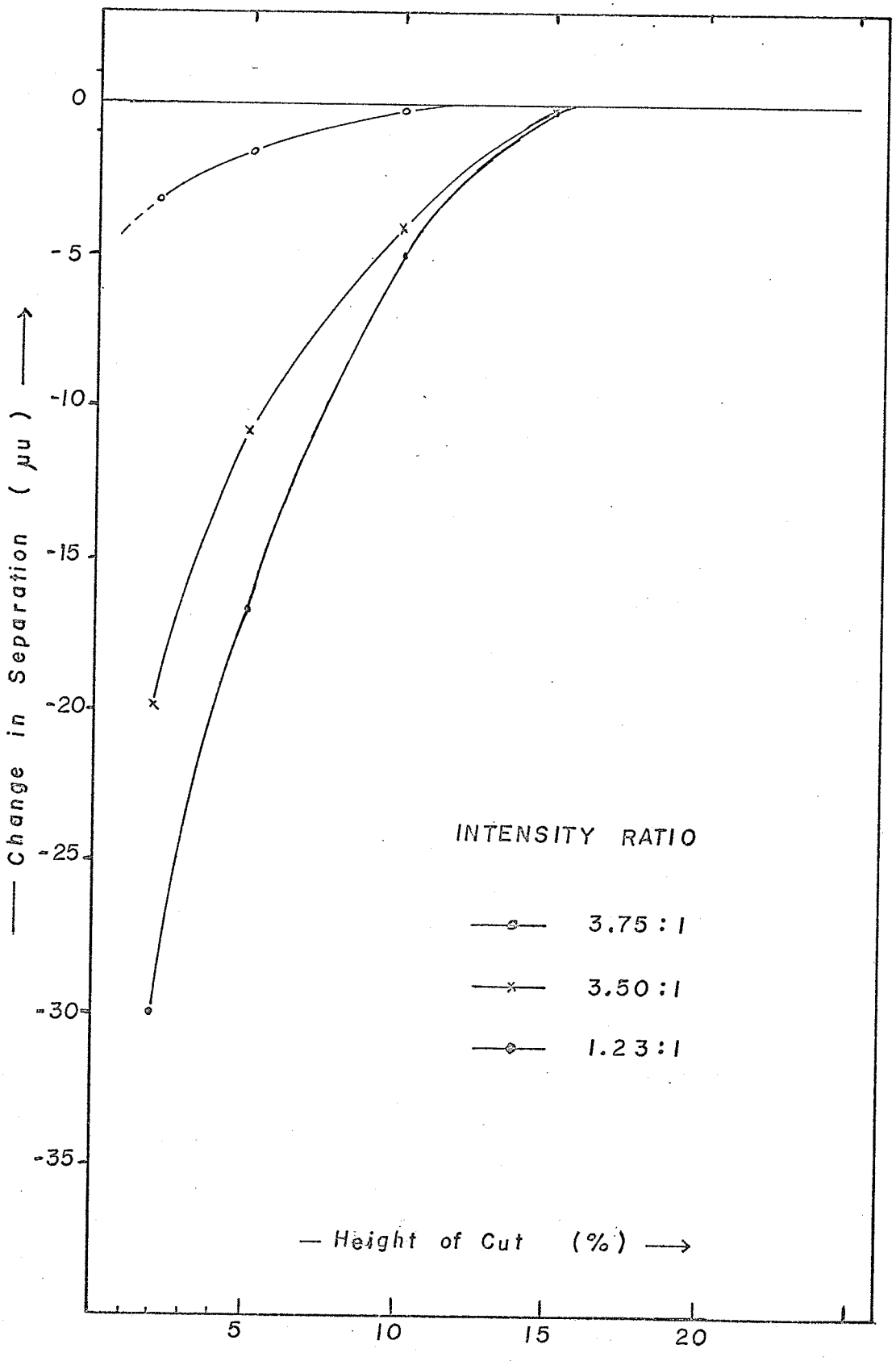
0
-5
-10
-15
-20
-25
-30
-35
— Change in Separation (μu) ⟶
INTENSITY RATIO
3.75 : 1
3.50 : 1
1.23 : 1
— Height of Cut (%) ⟶
5
10
15
20